Inter-Carrier Interference Suppression in Orthogonal Frequency Division Multiple Access (OFDMA) Systems Uplink

Hou Sheng-Wei

B.Eng., University of Science & Technology of China

A Dissertation submitted to the Department of Electrical & Computer Engineering in partial fulfillment of the requirements for the degree of Doctor of Philosophy

at

National University of Singapore

2008

Acknowledgements

At the end of my PhD study at the National University of Singapore, I would like to give my sincerest gratitude to my supervisor during the last three years, Professor Ko Chi Chung, for his guidance and assistance throughout the whole candidature. Not only this thesis and my research work, but also my personal development at NUS have benefited from his insight and support. It is my fortune to receive this valuable experience, without which none of what I have today would come true.

My parents, who always stand beside me, have given me their greatest understanding and support in all these years. Special thanks to my mother, she devotes her life to my education and always gives me the courage to face challenges, all of which have become stepping stones leading to the future.

Also, I am very thankful to the officemates at Communications Lab for their great friendship through my study at Singapore.

Contents

List of Figures

List of Tables

List of Abbreviations

4G	fourth generation (communication technologies)	MIMO	multiple input multiple output
BEM	basis expansion model	ML	maximum likelihood
BER	bit error rate	MMSE	minimum mean square error
BS	base station	MS	mobile station
CDMA	code division multiple access	MSE	mean square error
CFO	carrier frequency offset	OFDM	orthogonal frequency division multiplexing
CP	cyclic prefix	OFDMA	orthogonal frequency division multiple access
CRLB	Cramer-Rao Lower Bound	PIC	parallel interference cancellation
DFT	discrete Fourier transform	P/S	parallel to sequential
FDMA	frequency division multiple access	QPSK	quaternary phase shift keying
FFT	fast Fourier transform	SDMA	space division multiple access
IBI	inter-block interference	SB	subspace
ICI	inter-carrier interference	SER	symbol error rate
IFFT	inverse fast Fourier transform	SIC	successive interference cancellation
ISI	inter-symbol interference	SIR	signal-to-interference power ratio
LMMSE	linear minimum mean square error	SINR	signal-to-interference-plus-noise power ratio
LMS	least mean square	SNR	signal-to-noise power ratio
LS	least square	S/P	sequential to parallel
MAI	multiple access interference	TDMA	time division multiple access
MF	matched filtering	WiMAX	worldwide interoperability microwave access

Summary

In current broadband evolution of wireless communications, Orthogonal Frequency Division Multiplex (OFDM) is widely accepted as a major technique for many future broadband wireless systems. OFDMA, a multiuser OFDM using Frequency Division Multiple Access (FDMA), becomes a paramount candidate to support multiple access in future broadband wireless systems due to its advantages over existing multi-access techniques.

In uplink transmission, OFDMA suffers from Inter-Carrier Interference (ICI) caused by subcarrier frequency misalignment, which can be due to Carrier Frequency Offset (CFO) and Doppler effects. In particular, different users have independent frequency misalignment and thus CFO compensation used in single-user OFDM fails to suppress the ICI in an OFDMA system. In this dissertation, the use of multiuser detection schemes is developed to suppress ICI at the receiver after transmission through time and frequency selective channels. Both linear and non-linear detection techniques are considered and investigated. Minimum Mean Square Error (MMSE) and MMSE with Successive Detection (MMSE-SD) are proposed for possible use in OFDMA uplink. It is shown that the MMSE scheme is optimal linear scheme in terms of maximizing system rate, and the MMSE-SD is capable of exploiting the Doppler diversity from time-varying channels.

Since channel information is requisite knowledge to ICI suppression, estimation of the doubly selective fading channel is investigated in Chapter 4. To avoid performance

degradation caused by ICI in frequency domain, a time domain estimation scheme is proposed based on Basis Expansion Model. Both analytical and simulation results demonstrate that the proposed scheme obtains significant accuracy improvement. Moreover, the proposed ICI suppression schemes used in conjunction with the proposed channel estimation scheme are also evaluated.

Chapter 5 particularly presents a study on interleaved OFDMA system uplink, since a novel signal model can be designed in such a system, which obtains low complexity in ICI suppression. The design is considered in a static multipath fading channel and compared with current studies. Analytical and simulation results are presented to demonstrate that performance can be improved with reduced complexity.

In summary, this dissertation presents two important issues in physical layer design of OFDMA system. Improved ICI suppression and channel estimation schemes are proposed and analyzed for the use in mobile applications with time and frequency selective fading channels.

Chapter 1

Introduction

An explosive increase in the demand on multimedia information has lately motivated a high-data-rate evolution in wireless industry characterized by the change from narrowband to broadband. Under this evolution, signal modulation techniques will also be changed from single-carrier modulation to multicarrier modulation [1]. Conventional single-carrier modulation suffers from Inter-Symbol Interference (ISI) in a multipath fading channel and thus shows obvious limitation when used in broadband high-rate systems. Complicated channel equalization techniques are needed to remove the ISI in order to maintain performance. On the other hand, the use of multicarrier modulation is able to improve system immunity to multipath fading, because a high-rate data stream is separated into several low-rate data streams which are transmitted through different subcarriers. Design of channel equalization techniques in a multicarrier system thus can be dramatically simplified.

Amongst various multicarrier modulation schemes, Orthogonal Frequency Division Multiplexing (OFDM) has become a popular scheme since it can be readily implemented through a Fast Fourier Transform (FFT) module. OFDM also becomes a prime theme in the evolution towards future broadband wireless technologies and a promising candidate in several broadband wireless systems, such as Universal Mobile Telecommunications System (UMTS)[2], IEEE 802.11 and IEEE 802.16 [3]-[6].

1.1 OFDM-based Wireless Communications

1.1.1 Principles of OFDM

In OFDM modulation, a series of information symbols are placed onto uniformly spaced orthogonal subcarriers (the subcarriers that are orthogonal to each other during signaling interval). Fig.1.1 depicts the spectrum of an OFDM-modulated signal. To attain highest spectra efficiency, the spacing between subcarriers is chosen to be the smallest distance that ensures orthogonality.

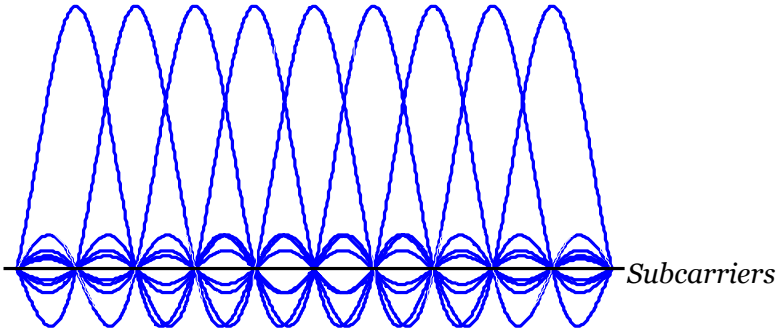

Fig.1.1: Spectra of an OFDM-modulated Signal.

A. FFT Implementation of OFDM

Let $X(k)$, $k = 0,1...N-1$, denote the information symbols. The signal after OFDM modulation can be described as

$$x(t) = \sum_{k=0}^{N-1} X(k) e^{j2\pi f_k t}, \qquad 0 \le t \le T, \quad (1\text{-}1)$$

where $f_k = f_0 + k\Delta f$ stands for the uniformly spaced subcarriers, and T is OFDM signaling interval. To ensure the orthogonality amongst waveforms $e^{j2\pi f_k t}$ over the interval $0 \le t \le T$, it is necessary that $\Delta f \cdot T = 1$, which is generally referred to as OFDM orthogonal condition. As a result of the orthogonality, information symbol

$X(k)$ can be easily demodulated from $x(t)$ by using

$$X(k)=\frac{1}{2\pi}\int_0^T x(t)e^{-j2\pi f_k t}dt\,, \qquad k=0,1...N-1\,. \quad (1\text{-}2)$$

Clearly, the modulation given by (1-1) and demodulation given by (1-2) have the same form as discrete-time Fourier transform and its inverse. If the OFDM signal (1-1) is sampled in time domain at a sampling period of T/N, it follows

$$x(n)=\sum_{k=0}^{N-1}X(k)e^{\frac{j2\pi f_k nT}{N}}=\sum_{k=0}^{N-1}X(k)e^{\frac{j2\pi n(f_0+k\Delta f)T}{N}}\,. \quad (1\text{-}3)$$

Using the orthogonal condition $\Delta f\cdot T=1$ and setting $f_0=0$ to eliminate the common phase shift,

$$x(n)=\sum_{k=0}^{N-1}X(k)e^{\frac{j2\pi nk}{N}}\,,$$

$$0\le k\le N-1\,,\ \ 0\le n\le N-1\,. \quad (1\text{-}4)$$

Equation (1-4) gives digital OFDM modulation. It is apparent that the digital OFDM modulation essentially uses Inverse Discrete Fourier Transform (IDFT) to modulate information symbols. And it is straightforward to see that the information symbol can be demodulated by using DFT at the receiver. In practical systems, FFT, the well-known fast algorithm for DFT, is used in digital OFDM modulation and demodulation modules.

B. Cyclic Prefix

When transmitted in a multipath fading channel, multiple replicas of an OFDM block will be received at the receiver, and this will give rise to Inter-Block Interference (IBI). To avoid the distortion due to IBI, a guard interval, specially named as Cyclic Prefix (CP), is appended at the head of each OFDM block. The use of CP helps to

simplify equalization. Specifically, after removing CP at the receiver, the received signal in frequency domain is simply the transmitted information symbols scaled by channel frequency responses, and therefore equalization can be simply done with a multiplication. Fig.1.2 shows a typical structure of CP. As shown below, a CP is normally a copy of the ending portion of the associated OFDM signal.

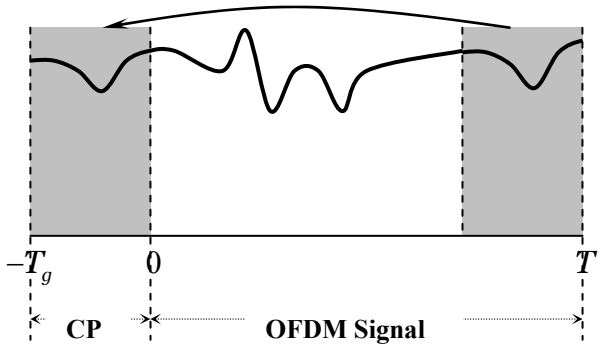

Fig.1.2: A Cyclic Prefix used in an OFDM system

With the aforementioned basic modules, a block diagram of OFDM transmitter and receiver are illustrated in Fig.1.3.

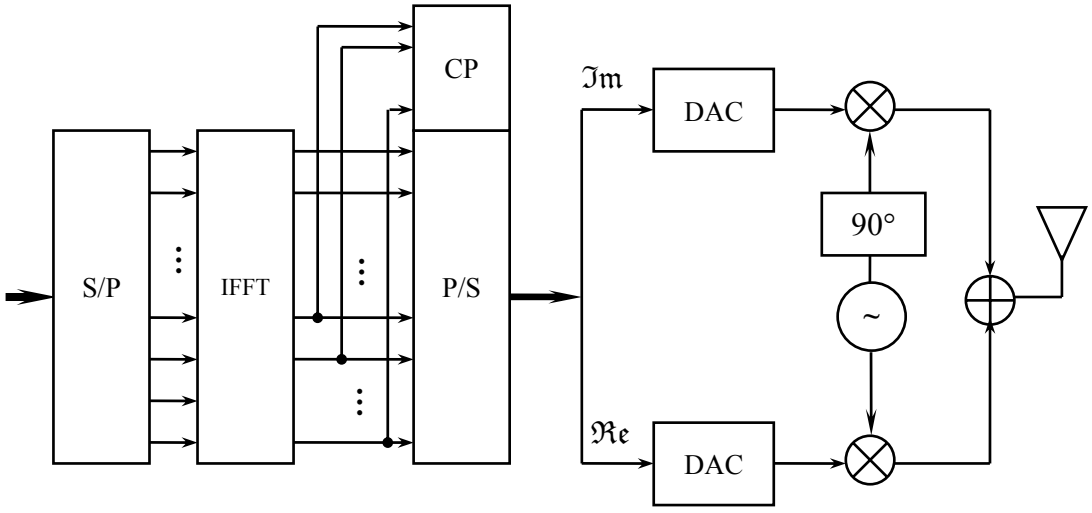

(a)

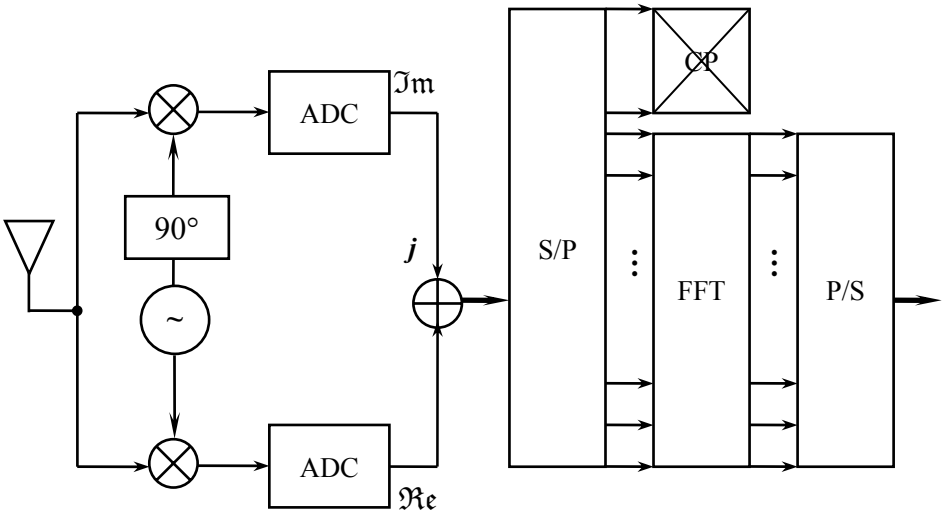

(b)

Fig.1.3: Block diagrams of (a) OFDM transmitter with a single antenna (b) OFDM receiver with a signal antenna.

1.1.2 OFDM-based Multiple Access

When used to support multiuser communications, OFDM can be used in combination with all types of multiple access schemes to share resources among different users. Typical OFDM-based multiple access techniques include Time Division Multiple Access (OFDM-TDMA), Code Division Multiple Access (OFDM-CDMA or MC-CDMA) and Frequency Division Multiple Access (OFDM-FDMA). These schemes are briefly introduced as below.

A. OFDM-TDMA

As illustrated in Fig.1.4(a), OFDM-TDMA places different users into different time slots. Each user occupies the whole bandwidth in an exclusive time slot. The time duration, in which every user accomplishes transmission once, is one frame.

B. OFDM-CDMA

OFDM-CDMA differentiates users by assigning each of them a subset of codes. As can be seen from Fig.1.4(b), all the users occupy the same bandwidth and communicate simultaneously. According to different combination fashions of OFDM and CDMA, OFDM-CDMA can be categorized as Multicarrier CDMA (MC-CDMA), Multicarrier DS-CDMA and Multitone CDMA [8].

C. OFDM-FDMA

OFDM-FDMA is generally termed as Orthogonal Frequency Division Multiple Access (OFDMA). As can be seen in Fig.1.4(c), each user is exclusively assigned with a subset of subcarriers and all the users communicate simultaneously. Subcarrier allocation in OFDMA is fairly flexible and thus attracts considerable research interest in the field of cross layer design. Subcarrier allocation in OFDMA can be either static allocation or dynamic allocation. Static allocation can be further categorized into Block, Interleaved and Hybrid schemes, which are sketched in Fig.1.4(c).

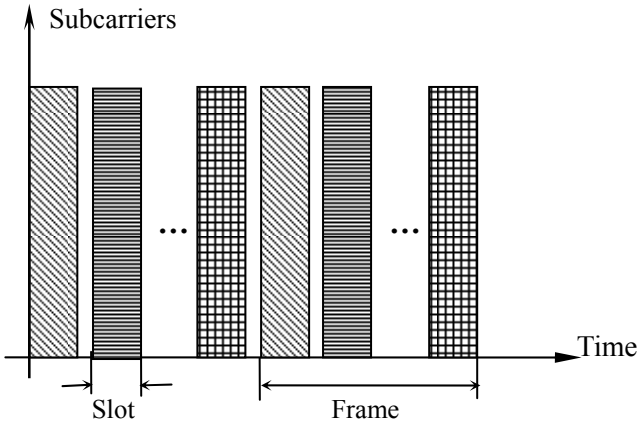

(a) OFDM-TDMA

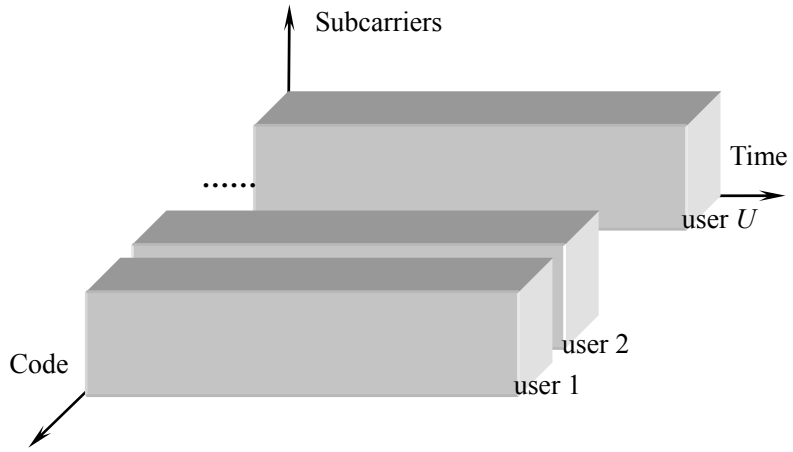

(b) OFDM-CDMA

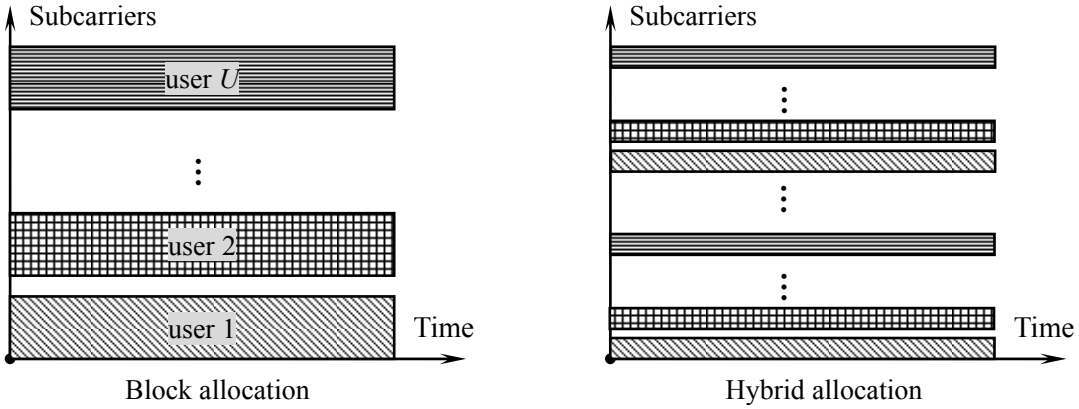

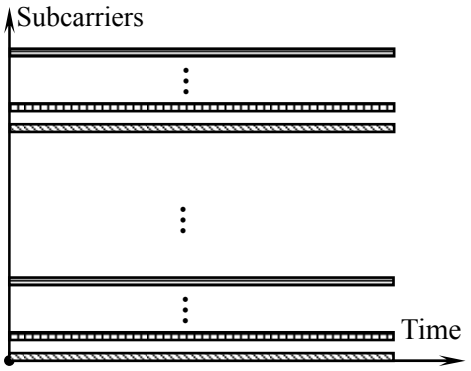

Interleaved allocation

(c) OFDM-FDMA with different subcarrier allocation schemes.

Fig.1.4: Typical multiple access techniques used with OFDM.

A number of studies have been dedicated to compare the above multiple access schemes in OFDM systems [9]. Table 1.1 presents comparisons on modulation,

flexibility and signaling overhead between different OFDM multiple access techniques.

TABLE 1-1. COMPARISON OF OFDM-BASED MULTIPLE ACCESS SCHEMES

	OFDM-TDMA	OFDM-FDMA	OFDM-CDMA
Modulation Scheme	Coherent or Incoherent	Coherent or Incoherent	Coherent only
Flexibility in adaptation	Adaptive modulation	Adaptive modulation Adaptive allocation	No adaptation
Signaling Overhead	Low	Moderate	High

1.2 OFDMA: Advantages and Challenges

Amongst all the multiple access techniques mentioned above, OFDMA receives the widest interest from both industry and academia. Particularly, OFDMA has been accepted as the air interface in a number of leading technologies for broadband communications, such as the well-known IEEE802.16e (WiMAX) system. In this section, some important advantages of the OFDMA technique, and the challenges in OFDMA system design are introduced and discussed.

A. Advantages of OFDMA

One major advantage of OFDMA is its flexibility on radio resource allocation, such as subcarrier, bit and power allocation. By using wisely designed scheduling algorithms, the so-called Multiuser Diversity, which is embedded in multipath fading channels, can be exploited to improve the overall system capacity [10]-[12]. Moreover, the flexibility on resource allocation also makes OFDMA a promising technique to accommodate variable data rate and differentiated Quality of Service (QoS) [11][13]-[16]. In previous study, it has been shown that OFDMA, by using intelligent resource allocation, outperforms the OFDM-TDMA and OFDM-CDMA systems in

overall system rate, Bit Error Rate (BER) performance, immunity to narrow-band interferences[7][17]. Due to these attractive features, OFDMA has been widely adopted. However, OFDMA itself also has some disadvantages that give rise to some challenging issues in system design.

B. Challenges

As a descendant of OFDM technique, OFDMA inherits a major disadvantage from OFDM: it is sensitive to frequency asynchronism. More specifically, carrier frequency misalignment commonly seen between Mobile Station (MS) and Base Station (BS) gives rise to Carrier Frequency Offset (CFO), which in turn induces Inter-Carrier Interference (ICI). It is ICI that causes severe performance degradation to OFDM and OFDMA systems. Particularly in OFDMA, this disadvantage becomes even more challenging. Specifically, the carrier frequencies used by different transmitters are fairly unlikely to be exactly the same, and signals transmitted from these transmitters also go through independent impairments during wireless transmission. Different users thus have different CFO at the receiver. As a result, these offsets cannot be removed by merely CFO compensation. Suppressing the ICI thus becomes a major challenge in OFDMA physical layer design, and also main scope of the study in this dissertation.

1.3 Inter-Carrier Interference Suppression in OFDMA Uplink

A simple idea to suppress ICI is to recover the frequency synchronism between transmitter and receiver. This is what researchers had been trying to do in early studies

[18]-[22]. A frequency synchronization scheme commonly studied for OFDMA systems is termed as Feedback-Adjustment, in which all the users' CFO are estimated at the receiver and sent back to each user through feedback channel. Every user then adjusts its own oscillator to eliminate the CFO. An obvious disadvantage of feedback adjustment is the long processing delay in the feedback process and extra cost on feedback channel. Therefore, the feedback-adjustment approach is generally used for the purpose of coarse frequency synchronization to reduce the frequency offset into a moderate value. After coarse synchronization, data transmission starts and feedback may be unsuitable as data transmission is sensitive to large delay, particularly in mobile or multimedia communications. Therefore, in the stage of data transmission, it is a preferred choice that using detection techniques to suppress the CFO-induced ICI at the receiver, instead of the feedback-adjustment [23].

Very recently, detection-based ICI suppression attracts considerable interest. While a number of studies have addressed this issue (specific review of these studies will be presented in Chapter 2), most of them are incremental work based on the conventional single-user OFDM detector, whose performance was analyzed in [24]. The conventional detector requires multiple FFT demodulation modules, and therefore involves considerable computational complexity. To solve this problem, a variant of this detector has been proposed in [25]. Specifically, multiple FFT modules have been reduced to only one by compensating for multiuser CFO through circular convolution after FFT demodulation. A number of sequent studies tried to improve performance by canceling ICI from the conventional detector or the low-complexity variant.

One design sacrifice in these studies is the lack of consideration on large scale fading. Most studies simply assume equal powers at the receiver when evaluating performance. In practice, it is unlikely that different users still have the same power after transmission. More importantly, power difference has significant impact on the performance of ICI suppression. In the studies of CDMA, this issue is known as the near-far effect [34]-[38]. Another insufficiency in previous studies is the assumption of static or quasi-static channel in signal modeling. Although the ICI caused by CFO is studied, the ICI caused by channel variation, which is commonly seen in mobile communications, has not been explicitly considered.

The contributions of this work include:

1. Research on ICI suppression is extended to time and frequency selective fading channels, and a signal model suitable for general OFDMA systems is obtained.
2. Both linear and nonlinear cancellation schemes are studied as an effort to establish a framework for the study on ICI suppression. Some of current studies can be considered as special cases of the detectors investigated herein.
3. Research on channel estimation is also extended to time and frequency selective fading channels, with Basis Expansion Model (BEM) formulated to ensure tracking multiuser CIR in time domain and thus bypass the issue of ICI during channel estimation.
4. Low complexity detection structure is obtained for interleaved OFDMA system.

1.4 Outline

The aim of this dissertation is to investigate the detection-based ICI suppression for OFDMA uplink in a time and frequency selective fading channel. In detail, contents of the remaining chapters are arranged as follows:

Chapter 2 presents a review on earlier studies of ICI suppression in OFDMA uplink. Chapter 3 investigates ICI suppression in a time and frequency selective fading channel. A signal model is firstly formulated and then several ICI suppression schemes are discussed and compared.

As a piece of knowledge requested in ICI suppression, channel information should be estimated prior to ICI suppression. Chapter 4 investigates the issue of channel estimation. In detail, basis expansion model is adopted to develop possible estimation techniques, to track multiuser doubly selective fading channels in OFDMA uplink.

Chapter 5 particularly takes the interleaved OFDMA system into account and formulates a novel signal model, which obtains low complexity in ICI suppression.

Chapter 6 presents some conclusions on the basis of the research covered in this dissertation, and also gives some possible directions for future work.

Chapter 2

Inter-Carrier Interference in OFDMA System Uplink

As mentioned in Chapter 1, suppression of Inter-Carrier Interference (ICI) caused by frequency asynchronism is crucial in the design of OFDM/OFDMA systems. In a single-user OFDM system, ICI can be easily suppressed via CFO compensation and equalization. In an OFDMA system, however, different users have different CFO and channel conditions, and therefore the issue of ICI suppression becomes more complicated. It is thus this chapter's objective that giving important background and review of latest notable research in the area of ICI suppression for OFDMA uplink.

This chapter is organized as follows. First, relevant background of ICI in an OFDMA uplink is introduced. Second, previous studies on the issue of ICI suppression in OFDMA uplink are reviewed.

2.1 Frequency Asynchronism and ICI in OFDMA Uplink

For the convenience of statement, the discussion is for now given to a static channel, in which asynchronism is due to CFO. Frequency asynchronism due to both CFO and channel variation will be considered in Chapter 3. Mathematically, frequency asynchronism appears to be a phase shift in the time domain signal. The received signal with phase shift due to CFO is given by

$$r_u(n) = \sum_{k=0}^{N-1} X_u(k) H_u(k) e^{\frac{j2\pi(f_k+f_u)nT}{N}} = \sum_{k=0}^{N-1} X_u(k) H_u(k) e^{\frac{j2\pi(k+\varepsilon_u)n}{N}} \quad (2\text{-}1)$$

where $H_u(k)$ is channel frequency response (static or semi-static channel) on subcarrier k, f_u is CFO of user u and ε_u stands for the CFO normalized with respect to subcarrier spacing $\frac{1}{T}$, i.e., $\varepsilon_u = f_u T$. Clearly, in a single-user OFDM system, the CFO-induced ICI can be readily suppressed by compensating for the phase shift before FFT demodulation. In an OFDMA uplink, on the other hand, due to the coexistence of multiple users, CFO compensation for one user is not helpful to compensating for other users' CFO. As a result, the ICI caused by other users' CFO cannot be eliminated. This implies that the ICI in an OFDMA uplink has two components, one is from the subcarriers used by user him/herself and the other is from other users. The former is generally termed as self ICI, while the latter is termed as cross ICI, or Multiple Access Interference (MAI). It is the MAI that makes ICI suppression a challenging issue in an OFDMA uplink.

To deal with the issue, considerable efforts have been made recently. Notable studies in this field are reviewed in next section.

2.2 A Review on Current ICI Suppression Approaches

2.2.1 Conventional Detector

As was mentioned in Chapter 1, the earliest and simplest suppression scheme is to employ a conventional detector, which deploys multiple single-user OFDM detection branches at the OFDMA BS receiver. The block diagram of such a detector is shown in

Fig.2.1(a). Two concerns are generally shown for this detector: First, it is clear that the use of multiple FFT demodulation modules leads to relatively large complexity. Second, as discussed in Section 2.1, CFO compensation is unable to remove MAI from the mixed signal and therefore residual ICI still exists after detection. To solve the first problem, a variant of the conventional detector has been proposed in [25]. CFO compensation is performed after FFT demodulation by using circular convolution and only one FFT demodulation module is needed. The block diagram of this variant is shown in Fig.2-1(b).

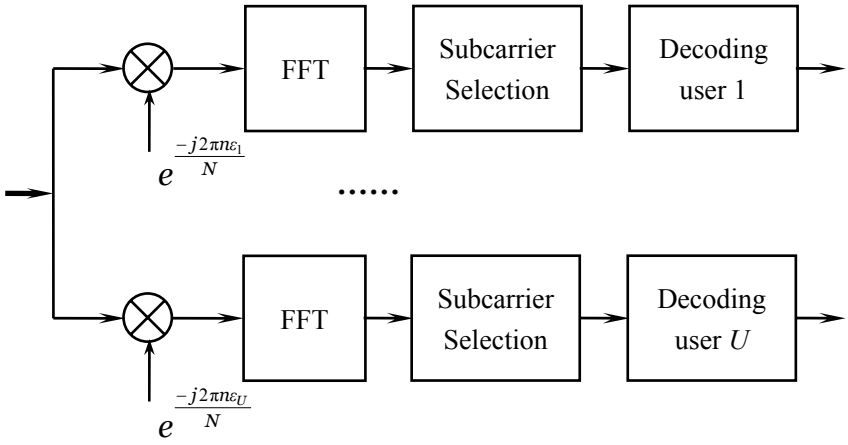

(a)

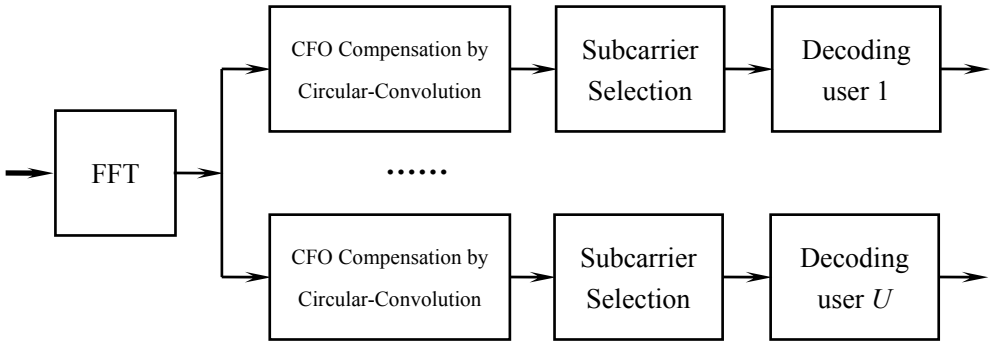

(b)

Fig.2.1: (a) Conventional OFDMA detector (b) Low-complexity variant based on post-FFT circular convolution.

Although complexity can be reduced, the performance of MAI suppression is still to be improved. For this reason, a number of studies have made attempts on the use of various interference cancellation algorithms to further improve performance of this detection scheme.

2.2.2 Supplementary Schemes based on Conventional Detection

In [26], Edge Sidelobe Suppression (ESS) has been developed to remove the MAI in a block OFDMA system. As shown by the authors, ESS is able to reduce the error floor in BER performance and can be realized by using lookup tables. However, ESS may not be suitable for other OFDMA systems than block OFDMA. In [27], Parallel Interference Cancellation (PIC) has been used to mitigate MAI after conventional detection. Specifically, interference signals are reconstructed via circular convolution and cancelled iteratively. Although it employs the low-complexity variant of the conventional detector, the use of circular convolution, signal reconstruction and iterative cancellation increases overall complexity. Moreover, in terms of BER performance, PIC scheme is capable of reducing error floor, but not eliminating the error floor. In [30], Selective Parallel Interference Cancellation (SPIC) and Successive Interference Cancellation (SIC) schemes were investigated and compared with the PIC scheme. It is shown that the SIC scheme gives slightly better performance than PIC and SPIC schemes, and the latter two schemes generate close performance.

2.2.3 Non Conventional Detector-based Schemes

In addition to the aforementioned schemes, several novel detection structures have

also been proposed. In [28], the author proposed an MMSE detection for the interleaved OFDMA uplink by exploring the periodicity embedded in an interleaved OFDMA block. According to the results presented in [29], an important advantage of the scheme is its low complexity. However, this scheme is only suitable for the use in an interleaved OFDMA system, since the periodicity is inapplicable in other OFDMA systems. In [31], the author developed another MMSE detection structure, which can be used in all types of OFDMA systems. It has been shown by the author that the PIC scheme proposed in [27] is a special case of the adaptive realization of this MMSE scheme. The author of [31] also developed a multistage linear parallel interference cancellation in [32]. In [33], the author investigated optimal demodulation of multicarrier multiuser signals on the basis of Maximum A-Posterior (MAP) rule. In addition, iterative detection has also been developed for the MAP detection to reduce the complexity. The study in [33] gives a theoretical framework of the ICI suppression in multicarrier systems. However, the complexity is still a concern in practical applications.

2.3 Problem Definition

Although the previous studies have gained considerable improvement on the performance of ICI suppression in OFDMA uplink, two important issues have not been clearly identified due to some common assumptions used in these studies: First, the impact of near-far problem has not been taken into account in all the performance assessment that have been done so far. Second, ICI suppression in time-varying

multipath channels is yet to be considered as most of the studies made a common assumption that the channel is either static or semi-static.

2.3.1 Near-far Problem in OFDMA Uplink

In most of the previous studies on ICI suppression, large-scale fading has not been considered. A common assumption is that the signals from all the users have the same power at the BS receiver. While this assumption may simplify the theoretical analysis, it is not a practical assumption because signals from different users usually go through different propagation loss and have different power at the BS. More importantly, the power difference, which is known as near-far problem in CDMA systems [34]-[38], affects performance of ICI suppression. A notable example is a simulation result presented in [27]. Specifically, the PIC scheme was simulated under the scenario that users have different powers at the BS and the result shows that performance degradation becomes unacceptable when the Signal-to-Interference power Ratio (SIR) is lower than -10dB. The authors suggested using power control to prevent severe performance degradation in the event of near-far problem. Although power control is an option to cope with the near-far problem, its additional processing delay and complexity may not be suitable for some delay-sensitive communications, such as multimedia and mobile communications. Therefore, having resistance to near-far problem in ICI suppression is important for some OFDMA applications.

2.3.2 ICI Suppression in Time-selective Fading Channels

In the latest IEEE802.16e standard (also known as mobile WiMAX), OFDMA has

been appointed to support mobile broadband access [39][40]. According to the physical layer specification, the maximum allowable velocity of MS is 120km/s. A simple calculation shows that the maximal normalized Doppler offset f_dT corresponding to this velocity may reach 5% or even higher. In such a scenario, channel variation within each OFDMA block is obvious and cannot be neglected [41]. In current studies, however, it is commonly assumed that wireless channel does not change within each OFDMA block. Therefore, extending the research into doubly selective channel is of remarkable significance to practical use.

In the remainder of this dissertation, investigation will be aimed at developing near-far resistant ICI suppression techniques under time and frequency selective fading channels.

Chapter 3

ICI Suppression in Doubly Selective Fading Channels

For OFDM transmission in time and frequency selective channels, in addition to CFO, channel variation also causes frequency asynchronism in the signal received at the receiver [42]-[47]. More specifically, channel variation induces spectra dispersion, which appears to be a series of CFO values, which disrupt orthogonality between subcarriers and induce ICI. ICI suppression in time selective channels has been extensively considered for single-user OFDM [48]-[54]. However, a signal model of OFDMA uplink has not been developed in a time selective channel. In this chapter, efforts are made to establish the signal model and develop appropriate ICI suppression schemes for OFDMA uplink in the doubly selective fading channel. At the moment, channel information is provisionally assumed to be perfectly known at the receiver. The issue of channel estimation will be considered in Chapter 4.

Section 3.1 introduces basic concepts relevant to time and frequency selective channels. Section 3.2 develops a signal model under a doubly selective fading channel for OFDMA uplink. Section 3.3 investigates linear and non-linear suppression schemes to clean ICI. Numerical results and discussions are presented in Section 3.4.

3.1 Time and Frequency Selective Fading Channels

In wireless and mobile communications, due to reflection and scattering of the radio wave on obstacles as well as motion of terminals, it is a usual case that Channel

Impulse Response (CIR) is dispersive in both time and frequency domain [55][56]. A general expression of the CIR is given by

$$h(t,\tau) = \sum_{l=0}^{L-1} h_l(t)\,\delta(\tau - \tau_l T_s), \tag{3-1}$$

where T_s is sampling period and LT_s is delay spread. A transmitted signal $s(t)$ is received as given by

$$\begin{aligned} r(t) &= s(t) * h(t,\tau) \\ &= \int_{\tau=-\infty}^{+\infty} s(t-\tau) \sum_{l=0}^{L-1} h_l(t)\,\delta(\tau - \tau_l T_s) d\tau, \\ &= \sum_{l=0}^{L-1} h_l(t)\, s(t - \tau_l T_s) \end{aligned} \tag{3-2}$$

where $*$ is the linear convolution operator.

3.1.1 Multipath Propagation and Frequency Selective Fading

From the Fourier transform of (3-1) over multipath index τ, it is apparent that time dispersion gives rise to fluctuations in frequency domain. More multipaths give rise to larger fluctuations. For this reason, the term 'frequency selective fading' is interchangeably used with 'multipath fading'.

In time domain, the presence of multipath fading causes interference between successive symbols, i.e., Inter-Symbol Interference (ISI). However, if the symbol duration is much longer than the delay spread, the impact of ISI would be insignificant. In OFDM systems, duration of one OFDM symbol is much larger than delay spread due to the use of a Cyclic Prefix. After the CP is discarded at the receiver, ISI is removed, and therefore multipath fading does not lead to a severe problem in an OFDM system.

3.1.2 Time Variation and Time Selective Fading

According to the time-frequency duality, variation or fluctuation in time domain gives rise to dispersion in frequency domain. Degree of the variation depends on the relation between symbol duration T and channel coherent time T_c (the time interval during which channel correlation is higher than some predetermined value, say 0.8). Generally speaking, a channel is regarded as static or quasi-static if $T \le 0.01T_c$ [41]. In an OFDM system, basic unit for transmission is one OFDM block, whose duration can be as long as $0.1T_c$. Therefore, the ICI due to time selectivity is a crucial problem to be solved.

Next section presents a signal model for OFDMA uplink in doubly selective channels.

3.2 OFDMA Signal in Doubly Selective Fading Channels

Consider an OFDMA system with *N* subcarriers and a total of *U* users. All the users communicate with the BS through uncorrelated time and frequency selective fading channels. The diagram of an OFDMA transmitter at user's terminal is shown in Fig.3.1.

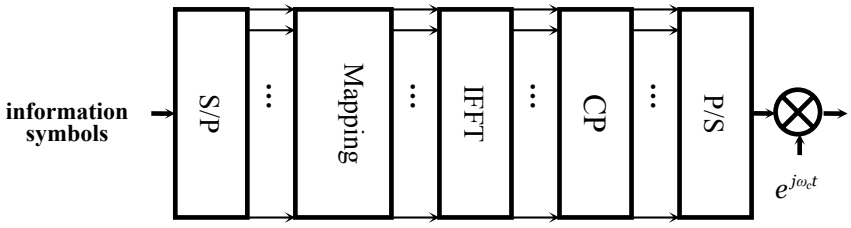

Fig.3.1: Transmitter block diagram for each user in an OFDMA uplink.

As shown in Fig.3.1, at transmitter of an arbitrary user *u*, information symbols are grouped and padded with zero at the mapping module to form a block

$\left[X_u(0), X_u(1)...X_u(N-1)\right]$, and then fed into an IFFT module. In the resulting OFDMA block, information symbols are placed on the subcarriers used by user *u*, while zero elements are put onto the subcarriers occupied by other users. After IFFT modulation, a cyclic prefix is added at the head of each OFDMA block to avoid the distortion due to Inter-Block Interference. After CP is added, the signal can be mathematically expressed as

$$x_u(n) = \frac{1}{\sqrt{N}} \sum_{k=0}^{N-1} X_u(k) \exp\left(j2\pi nk/N\right),$$

$$-N_g \le n \le N-1, \quad \text{(3-3)}$$

where N_g is the length of CP. In an OFDMA system, time-domain dispersion is not only due to multipath propagation, but also delay between users. To this end, the length of cyclic prefix should be larger than the overall delay spread resulting from multipath fading and time asynchronism between users. The signal given by (3-3) is then fed into RF modules where a radio frequency signal is generated and transmitted into wireless channels. The channel model used in this study is Wide-Sense Stationary Uncorrelated Scattering (WSSUS) doubly selective with delay spread *L*. In particular, the channel may vary within the duration of each OFDMA block.

After transmission, the signal received from user *u* is given by

$$\begin{aligned} r_u(n) &= \sum_{l=0}^{L-1} h_u(n,l)\, x_u(n-l) + z(n) \\ &= \frac{1}{\sqrt{N}} \sum_{k=0}^{N-1} X_u(k)\, \bar{H}_u(n,k) \exp\left(j2\pi nk/N\right) + z(n) \end{aligned}, \quad \text{(3-4)}$$

where $h_u(n,l)$ stands for path *l* of the channel associated with user *u* and

$$\bar{H}_u(n,k) = \sum_{l=0}^{L-1} h_u(n,l) \exp\left(-j2\pi lk/N\right) \quad \text{(3-5)}$$

is the frequency domain CIR on subcarrier *k* at time *n*, and $z(n)$ is a complex white noise with variance σ_n^2. After front-end processing, due to time and frequency misalignment between transmitter and BS, time offset and CFO are induced into the baseband signal. After discarding CP, the baseband signal becomes

$$r_u(n) = \frac{1}{\sqrt{N}} \sum_{k=0}^{N-1} X_u(k) \bar{H}_u(n,k) \exp\left[j2\pi (n - n_u)(k + \varepsilon_u)/N \right] + z(n),$$

$$0 \le n \le N-1, \quad (3\text{-}6)$$

where n_u and ε_u are time offset and CFO, normalized with respect to sampling period T_s and subcarrier spacing $1/NT_s$, respectively. In practice, a coarse time and frequency synchronization would have been accomplished before the commencement of data transmission. Therefore, these two offsets n_u and ε_u are their residual values and usually appear as a fractional of the sampling period and subcarrier spacing. As described in [19], the fractional time offset n_u simply introduces a linear phase shift across the subcarriers, and thus it can be combined into the channel frequency response and compensated for in a channel equalizer. Therefore, the baseband signal given by (3-6) can be rewritten into

$$r_u(n) = \frac{1}{\sqrt{N}} \sum_{k=0}^{N-1} X_u(k) H_u(n,k) \exp\left[j2\pi n (k + \varepsilon_u)/N \right] + z(n),$$

$$0 \le n \le N-1, \quad (3\text{-}7)$$

where $H_u(n,k) = \bar{H}_u(n,k) \exp\left[-j2\pi n_u (k + \varepsilon_u)/N \right]$ is the equivalent frequency channel response. From (3-7), the mixed signal due to all the users is given by

$$r(n) = \frac{1}{\sqrt{N}} \sum_{u=1}^{U} \exp\left(\frac{j2\pi n \varepsilon_u}{N} \right) \sum_{k=0}^{N-1} X_u(k) H_u(n,k) \exp\left(\frac{j2\pi nk}{N} \right) + z(n),$$

$$0 \le n \le N-1. \quad (3\text{-}8)$$

In (3-8), since information symbols have been padded with zero, symbol $X_u(k)$ is zero if subcarrier *k* is not used by user *u*. To concisely express an OFDMA block in matrix form, a masking variable $m_u(k)$ is introduced. Specifically,

$$m_u(k) = \begin{cases} 0 & \text{subcarrier } k \text{ is not used by user } u \\ 1 & \text{subcarrier } k \text{ is used by user } u \end{cases}, \text{ for } u=1,\ 2\ldots U. \qquad (3\text{-}9)$$

Following (3-8) and (3-9), an OFDMA block can be expressed in matrix form given by

$$\boldsymbol{r} = \sum_{u=1}^{U} \boldsymbol{D}_u \boldsymbol{H}_u \boldsymbol{M}_u \boldsymbol{X} + \boldsymbol{Z}\,, \qquad (3\text{-}10)$$

where

$$\boldsymbol{D}_u = \mathrm{diag}\left[\exp\left(j2\pi n\varepsilon_u / N\right)\right]_{n=0,1\ldots N-1}, \qquad (3\text{-}11)$$

$$\boldsymbol{H}_u = \frac{1}{\sqrt{N}} \begin{bmatrix} H_u(0,0) & H_u(0,1) & \ldots & H_u(0,N-1) \\ H_u(1,0) & H_u(1,1)e^{\frac{j2\pi}{N}} & \ldots & H_u(1,N-1)e^{\frac{j2\pi(N-1)}{N}} \\ \ldots & \ldots & \ldots & \ldots \\ H_u(N-1,0) & H_u(N-1,1)e^{\frac{j2\pi(N-1)}{N}} & \ldots & H_u(N-1,N-1)e^{\frac{j2\pi(N-1)^2}{N}} \end{bmatrix}, \qquad (3\text{-}12)$$

$$\boldsymbol{M}_u = \mathrm{diag}\left[m_u(k)\right]_{k=0,1\ldots N-1}, \qquad (3\text{-}13)$$

and $\boldsymbol{X} = \left[X(0)\ X(1)\ \ldots\ X(N-1)\right]^T$ contains information symbols on all the subcarriers. Note that the matrix $\boldsymbol{H}_u$ is essentially the Hadamard product† between the channel frequency response matrix

† Hadamard Product: For two matrices of the same dimensions $\boldsymbol{A}$ and $\boldsymbol{B}$, the Hadamard product or entry-wise product is defined by $[\boldsymbol{A} \bullet \boldsymbol{B}]_{ij} = [\boldsymbol{A}]_{ij}[\boldsymbol{B}]_{ij}$.

$$\begin{bmatrix} H_u(0,0) & H_u(0,1) & \dots & H_u(0,N-1) \\ H_u(1,0) & H_u(1,1) & \dots & H_u(1,N-1) \\ \dots & \dots & \dots & \dots \\ H_u(N-1,0) & H_u(N-1,1) & \dots & H_u(N-1,N-1) \end{bmatrix}, \tag{3-14}$$

and IFFT matrix:

$$\boldsymbol{F} = \frac{1}{\sqrt{N}} \begin{bmatrix} 1 & 1 & \dots & 1 \\ 1 & e^{\frac{j2\pi}{N}} & \dots & e^{\frac{j2\pi(N-1)}{N}} \\ \dots & \dots & \dots & \dots \\ 1 & e^{\frac{j2\pi(N-1)}{N}} & \dots & e^{\frac{j2\pi(N-1)^2}{N}} \end{bmatrix}. \tag{3-15}$$

Apparently, channel variation disrupts orthogonality between column vectors of the IFFT matrix.

As a special case, if channel is invariant, the Hadamard product will degenerate to

$$\boldsymbol{H}_u = \boldsymbol{F}\boldsymbol{H}_S, \tag{3-16}$$

and the signal model given by (3-10) degenerates to

$$\boldsymbol{r}_{Static} = \left(\sum_{u=1}^{U} \boldsymbol{D}_u \boldsymbol{F} \boldsymbol{M}_u \right) \boldsymbol{H}_S \boldsymbol{X} + \boldsymbol{Z}, \tag{3-17}$$

where

$$\boldsymbol{H}_S = \mathrm{diag}\left[H(0) \quad H(1) \quad \dots \quad H(N-1) \right]. \tag{3-18}$$

In such a scenario, $\boldsymbol{H}_S$ does not affect orthogonality between the subcarriers.

In next section, the issue of ICI suppression is investigated on the basis of (3-10).

3.3 ICI Suppression for OFDMA Uplink

Let $\boldsymbol{A}$ denote $\sum_{u=1}^{U} \boldsymbol{D}_u \boldsymbol{H}_u \boldsymbol{M}_u$, (3-10) can be rewritten as

$$\boldsymbol{r} = \boldsymbol{A}\boldsymbol{X} + \boldsymbol{Z}. \tag{3-19}$$

Based on this signal model, multiuser detection techniques, that have been extensively studied for CDMA systems [35][36][57]-[59], can be developed for possible use in OFDMA systems.

3.3.1 Matched Filtering

Matched Filtering (MF) is the simplest cancellation algorithm that can be used for (3-19). In a MF detector, an OFDMA block is simply filtered by

$$\boldsymbol{W} = \boldsymbol{A}^H. \tag{3-20}$$

This processing essentially includes FFT demodulation, CFO compensation and channel equalization. To see this, when the MF is used in a static channel, from (3-17), $\boldsymbol{W}$ can be rewritten into

$$\boldsymbol{W}_S = \boldsymbol{H}_S^H \left(\sum_{u=1}^{U} \boldsymbol{D}_u \boldsymbol{F} \boldsymbol{M}_u \right)^H. \tag{3-21}$$

It is obvious that (3-21) describes what is done by a conventional OFDMA detector plus channel equalization. From this point of view, MF does nothing but FFT demodulation and CFO compensation. As was discussed in Chapter 2, this type of detection is ineffective and suffers from residual MAI.

More importantly, the existence of residual MAI in the output of matched filtering raise another issue – the near-far problem. Specifically, a user with strong power may

induce serious MAI onto other users, and therefore handicap the detection of a user with weaker power. A simulation is carried out to illustrate the performance in the event of near far problem. In the simulation, a desired user is placed 5m away from the BS, while the other users uniformly distribute within a circle centering at the BS with a 10m diameter. The system setup is shown in Fig.3.2.

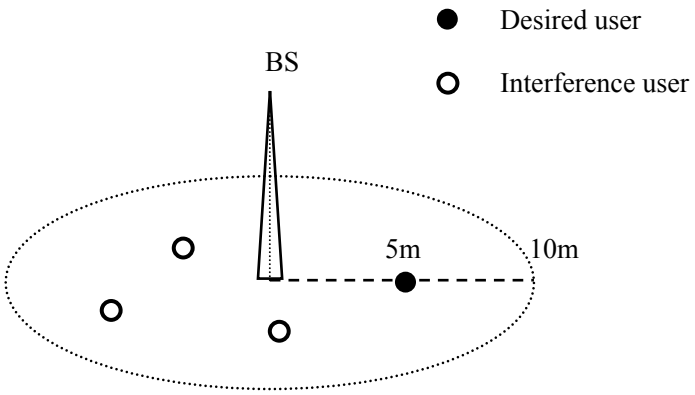

Fig.3.2: Near-far effect simulation system setup. The desired user locates at 5m from the BS, while interference users uniformly distribute in the circle. The desired user has a 30dB SNR at the BS. The large-scale fading is modeled by amplitude attenuation $1/\sqrt{d_u^{\beta}}$, where attenuation index β ranges from 2 to 4. In this example, $\beta = 3$.

The simulation result is shown in Fig.3.3. Obviously, the output SINR of a MF detector can be as low as -30dB due to the near-far problem. Therefore, as in CDMA systems, power control mechanism is stringently required when matched filtering (or the conventional OFDMA detector) is used. As a result, additional complexity becomes new price to pay in system design.

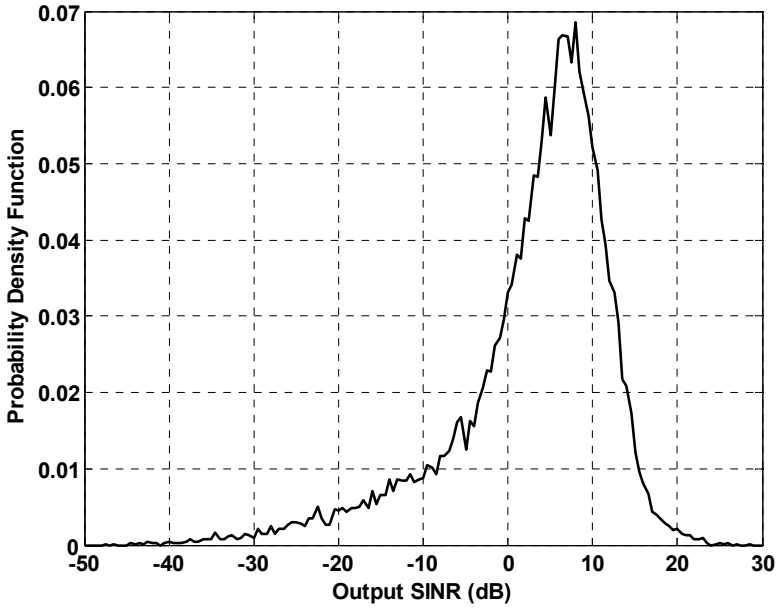

Fig.3.3: Probability density function of post-MF SINR, SNR = 30dB.

Although easy to implement, the MF detection has the following two major weaknesses:

1. sensitive to CFO and channel variations,
2. sensitive to near-far problem.

Finally, it is worthwhile to examine noise power after detection, since linear detection schemes may enhance the noise. As shown in Appendix A, the noise power after matched filtering is given by

$$p_{n,\mathrm{MF}} = \sigma_n^2 \sum_{i=1}^{r} |\lambda_i|^2 , \tag{3-22}$$

where λ_i is the eigenvalue and r is the rank of matrix $\boldsymbol{A}$. Since $\sum_{i=1}^{r} |\lambda_i|^2$ is limited, matched filtering does not suffer from severe noise enhancement problem, and therefore the performance is mainly limited by residual MAI.

3.3.2 Zero Forcing

Zero Forcing (ZF) is well known as decorrelating multiuser detector in CDMA systems [59]. It is a least square technique that attempts to completely remove interference from a mixed signal. Mathematically, ZF-based ICI suppression corresponds to the least square problem given by $\min_{\boldsymbol{W}} \left\| \boldsymbol{W}_{\mathrm{ZF}} \boldsymbol{A}\boldsymbol{X} - \boldsymbol{X} \right\|^2$, solving which yields

$$\boldsymbol{W}_{\mathrm{ZF}} = \left(\boldsymbol{A}^H \boldsymbol{A} \right)^{-1} \boldsymbol{A}^H, \tag{3-23}$$

which is essentially the Moore-Penrose pseudo inverse of matrix $\boldsymbol{A}$.

As shown in Appendix A, noise power in the output of ZF is given by

$$p_{n,\mathrm{ZF}} = \sigma_n^2 \sum_{i=1}^{r} \frac{1}{\left| \lambda_i \right|^2}. \tag{3-24}$$

It is obvious that the magnitude of noise power depends on those small eigenvalues. In practice, CFO and channel variations may lead to relatively high correlation between some columns of matrix $\boldsymbol{A}$, the resulting small eigenvalues give rise to serve enhancement on noise power. This is known as the noise enhancement problem for zero forcing. Noise amplification is plotted against the value of the minimal eigenvalue in Fig 3.4. It is obvious that noise enhancement increases without limit as the minimal eigenvalue decreases.

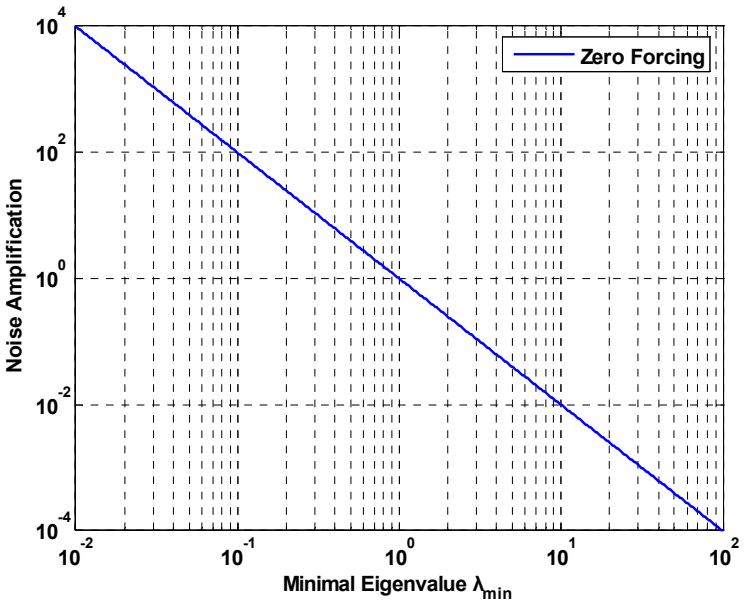

Fig 3.4: Noise enhancement of zero forcing ICI suppression. Whenever the subchannel correlation is high, the minimum eigenvalue approaches zero and noise enhancement increases without limit.

As a result, although ZF detection is capable of completely removing the ICI, the performance improvement gained from ICI cancellation sometimes may be completely cancelled by the enhanced noise power. This will be seen in simulation results in Section 3.4.

3.3.3 MMSE

MMSE technique attempts to suppress both interference and noise, and therefore avoids severe noise enhancement. Mathematically, based on the signal model given by (3-19), the MMSE ICI suppression corresponds to solving optimization problem

$$\min_{\boldsymbol{W}} \mathbb{E}\left\|\boldsymbol{W}_{\text{mmse}}\boldsymbol{r} - \boldsymbol{X}\right\|^2, \tag{3-25}$$

and the weight matrix $\boldsymbol{W}_{\text{mmse}}$ can be easily obtained by using Lagrange multiplier. Nevertheless, this is not the only method leading to the MMSE solution. In this dissertation, an optimal linear ICI suppression scheme that maximizes overall

achievable rate is derived and proven as an equivalent of the MMSE solution.

As described in [44][60], the overall achievable rate can be maximized if the SINR γ_k is maximized for all the subcarriers $k = 0,1...N-1$. After each OFDMA block is filtered by a weight matrix $\boldsymbol{W}$, the SINR on the *m*-th subcarrier (supposing it is used by user *u*) can be derived as follows.

First, signal power on subcarrier *m* is given by

$$\begin{aligned} p_m &= \mathbb{E}\left\{\boldsymbol{w}_m^H \boldsymbol{A}\boldsymbol{e}_m \boldsymbol{e}_m^T \boldsymbol{X}\boldsymbol{X}^H \boldsymbol{e}_m \boldsymbol{e}_m^T \boldsymbol{A}^H \boldsymbol{w}_m\right\} \\ &= \boldsymbol{w}_m^H \boldsymbol{A}\boldsymbol{e}_m \mathbb{E}\left\{\boldsymbol{e}_m^T \boldsymbol{X}\boldsymbol{X}^H \boldsymbol{e}_m\right\} \boldsymbol{e}_m^T \boldsymbol{A}^H \boldsymbol{w}_m \end{aligned}, \tag{3-26}$$

where $\boldsymbol{w}_m$ and $\boldsymbol{e}_m$ are the *m*-th column of weight matrix $\boldsymbol{W}$ and identity matrix $\mathbf{I}_N$.

Second, ICI power on subcarrier *m* is given by

$$\begin{aligned} &J_m \\ &= \mathbb{E}\left\{\sum_{q\neq m, q\in S_u} \boldsymbol{w}_m^H \boldsymbol{A}\boldsymbol{e}_q \boldsymbol{e}_q^T \boldsymbol{X}\boldsymbol{X}^H \boldsymbol{e}_q \boldsymbol{e}_q^T \boldsymbol{A}^H \boldsymbol{w}_m\right\} + \mathbb{E}\left\{\sum_{v\neq u}\sum_{p\in S_v} \boldsymbol{w}_m^H \boldsymbol{A}\boldsymbol{e}_p \boldsymbol{e}_p^T \boldsymbol{X}\boldsymbol{X}^H \boldsymbol{e}_p \boldsymbol{e}_p^T \boldsymbol{A}^H \boldsymbol{w}_m\right\} \\ &= \boldsymbol{w}_m^H \boldsymbol{A}\left[\sum_{q\neq m, q\in S_u} \boldsymbol{e}_q \mathbb{E}\left\{\boldsymbol{e}_q^T \boldsymbol{X}\boldsymbol{X}^H \boldsymbol{e}_q\right\} \boldsymbol{e}_q^T\right] \boldsymbol{A}^H \boldsymbol{w}_m + \boldsymbol{w}_m^H \boldsymbol{A}\left[\sum_{v\neq u}\sum_{p\in S_v} \boldsymbol{e}_p \mathbb{E}\left\{\boldsymbol{e}_p^T \boldsymbol{X}\boldsymbol{X}^H \boldsymbol{e}_p\right\} \boldsymbol{e}_p^T\right] \boldsymbol{A}^H \boldsymbol{w}_m \end{aligned}, \tag{3-27}$$

where S_u stands for the set of subcarriers occupied by user *u*. Without loss of generality, assuming that powers are uniformly allocated over all the subcarriers, the signal and ICI powers given by (3-26) and (3-27) become

$$p_m = \sigma_s^2 \boldsymbol{w}_m^H \boldsymbol{A}\boldsymbol{e}_m \boldsymbol{e}_m^T \boldsymbol{A}^H \boldsymbol{w}_m, \tag{3-28}$$

$$J_m = \sigma_s^2 \boldsymbol{w}_m^H \boldsymbol{A}\left(\mathbf{I}_N - \boldsymbol{e}_m \boldsymbol{e}_m^T\right) \boldsymbol{A}^H \boldsymbol{w}_m, \tag{3-29}$$

where σ_s^2 stands for the signal power assigned on each subcarrier.

Finally, noise power on subcarrier *m* is given by

$$\eta_m = \boldsymbol{w}_m^H \mathbb{E}\{\boldsymbol{Z}\boldsymbol{Z}\}\boldsymbol{w}_m = \sigma_n^2 \boldsymbol{w}_m^H \boldsymbol{w}_m . \quad (3\text{-}30)$$

According to (3-28), (3-29) and (3-30), the SINR γ_m is given by

$$\gamma_m = \frac{\boldsymbol{w}_m^H \boldsymbol{A}\boldsymbol{e}_m \boldsymbol{e}_m^T \boldsymbol{A}^H \boldsymbol{w}_m}{\boldsymbol{w}_m^H \left[\frac{\sigma_n^2}{\sigma_s^2}\mathbf{I}_N + \boldsymbol{A}\left(\mathbf{I}_N - \boldsymbol{e}_m \boldsymbol{e}_m^T\right)\boldsymbol{A}^H \right] \boldsymbol{w}_m} . \quad (3\text{-}31)$$

An optimization problem that maximizes γ_m can be expressed as

$$\max_{\boldsymbol{w}_m} \left\{ \boldsymbol{w}_m^H \boldsymbol{A}\boldsymbol{e}_m \boldsymbol{e}_m^T \boldsymbol{A}^H \boldsymbol{w}_m \right\}, \text{ subject to } \boldsymbol{w}_m^H \left[\frac{\sigma_n^2}{\sigma_s^2}\mathbf{I}_N + \boldsymbol{A}\left(\mathbf{I}_N - \boldsymbol{e}_m \boldsymbol{e}_m^T\right)\boldsymbol{A}^H \right] \boldsymbol{w}_m = 1,$$

$$\text{for } m = 0,1,...N-1 . \quad (3\text{-}32)$$

In fact, (3-32) corresponds to a standard generalized eigenvalue problem [61][62], with a solution given by

$$\boldsymbol{w}_m = \left(\frac{\sigma_n^2}{\sigma_s^2}\mathbf{I}_N + \boldsymbol{A}\boldsymbol{A}^H \right)^{-1} \boldsymbol{A}\boldsymbol{e}_m , \qquad m = 0,1...N-1 . \quad (3\text{-}33)$$

And the weight matrix $\boldsymbol{W}$ is expressed as

$$\boldsymbol{W} = \boldsymbol{A}^H \left(\frac{\sigma_n^2}{\sigma_s^2}\mathbf{I}_N + \boldsymbol{A}\boldsymbol{A}^H \right)^{-1} . \quad (3\text{-}34)$$

This is the optimal linear ICI suppression in terms of maximizing overall achievable rate. On the other hand, under the same assumption of uniform power allocation, the MMSE solution solved from (3-25) is given by

$$\boldsymbol{W}_{\text{mmse}} = \left(\frac{\sigma_n^2}{\sigma_s^2}\mathbf{I}_N + \boldsymbol{A}^H \boldsymbol{A} \right)^{-1} \boldsymbol{A}^H . \quad (3\text{-}35)$$

According to the following lemma, the linear ICI suppression schemes given by (3-34) and (3-35) are the same.

Lemma: If matrix $\boldsymbol{E}$ has full column rank, matrix $\boldsymbol{G}$ is nonsingular, for an arbitrary $\sigma^2 \neq 0$, the following equality is true:

$$\boldsymbol{G}\boldsymbol{E}^H\left(\boldsymbol{E}\boldsymbol{G}\boldsymbol{E}^H+\sigma^2\boldsymbol{I}\right)^{-1}=\left(\boldsymbol{E}^H\boldsymbol{E}+\sigma^2\boldsymbol{G}^{-1}\right)^{-1}\boldsymbol{E}^H$$

Proof: See Appendix B.

Although uniform power allocation is assumed in the above derivation, it is straightforward to extend the result to arbitrary power allocation schemes. In this point of view, MMSE is the optimal linear ICI suppression scheme. Hence, it is expected that the MMSE should be able to produce reasonably good cancellation on both ICI and noise. According to the results given in Appendix A, the noise power after MMSE detection is given by

$$p_{n,\mathrm{MMSE}}=\sigma_n^2\sum_{i=1}^{r}\frac{1}{\left(|\lambda_i|+\dfrac{\sigma_n^2}{|\lambda_i|}\right)^2}, \tag{3-36}$$

In Fig.3.5, noise amplification is plotted against the minimum eigenvalue under unit noise power $\sigma_n^2=1$. Clearly, unlike ZF, MMSE puts a limit on noise amplification.

Finally, it is worthwhile to point out that, if the channel is static, the MMSE scheme developed here degenerates to the MMSE scheme proposed in [31].

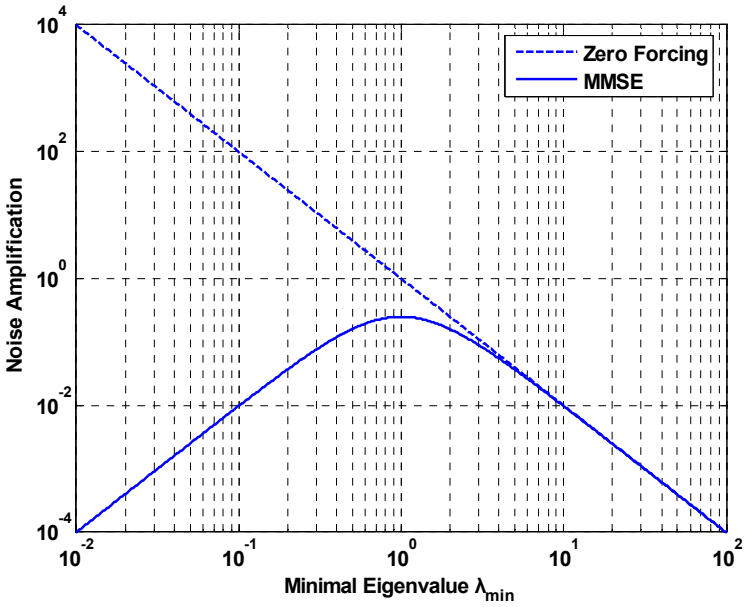

Fig.3.5: Noise enhancement characteristic of MMSE ICI suppression. Unlike zero forcing, MMSE has a limited value on noise enhancement.

3.3.4 MMSE Successive Detection

As discussed in [63], combining Successive Detection (SD) post-decoding with MMSE pre-detection maximizes mutual information and incurs no performance loss compared with complicated joint multiuser decoding, which is devoted to achieve the total channel capacity. With this result, the MMSE-SD scheme can be also used to suppress ICI in OFDMA uplink. Specifically, we propose the use of ordered SD on a per-user basis. The order of detection is determined by comparing post-MMSE SINR of undetected users. The user with the highest post-MMSE SINR will be detected and decoded. The signal of the decoded user is then reconstructed and subtracted from the multiuser signal. The resultant multiuser signal enters a new round of MMSE-SD detection until all the users are detected. We note that a per-subcarrier MMSE-SD has been studied in [64] for a single-user OFDM system and gains significant performance improvement. It can be also used in OFDMA system, but obviously involves much

higher complexity. Hence, the proposed scheme presents a trade-off between performance and complexity. The flowchart and mathematical description of the MMSE-SD algorithm are shown in Fig.3.6 and Table 3-1, respectively.

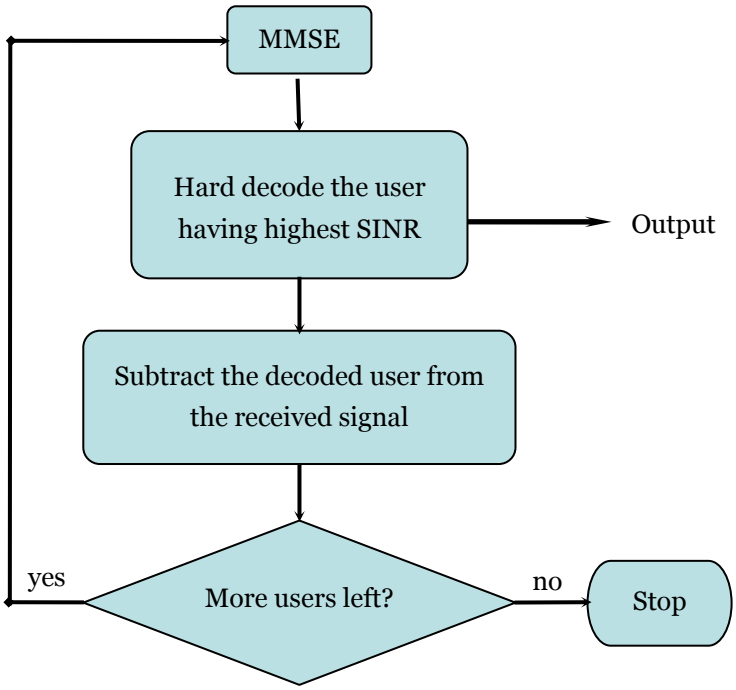

Fig.3.6: Flowchart of MMSE-SD detection

TABLE 3-1. MMSE-SUCCESSIVE DETECTION (MMSE-SD)

Initialization: $j=1$, $\boldsymbol{A}_1=\boldsymbol{A}$, $\boldsymbol{Y}_1=\boldsymbol{Y}$

Step 1: Calculate the MMSE detection output SINR for each user, select the highest one

$$\boldsymbol{W}_j=\left(\frac{\sigma_0^2}{\sigma_s^2}\mathbf{I}_N+\boldsymbol{A}_j^H\boldsymbol{A}_j\right)^{-1}\boldsymbol{A}_j^H,$$

$$u_j=\arg\max_{u\in U}\{\mathrm{SINR}_u\}=\arg\max_{u\in U}\left\{\frac{\mathrm{trace}\left[\left\|\boldsymbol{M}_u\boldsymbol{W}_j\boldsymbol{A}_j\right\|^2\right]}{\mathrm{trace}\left[\left\|\boldsymbol{M}_u\boldsymbol{W}_j\boldsymbol{A}_j\left(\mathbf{I}_N-\boldsymbol{M}_u\right)\right\|^2\right]+\sigma_n^2\mathrm{trace}\left[\left\|\boldsymbol{M}_u\boldsymbol{W}_j\right\|^2\right]}\right\}$$

where U is the set formed by the users to be detected.

Step 2: Decode the selected user, $\hat{\boldsymbol{X}}_{u_j}=\mathrm{sign}\left\{\boldsymbol{M}_{u_j}\boldsymbol{W}_j\boldsymbol{Y}_j\right\}$

Step 3: Subtract the decoded user from the original signal

$\boldsymbol{Y}_{j+1}=\boldsymbol{Y}_j-\boldsymbol{A}_j\boldsymbol{M}_{u_j}\hat{\boldsymbol{X}}_{u_j}$, $\boldsymbol{A}_{j+1}=\boldsymbol{A}_j\left(\mathbf{I}_N-\boldsymbol{M}_{u_j}\right)$, $U=U-u_j$

$j=j+1$, go back to Step 1. Stop when all users are decoded.

3.4 Performance Analysis

3.4.1 Post-detection SINR

As will be used soon, SINR after ZF and MMSE detection is listed here. From the detection weight matrix of ZF (3-23) and MMSE (3-35), it is not difficult to derive their post-detection SINR as shown in Table 3-2.

TABLE 3-2: POST-DETECTION SINR FOR ZF AND MMSE

	Post-detection SINR for subcarrier m, m=0, 1… N-1.
ZF	$\gamma_m=\dfrac{\sigma_s^2}{\sigma_n^2\boldsymbol{e}_m^H\left(\boldsymbol{A}^H\boldsymbol{A}\right)^{-1}\boldsymbol{e}_m}$
MMSE	$\gamma_m=\dfrac{\boldsymbol{e}_m^H\boldsymbol{A}^H\boldsymbol{R}_{yy}^{-1}\boldsymbol{A}\boldsymbol{e}_m}{1-\boldsymbol{e}_m^H\boldsymbol{A}^H\boldsymbol{R}_{yy}^{-1}\boldsymbol{A}\boldsymbol{e}_m}$, $\boldsymbol{R}_{yy}=\boldsymbol{A}\boldsymbol{A}^H+\dfrac{\sigma_n^2}{\sigma_s^2}\boldsymbol{I}$

In Section 3.5, these results will be used to calculate theoretical symbol error rate.

3.4.2 Sensitivity to Channel Estimation Error

When the proposed MMSE and MMSE-SD detection schemes are practically implemented, the matrix $\boldsymbol{A}$ is unknown to the receiver and should be estimated before detection. Specifically, CFO and CIR have to be estimated by estimators and used to calculate $\boldsymbol{A}$. Estimation error is unavoidable and thus it is worthwhile to study robustness of the proposed detectors against these errors. Analysis in this section focuses on studying the impact of CIR estimation error. Similar analysis on the impact of CFO estimation error is given in Chapter 5.

Let $\hat{\boldsymbol{A}} = \left[\hat{\boldsymbol{\theta}}_1 \;\; \hat{\boldsymbol{\theta}}_2 \;\; ... \;\; \hat{\boldsymbol{\theta}}_N \right]$ denote the estimate of $\boldsymbol{A}$. First, it is easy to show that the SINR after linear detection is given by

$$\gamma_m = \frac{\left|\alpha_m\right|^2 \sigma_m^2}{\sum_{l \neq m} \left|\alpha_l\right|^2 \sigma_l^2 + \left\|\boldsymbol{w}_m\right\|^2 \sigma_n^2}, \qquad \text{for } m = 1,2...N, \quad (3\text{-}37)$$

where $\alpha_m = \boldsymbol{w}_m^H \boldsymbol{\theta}_m$ and σ_m^2 is the signal power carried by subcarrier *m*. In [36], γ_m has been derived for zero forcing detectors and the result can be also used for MMSE detectors in high SNR region. Mathematically, the post-ZF detection SINR is given by

$$\gamma_m = \frac{\sigma_m^{-2} \left|c_m^*\right|^2}{\sum_{l \neq m} \sigma_l^{-2} \left|c_l^*\right|^2 + \sigma_n^2 \mathbf{c}^H \boldsymbol{P}^{-1} \left(\boldsymbol{A}^H \boldsymbol{A}\right)^{-1} \boldsymbol{P}^{-1} \mathbf{c}}, \qquad \text{for } m = 1,2...N, \quad (3\text{-}38)$$

where

$$\boldsymbol{P} = \mathrm{diag}\left[\sigma_1^2 \;\; \sigma_2^2 \;\; ... \;\; \sigma_N^2 \right], \quad (3\text{-}39)$$

and c_m is the *m*-th entry of column vector $\boldsymbol{c}$, which is defined and derived in next paragraph.

From a subspace point of view, a mismatched vector $\hat{\boldsymbol{\theta}}_m$ has two components: one in signal subspace and the other one in noise subspace [36]. Mathematically,

$$\hat{\boldsymbol{\theta}}_m = \boldsymbol{\theta}_m^s + \boldsymbol{\theta}_m^n = \boldsymbol{A}\boldsymbol{c} + \boldsymbol{\theta}_m^n . \tag{3-40}$$

where $\boldsymbol{\theta}_m^s$ and $\boldsymbol{\theta}_m^n$ stand for the signal-subspace and noise-subspace components, respectively; and vector $\boldsymbol{c}$ is the coordinate vector of $\boldsymbol{\theta}_m^s$ when signal subspace is spanned by $\boldsymbol{A}$. Besides, it is easy to see that

$$\hat{\boldsymbol{\theta}}_m = \boldsymbol{\theta}_m + \Delta\boldsymbol{\theta}_m = \boldsymbol{A}\boldsymbol{e}_m + \left(\sum_{u=1}^{U} \boldsymbol{D}_u \Delta\boldsymbol{H}_u \boldsymbol{M}_u \right) \boldsymbol{e}_m , \tag{3-41}$$

where $\Delta\boldsymbol{\theta}_m$ stands for the mismatch between $\hat{\boldsymbol{\theta}}_m$ and $\boldsymbol{\theta}_m$, $\Delta\boldsymbol{H}_u$ is the estimation error on CIR. Combing (3-40) and (3-41), it follows that

$$\boldsymbol{A}\boldsymbol{c} + \boldsymbol{\theta}_m^n = \boldsymbol{A}\boldsymbol{e}_m + \left(\sum_{u=1}^{U} \boldsymbol{D}_u \Delta\boldsymbol{H}_u \boldsymbol{M}_u \right) \boldsymbol{e}_m . \tag{3-42}$$

Premultiplying (3-42) by $\boldsymbol{A}^H$ and solving the resulting equation yields

$$\boldsymbol{c} = \boldsymbol{e}_m + (\boldsymbol{A}^H \boldsymbol{A})^{-1} \boldsymbol{A}^H \left(\sum_{u=1}^{U} \boldsymbol{D}_u \Delta\boldsymbol{H}_u \boldsymbol{M}_u \right) \boldsymbol{e}_m . \tag{3-43}$$

The property that signal subspace is orthogonal to noise subspace, or $\boldsymbol{A}^H \boldsymbol{\theta}_m^n = \boldsymbol{0}$, has been used to obtain (3-43). Substituting (3-43) into (3-38), the post-ZF SINR (or the asymptotic post-MMSE SINR) is obtained as a function of the channel estimation error.

3.5 Numerical Results and Discussions

In this section, numerical results will be given through simulations. System setup and parameters used in the simulations are as below:

1. 64-subcarrier 4-user OFDMA system using interleaved subcarrier allocation.

2. QPSK is used to modulate uncoded information bits.
3. Doubly selective 3-ray Rayleigh fading channel, with a 4.2 μs delay spread.
4. Unless otherwise specified, normalized Doppler spread f_dT is set to be 0.05, where T is the duration of one OFDMA block.
5. Unless otherwise specified, CFO of the four users are 0.15, -0.1, 0.2 and 0.1.
6. CIR is assumed to be perfectly known.

Example 1. Comparison between MF, ZF, MMSE and MMSE-SD

In Fig.3.7, average Symbol Error Rate (SER) is plotted versus SNR for MF, ZF, MMSE and MMSE-SD schemes. As can be seen, MF suffers from ICI and shows a high error floor. ZF performs much better than MF, but worse than MMSE due to noise enhancement. MMSE-SD outperforms MMSE and gives the best performance. The results imply that using MF is not feasible in the scenario being studied, and thus this scheme will not be discussed any further.

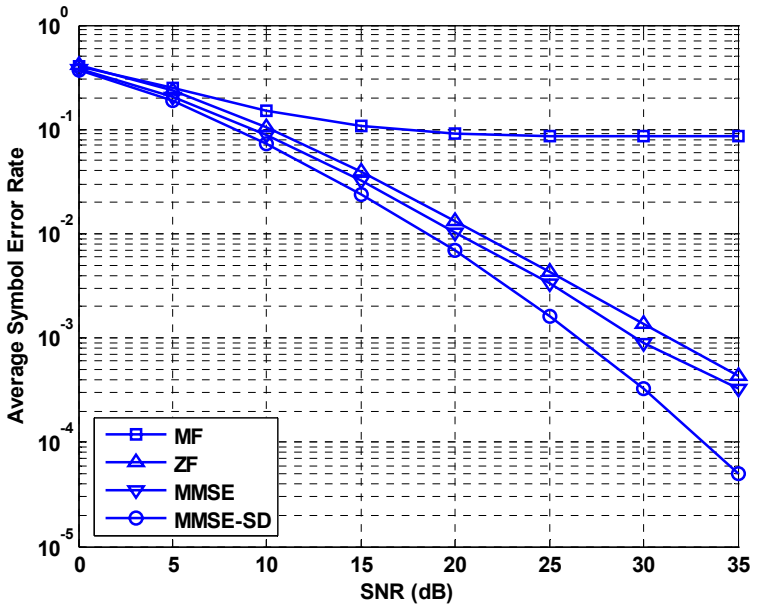

Fig.3.7: Average symbol error rates versus SNR with perfect CIR, normalized Doppler spread $f_dT = 0.05$.

Example 2. SER versus normalized Doppler spread f_dT

In Fig.3.8, average SER is plotted against normalized Doppler spread f_dT for ZF, MMSE and MMSE-SD schemes. As a benchmark, theoretical SER for QPSK modulation is also plotted in the same figure. The theoretical SER is calculated through

$$P_m = 2Q\left(\sqrt{\gamma_m}\right)\left[1-0.5Q\left(\sqrt{\gamma_m}\right)\right], \qquad \text{for } m=1,\ 2\ldots N\text{-}1,$$

on every subcarrier and the theoretical SER is obtained by averaging P_m over all the subcarriers.

As can be seen, ZF has the worst performance due to noise enhancement. MMSE gives much better performance since both ICI and noise are suppressed. As channel changes faster, MMSE is also slightly degraded since residual ICI increases. MMSE-SD produces the best performance. More importantly, by using MMSE-SD, an improvement in performance can be seen as channel changes faster. As will be shown later in Chapter 4, a time-selective channel gives rise to not only ICI, but also a form of time diversity – Doppler diversity. While ICI degrades performance, Doppler diversity improves performance. Provided that ICI can be effectively eliminated, the higher the channel variation is, the larger the Doppler diversity and the better the performance are. The results in Fig.3.8 demonstrate that the MMSE-SD scheme is able to effectively exploit gain from Doppler diversity in OFDMA uplink. With this result, the MMSE and MMSE-SD schemes are proposed for possible use in OFDMA systems uplink as an ICI suppressor.

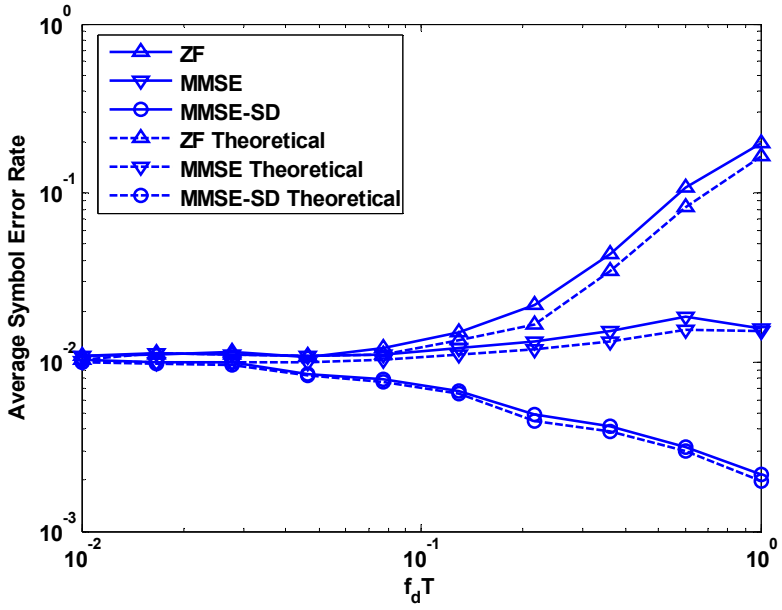

Fig.3.8: Average symbol error rates versus f_dT with perfect CIR, SNR=20dB.

Example 3. Near-far Resistance

To examine immunity of the proposed detection techniques to near–far effects, we fix the power of user 1 at the BS and assume the other three interfering users to have the same Interference Signal power Ratio (ISR) over user 1. The SER of user 1 is then simulated and plotted versus ISR in Fig.3.9. As can be seen, if perfect CIR is available, both MMSE and MMSE-SD are resistant to near-far effects. Particularly, since successive detection scheme detects strong users prior to weak users, weak users will encounter less interference in the MMSE-SD detection. As a result, the MMSE-SD scheme earns more performance gain than the MMSE scheme for weak users.

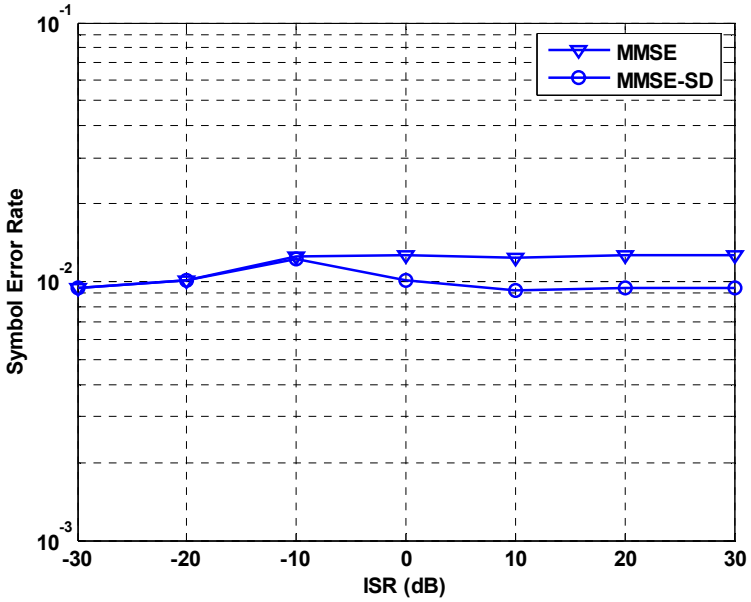

Fig.3.9: Symbol error rate against Interference Signal power Ratio, SNR = 20 dB, $f_d T = 0.05$. Every interfering user induces the same ISR over user 1.

Example 4. Sensitivity to Channel Estimation Error

Using the result obtained in Section 3.4.2, we model channel estimation error as complex white Gaussian noise $\mathcal{CN}\left(0,\sigma_e^2\right)$, with σ_e^2 being the estimation Mean Square Error (MSE). The post-MMSE SINR is plotted versus σ_e^2 in Fig.3.10. Apparently performance degradation is insignificant when $\sigma_e^2 < 0.01$. As will be shown soon, this accuracy can be readily obtained by a properly designed estimator. It is also interesting to note that, the detection performance becomes more sensitive to channel estimation error when SNR increases. This can be explained from (3-38). Specifically, channel estimation error gives rise to extra ICI, and from the denominator of (3-38), the post-MMSE SINR is primarily limited by ICI at high SNR. Therefore, degradation due to channel estimation error is more obvious at high SNR region. On the other hand, if SNR is low, SINR is primarily limited by noise and thus the degradation caused by ICI is relatively small.

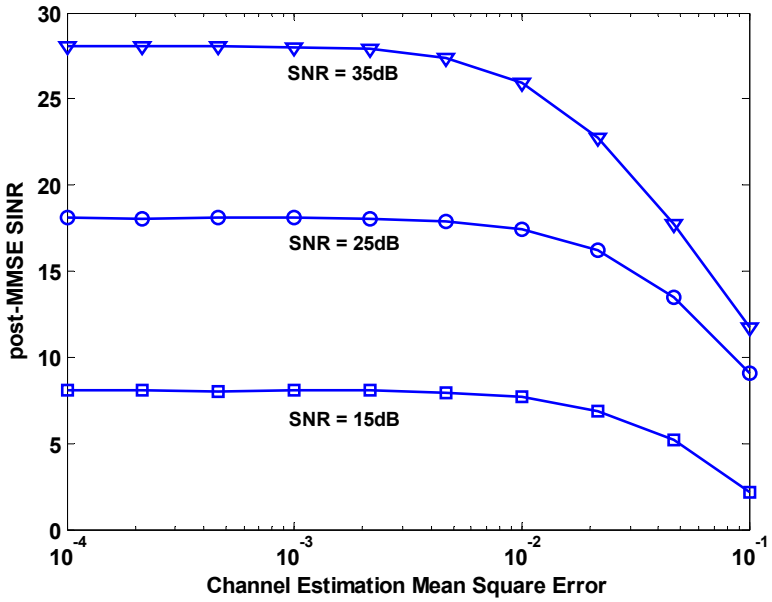

Fig.3.10: Post-MMSE SINR versus channel estimation MSE, $f_d T = 0.05$.

Chapter 4

Basis Expansion Model (BEM) based Channel Estimation for OFDMA Uplink

As can be seen in Chapter 3, channel information is prerequisite to ICI suppression techniques. Therefore, further investigation should be given to the issue of doubly selective channel estimation in OFDMA uplink, which is the subject of this chapter. In this chapter, a Basis Expansion Model (BEM) is chosen to reformulate OFDMA uplink signal, on the basis of which the BEM-based channel estimation techniques are investigated.

Section 4.1 presents a review of previous studies on OFDMA uplink channel estimation. In Section 4.2, existing time-varying channel modeling schemes are reviewed. An oversampled basis expansion model is formulated for OFDMA uplink. In Section 4.3, BEM-based channel estimation algorithms are developed under both time-domain and frequency-domain pilot patterns. Finally in Section 4.4, numerical results and discussions are presented to demonstrate the performance.

4.1 Current OFDMA Uplink Channel Estimation Schemes

OFDMA uplink channel estimation lately received considerable research interest and has been investigated in several studies. In [72], a searching algorithm based on maximum-likelihood has been developed to jointly estimate multiuser CFO and CIR. To reduce the high complexity of searching over multidimensional domain, alternating

projection method was used to search in a series of mono-dimensional searches. In [73], iterative algorithms were developed to accomplish channel and CFO estimation as well as signal detection. In [75], a subspace method was developed to track OFDMA uplink channels. It solves error floor in highly frequency-selective channels. In [76], irregular sampling techniques are developed to estimate OFDMA uplink channels. In [77], the BEM was independently studied for the purpose of OFDMA uplink channel estimation. However, the studies given in [72][73][75]-[77] are all based on the assumption that channel is semi-static. As on of few studies provided for doubly selective channels, [74] investigated the impact of mobility on OFDMA uplink channel estimation. A general doubly selective fading channel was considered and the ICI is considered as a noise component. Linear MMSE and Gauss-Markov techniques were investigated to estimate channel in frequency domain. Obviously, till now most of the studies on OFDMA uplink channel estimation are still in static or semi-static channels. Explicit study on estimation of time-selective channels is called for.

In this chapter, accuracy improvement on channel estimation is obtained from a simple consideration: estimating channel in time domain. As ICI always shows up in frequency domain and degrades estimation accuracy, time domain estimation is able to prevent the degradation and obtain more accurate estimates.

With this in mind, an appropriate signal model and pilot pattern should be formulated to enable channel estimation in time domain.

4.2 Basis Expansion Model for OFDMA Uplink Channels

4.2.1 An Overview on Modeling Doubly Selective Fading Channels

A doubly selective fading channel can be illustrated by a tapped-delay line shown in Fig.4.1.

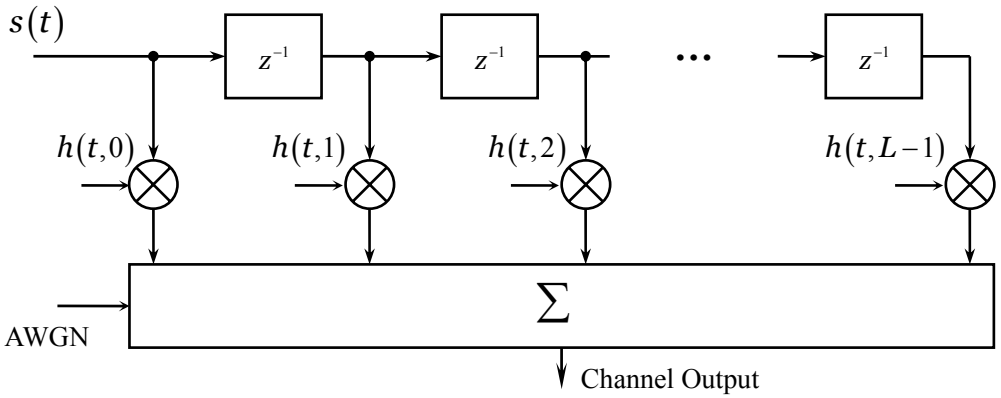

Fig.4.1: Delay-tapped line representation of a doubly selective fading channel. Each delay branch stands for a path.

For a channel whose coherence time is in the order of hundreds of symbol durations, static assumption is reasonable and adaptive algorithms are usually deployed to track the variation. On the other hand, for the channel whose coherence time is only about several symbols, static assumption is invalid. In this scenario, on-line channel estimation and equalization are normally required.

To mathematically describe temporal evolution of path gains, channel modeling methods have been extensively studied. Different modeling schemes may lead to different estimation algorithms. Existing channel modeling schemes can be roughly categorized as Statistical Modeling and Deterministic Modeling. Specifically, in

statistical modeling schemes, uncorrelated stationary random processes are employed to describe time evolution of the channel. The random process is generally assumed to be Gaussian with nonzero mean for Rician fading or zero mean for Rayleigh fading, depending on whether line of sight paths exist or not [79]-[82]. To track a channel under such a modeling method, Kalman filter is used to estimate the taps [83]-[87]. Specifically, if the time-varying taps can be modeled as AR or ARMA processes, both the model parameters and the model order can be known, then the channel can be optimally tracked using the Kalman filter. However, these primary parameters may not easy to acquire in practice.

On the other hand, as a deterministic modeling scheme, Basis Expansion Modeling (BEM) has recently received considerable interest in cellular radio applications [65]-[71]. BEM assigns time evolution of a channel to a series of bases and the resultant basis coefficients can be considered as invariant in a prolonged period of time. In other words, BEM transforms a fast fading channel path gain into a series of slow fading bases coefficients. So far, both exponential bases [65][68][69] and polynomial bases [88][89] have been studied for such a purpose. Deterministic modeling and associated channel estimation schemes release the requirements in statistical modeling that training sequence should be white or random. Moreover, unlike the statistical approach, reliable channel identification can be obtained with short training sequence as long as SNR is high enough. Motivated by these advantages, it is the objective of this chapter that formulating exponential BEM and developing the corresponding channel estimation for OFDMA system uplink. Henceforth, for the ease

of statement and without any confusion, the term BEM is used to refer the exponential bases expansion model.

4.2.2 Basis Expansion Model

The BEM is essentially a Fourier bases approximation of channel variation. Specifically, Fourier transform of a CIR over time (also known as *Spread Function*) completely characterizes the nature of its variation, and moreover, the spread function is bandlimited within $[-f_d \quad f_d]$, with

$$f_d = \frac{\upsilon f_c}{c}, \tag{4-1}$$

where υ is velocity of the mobile station, f_c is central carrier frequency of the band and c stands for the speed of light. Therefore, Fourier bases sampled in the Doppler frequency domain admit an enough accurate approximation of CIR [79][90]. A path $h(t,\tau)$ can be approximated by a linear superposition of finite Fourier bases over a time period $[0 \quad T]$, as given by

$$\begin{aligned} h(t,\tau) &= \delta(t-\tau)\sum_{q=-\infty}^{+\infty} a_q \exp\left(j2\pi t f_q\right) \\ &\simeq \delta(t-\tau)\sum_{q=-Q}^{Q} a_q \exp\left(j2\pi t f_q\right) \end{aligned}, \quad 0 \le t \le T, \tag{4-2}$$

where f_q is the sampled Doppler frequency and a_q is the associated basis coefficient. Principle of BEM is illustrated in Fig.4.2.

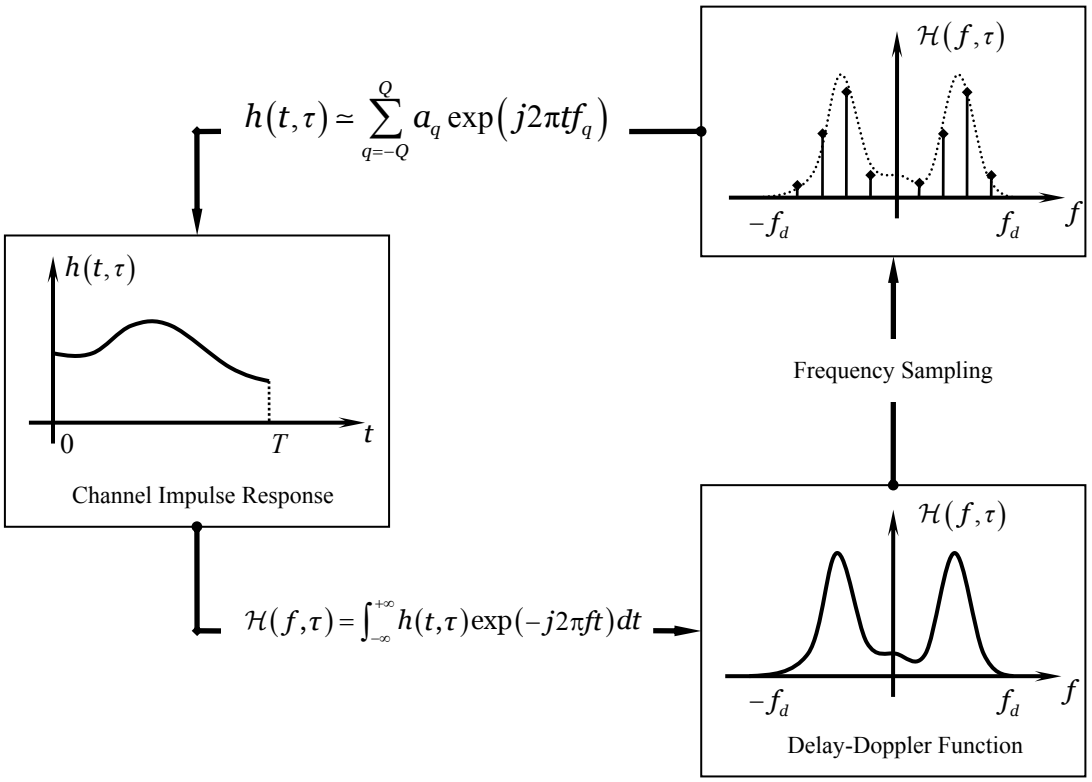

Fig.4.2: Sampling in Doppler frequency domain and BEM representation of time-varying channel.

With sampling in time domain, the discrete-time version of (4-2) is given by

$$\begin{aligned} h(n,l) &= h\left(t = nT_S,\ \tau = lT_S\right) \\ &= \delta(n-l)\sum_{q=-Q}^{Q} a_q \exp\left(j2\pi n T_S f_q\right), \end{aligned}$$

$$0 \le n \le N-1 = \lfloor T/T_S \rfloor,\ \ 0 \le l \le L-1 = \lfloor \tau_{\max}/T_S \rfloor \quad (4\text{-}3)$$

where T_S stands for time-domain sampling period, $\tau_{\max}$ stands for delay spread and Q is the highest Fourier basis order. If the BEM bases are selected as to be

$$f_q = \frac{q}{gT}, \qquad -\lceil gf_{\max}T \rceil \le q \le \lceil gf_{\max}T \rceil, \quad (4\text{-}4)$$

(4-3) can be written as

$$h(n,l)=\delta(n-l)\sum_{q=-Q}^{Q}a_q\exp\left(\frac{j2\pi nq}{gN}\right), \tag{4-5}$$

where g is a positive integer defining the sampling resolution in Doppler domain. If $g=1$, (4-5) is termed as conventional BEM. If $g>1$, (4-5) is termed oversampled BEM. For the convenience of statement, g is referred to as oversampling index in the following discussions. Intuitively, larger oversampling index leads to higher frequency domain resolution, and thus higher modeling accuracy. This is demonstrated by simulation results shown in Fig.4.3.

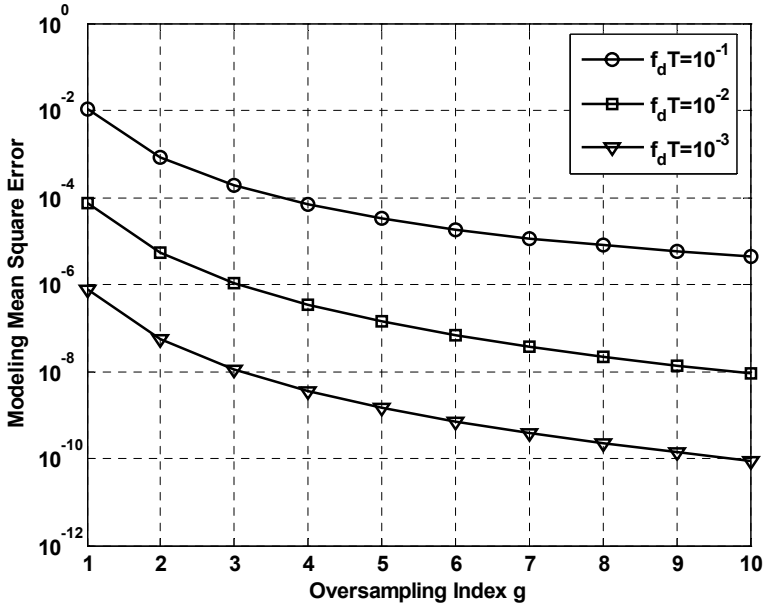

Fig.4.3: Mean Square Error (MSE) of BEM modeling versus oversampling index.

From (4-5), for a signal $s(n)$, it is easy to see that after transmission the received signal can be expressed as

$$\begin{aligned} r(n) &= h(n,l)*s(n)+z(n) \\ &= \sum_{q=-Q}^{Q}a_q\exp\left(\frac{j2\pi nq}{gN}\right)s(n-l)+z(n)\end{aligned}, \tag{4-6}$$

where the operator $*$ stands for linear convolution.

4.2.3 BEM-based Signal Model for OFDMA Uplink

Following (4-6), each OFDMA block received from user *u* can be written as

$$\begin{aligned} r_u(n) &= \exp\left(\frac{j2\pi n\varepsilon_u}{N}\right)\sum_{l=0}^{L-1} h_u(n,l)\,x_u(n-l)+z(n) \\ &= \sum_{q=-Q}^{Q} d_{u,q}(n)\sum_{l=0}^{L-1} a_u(q,l)\,x_u(n-l)+z(n) \end{aligned}, \qquad 0\le n\le N-1, \quad (4\text{-}7)$$

where

$$d_{u,q}(n)=\exp\left[\frac{j2\pi\left(\varepsilon_u+\frac{q}{g}\right)n}{N}\right]$$

is the phase offset induced by both CFO ε_u and channel variations. As can be seen, one time-selective path introduces $2Q+1$ replicas of the original signal $x_u(n)$. This is identified as a sort of diversity - Doppler diversity [90]-[94]. On the other hand, time selectivity also gives rise to more CFOs q/g. Although the Doppler diversity brings diversity gain to improve system performance, CFO induces ICI and cancels the gain. Therefore, the diversity gain can be exploited to improve system performance provided that ICI can be effectively suppressed. This is in line with and supports the findings presented in Chapter 3.

(4-7) can be re-written in matrix form as given by

$$\boldsymbol{r}_u=\sum_{q=-Q}^{Q}\boldsymbol{D}_u(q)\boldsymbol{C}(\boldsymbol{x}_u)\boldsymbol{a}_u(q)+\boldsymbol{z}, \qquad (4\text{-}8)$$

where

$$\boldsymbol{D}_u(q)=\mathrm{diag}\left[d_{u,q}(0)\ \ d_{u,q}(1)\ \ \ldots\ \ d_{u,q}(N-1)\right], \qquad (4\text{-}9)$$

$$\boldsymbol{C}(\boldsymbol{x}_u)=\begin{bmatrix} x_u(0) & x_u(N-1) & \ldots & x_u(N-L+1) \\ x_u(1) & x_u(0) & \ldots & x_u(N-L+2) \\ \ldots & \ldots & \ldots & \ldots \\ x_u(N-1) & x_u(N-2) & \ldots & x_u(N-L) \end{bmatrix}, \tag{4-10}$$

$$\boldsymbol{a}_u(q)=\left[a_u(q,0)\ \ a_u(q,1)\ \ \ldots\ \ a_u(q,L-1)\right]^T. \tag{4-11}$$

By forming augmented matrices

$$\boldsymbol{D}_u=\left[\boldsymbol{D}_u(-Q)\boldsymbol{C}(\boldsymbol{x}_u)\ \ \ldots\ \ \boldsymbol{D}_u(0)\boldsymbol{C}(\boldsymbol{x}_u)\ \ \ldots\ \ \boldsymbol{D}_u(Q)\boldsymbol{C}(\boldsymbol{x}_u)\right], \tag{4-12}$$

$$\boldsymbol{a}_u=\left[\boldsymbol{a}_u(-Q)^T,\ \ldots\ \boldsymbol{a}_u(0)^T,\ \ldots\ \boldsymbol{a}_u(Q)^T\right]^T, \tag{4-13}$$

(4-8) can be rewritten as

$$\boldsymbol{r}_u=\boldsymbol{D}_u\boldsymbol{a}_u+\boldsymbol{z}. \tag{4-14}$$

Similarly, by forming augmented matrices

$$\boldsymbol{D}=\left[\boldsymbol{D}_1\mid\ \boldsymbol{D}_2\mid\ \ldots\ \ \boldsymbol{D}_U\right], \tag{4-15}$$

$$\boldsymbol{\mathcal{A}}=\left[\boldsymbol{a}_1^T\ \ \boldsymbol{a}_2^T\ \ \ldots\ \ \boldsymbol{a}_U^T\right]^T, \tag{4-16}$$

Finally, each OFDMA block due to all the users is given by

$$\boldsymbol{r}=\sum_{u=1}^{U}\boldsymbol{r}_u=\boldsymbol{D}\boldsymbol{\mathcal{A}}+\boldsymbol{z}. \tag{4-17}$$

Note that column vector $\boldsymbol{\mathcal{A}}$ contains all the BEM coefficients instead of channel responses. Under the above framework, BEM coefficients vector $\boldsymbol{\mathcal{A}}$ will be estimated first and then used to calculate users' CIR as given by (4-5).

4.3 BEM-based Channel Estimation for OFDMA Uplink

To track time selective channels, pilots or preamble symbols are usually needed. Pilots can be placed on time grid or frequency grid or both. In this dissertation, based on the consideration mentioned at the end of Section 4.1, a time domain pilot pattern used in [95]-[97] is adopted for OFDMA system uplink. The pilot pattern is shown in Fig.4.4 as below.

Fig.4.4: Pilot pattern for time-domain estimation, 'P' stands for pilot blocks, an data block corresponds to an OFDMA block.

Using this pilot pattern, multiuser CIR is first estimated from pilot blocks. The estimate is then used to reconstruct CIR in data blocks via an interpolation algorithm.

It is also noted that a time-frequency pilot pattern is adopted in IEEE802.16e standard [39] for WiMAX systems. The use of BEM under such a pilot pattern will also be considered in this section.

4.3.1 Time-domain Estimation

Under the pilot pattern shown in Fig.4.4, the matrix $\boldsymbol{D}$ in (4-17) is a piece of pre-knowledge to the receiver, and thus estimation can be performed before FFT demodulation. Typical estimators that can be used are Least Square (LS), Maximum-Likelihood (ML) and Linear Minimum Mean Square Error (LMMSE).

A. Least Square

The use of Least Square corresponds to solving the problem $\min_{\boldsymbol{G}_{LS}} \left\| \boldsymbol{G}_{LS}\boldsymbol{D}\boldsymbol{\mathcal{A}} - \boldsymbol{\mathcal{A}} \right\|^2$,

and the solution is given by

$$\boldsymbol{G}_{LS} = \left(\boldsymbol{D}^H \boldsymbol{D}\right)^{-1} \boldsymbol{D}^H, \tag{4-18}$$

which is essentially the Moore-Penrose pseudo inverse of $\boldsymbol{D}$. Consequently, the estimated BEM coefficient vector is

$$\hat{\boldsymbol{\mathcal{A}}} = \boldsymbol{G}_{LS}\boldsymbol{r} = \boldsymbol{\mathcal{A}} + \left(\boldsymbol{D}^H \boldsymbol{D}\right)^{-1} \boldsymbol{D}^H \boldsymbol{z}. \tag{4-19}$$

Since mean value of Gaussian noise $\boldsymbol{z}$ is zero and $\left(\boldsymbol{D}^H \boldsymbol{D}\right)^{-1} \boldsymbol{D}^H$ is deterministic, the LS estimator is unbiased. In addition, according to the result in [98], it is easy to see that the LS estimator (4-18) is the Best Linear Unbiased Estimator.

B. Maximum-Likelihood

As the noise is assumed to be Gaussian, the likelihood function associated with (4-17) is given by

$$\ln f\left(\boldsymbol{r} \mid \boldsymbol{\mathcal{A}}\right) = \ln\left[\left(2\pi\sigma_n^2\right)^{-\frac{N}{2}} e^{-\frac{(\boldsymbol{r}-\boldsymbol{D}\boldsymbol{\mathcal{A}})^H(\boldsymbol{r}-\boldsymbol{D}\boldsymbol{\mathcal{A}})}{2\sigma_n^2}}\right]. \tag{4-20}$$

It is then readily to show that the ML estimate solved by maximizing (4-20), or,

$$\frac{\partial \ln f\left(\boldsymbol{r} \mid \boldsymbol{\mathcal{A}}\right)}{\partial \boldsymbol{\mathcal{A}}} = 0, \tag{4-21}$$

is the same as the LS estimate given by (4-19). Therefore, for the time-domain pilot pattern, LS and ML estimators are the same.

C. Linear MMSE

In general, estimation MSE consists of errors due to variance and bias [99][100]. Although LS and ML have zero bias, they cannot guarantee the minimum MSE. A LMMSE estimator attempts to minimize the overall MSE by solving

$\min_{\boldsymbol{G}_M} \mathbb{E}\left\|\boldsymbol{\mathcal{A}} - \boldsymbol{G}_M \boldsymbol{r}\right\|^2$. It is easy to show that the estimator is given by

$$\boldsymbol{G}_M = \boldsymbol{R}\boldsymbol{D}^H \left(\boldsymbol{D}\boldsymbol{R}\boldsymbol{D}^H + \sigma_n^2 \boldsymbol{I}\right)^{-1}, \tag{4-22a}$$

where $\boldsymbol{R} = \mathbb{E}\left\{\boldsymbol{\mathcal{A}}\boldsymbol{\mathcal{A}}^H\right\}$ is the autocorrelation matrix of the BEM coefficients and can be pre-calculated as shown in Appendix C. Note that the matrix $\boldsymbol{D}$ given by (4-15) has dimension $L_P \times (2Q+1)LU$, where L_P is the length of each pilot block and $(2Q+1)LU$ is the number of parameters to be estimated. Correspondingly, a $L_P \times L_P$ matrix inverse is needed in (4-22a). As will be shown later, L_P should be equal to or larger than $(2Q+1)LU$ to guarantee estimation accuracy. By using the lemma given in Chapter 3, an equivalent estimator with lower matrix inversion complexity is given by

$$\boldsymbol{G}_M = \left(\boldsymbol{D}^H \boldsymbol{D} + \sigma_n^2 \boldsymbol{R}^{-1}\right)^{-1} \boldsymbol{D}^H. \tag{4-22b}$$

Clearly, in contrast to unbiased estimators, LMMSE is biased. The overall MSE, however, is minimized. In other words, LMMSE obtains the optimal trade-off between variance and bias.

4.3.2 Interpolation Algorithms

After estimating multiuser CIR through pilot blocks, making use of the correlation in time domain, there are a number of interpolation algorithms can be used to construct multiuser CIR in data blocks. Two typical algorithms: linear interpolation and MMSE interpolation are addressed below.

A. Linear Interpolation

If channel variation is obvious but not severe, it can be regarded as linear. This

applies to mobile communications with low to moderate speed. Mathematically, the CIR of each path in a data block is constructed as

$$h_{u,d}(n,l)$$
$$= h_{u,p}\left(L_P + N_g - 1, l\right) + \frac{h_{u,p+1}(0,l) - h_{u,p}\left(L_P + N_g - 1, l\right)}{M\left(N + N_g\right) + N_g + 1}\left[\left(d-1\right)\left(N + N_g\right) + N_g + 1 + n\right]$$

$$u = 1,2...U\ ,\ \ l = 0,1...L-1\ ,\ \ 1 \le d \le M\ ,\ \ 0 \le n \le N-1\ , \quad (4\text{-}23)$$

where d is the data block index, n is the sample index within each data block, p is the pilot block index and *M* is the number of data blocks between two successive pilot blocks. Linear interpolation scheme is shown as below.

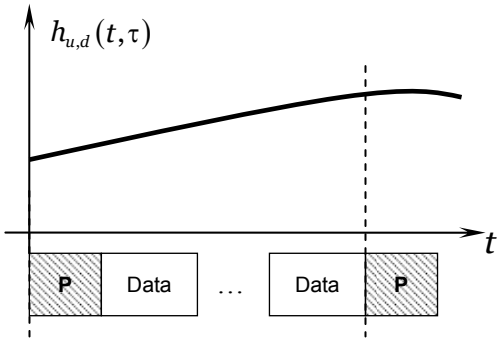

Although it is the simplest method to reconstruct the CIR of data blocks, its performance is guaranteed only if the Doppler effect is not too severe. For the scenario with severe Doppler effect ($f_d T > 0.1$, [96]), more advanced interpolation scheme can be used.

B. MMSE Interpolation

MMSE interpolation makes use of channel statistics to reconstruct CIR for data blocks. In the time-domain pilot pattern shown in Fig.4.4, taking K pilot blocks and

the $(K-1)M$ data blocks located between the pilot blocks, supposing estimation of the l-th path in the p-th pilot blocks is denoted by $\hat{\boldsymbol{h}}_u(p,l)$, $p = j, j+M+1 \ldots j+K(M+1)$, CIR of the l-th path in the d-th data block ($p+1 \le d \le p+M$) can be reconstructed by solving the MMSE problem

$$\min_{\boldsymbol{m}} E\left\|\boldsymbol{h}_u(d,l) - \boldsymbol{m}\hat{\boldsymbol{\mathcal{H}}}\right\|^2, \tag{4-24a}$$

where

$$\hat{\boldsymbol{\mathcal{H}}} = \left[\hat{\boldsymbol{h}}_u(j,l)^T, \hat{\boldsymbol{h}}_u(j+M+1,l)^T \ldots \hat{\boldsymbol{h}}_u(j+KM+K,l)^T\right]^T, \tag{4-24b}$$

is the augmented vector formed by CIR estimate of path l in all the K pilot blocks. The solution of (4-24) is the MMSE interpolation weight vector, as given by

$$\boldsymbol{m} = \boldsymbol{R}_{d\hat{\mathcal{H}}}\boldsymbol{R}_{\hat{\mathcal{H}}\hat{\mathcal{H}}}^{-1}, \tag{4-25}$$

where

$$\boldsymbol{R}_{d\hat{\mathcal{H}}} = \mathbb{E}\left[\boldsymbol{h}_u(d,l)\hat{\boldsymbol{\mathcal{H}}}^H\right], \tag{4-26}$$

$$\boldsymbol{R}_{\hat{\mathcal{H}}\hat{\mathcal{H}}} = \mathbb{E}\left[\hat{\boldsymbol{\mathcal{H}}}\hat{\boldsymbol{\mathcal{H}}}^H\right]. \tag{4-27}$$

Provided that channel statistics are known, (4-26) and (4-27) can be easily determined as shown in Appendix D.

4.3.3 Frequency-domain Estimation

As one of the latest standards using OFDMA, IEEE 802.16e (also known as mobile WiMAX) deploys the uplink channel pilot pattern shown in Fig.4.5(a). The basic unit in this pattern is a tile shown in Fig.4.5(b). In subcarrier allocation, each user is allocated

with 6 tiles.

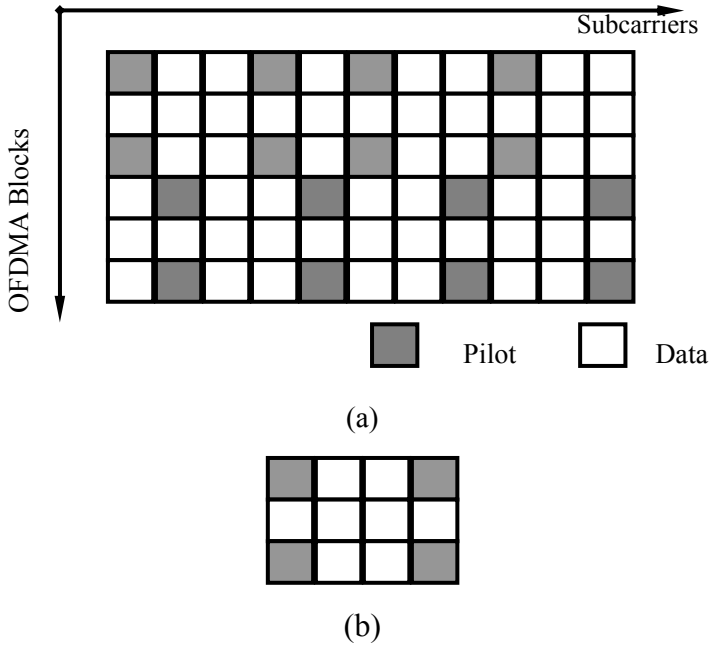

Fig.4.5: (a) Pilot pattern in mobile WiMAX uplink, (b) A tile.

By using this pilot pattern, estimation will be carried out after FFT demodulation. Moreover, the matrix $\boldsymbol{D}$ in (4-17) will be unknown to the receiver. Therefore, the signal model given by (4-17) should be revised. More specifically, ICI will appear after FFT demodulation and the ICI induced by data introduces extra uncertainty in addition to the Gaussian noise, since data are unknown at the stage of channel estimation. For this reason, data should be separated from pilots in the new signal model.

First, it is easy to see that (4-7) can be rewritten into another form in terms of frequency-domain symbols, as given by

$$\begin{aligned} & r_u(n) \\ &= \sum_{q=-Q}^{Q} d_{u,q}(n) \sum_{l=0}^{L-1} a_u(q,l) \frac{1}{\sqrt{N}} \sum_{k=0}^{N-1} X_u(k) e^{\frac{j2\pi(n-l)k}{N}} + z(n) \\ &= \sum_{q=-Q}^{Q} d_{u,q}(n) \left\{ \frac{1}{\sqrt{N}} \sum_{k=0}^{N-1} X_u(k) e^{\frac{j2\pi nk}{N}} \left[\sum_{l=0}^{L-1} a_u(q,l) e^{\frac{-j2\pi lk}{N}} \right] \right\} + z(n) \end{aligned} \quad ,$$

$$0 \le n \le N-1, \quad (4\text{-}28)$$

Following (4-28), an OFDMA block received from user u can be written in matrix form given by

$$\boldsymbol{r}_u = \sum_{q=-Q}^{Q} \boldsymbol{D}_u(q)\boldsymbol{F}\mathrm{diag}[\boldsymbol{X}_u]\sqrt{N}\boldsymbol{F}^H(1:N,1:L)\boldsymbol{a}_u(q) + \boldsymbol{z}, \quad (4\text{-}29)$$

where $\boldsymbol{F}^H(1:N,1:L)$ is the FFT matrix with rows 1 to N and columns 1 to L selected, $\boldsymbol{D}_u(q)$ and $\boldsymbol{a}_u(q)$ have been defined in (4-9) and (4-11). Separating the pilot and data components, (4-29) can be rewritten as

$$\begin{aligned}\boldsymbol{r}_u = &\sum_{q=-Q}^{Q} \boldsymbol{D}_u(q)\boldsymbol{F}\mathrm{diag}[\boldsymbol{\mathcal{P}}_u]\sqrt{N}\boldsymbol{F}^H(1:N,1:L)\boldsymbol{a}_u(q) \\ &+\sum_{q=-Q}^{Q} \boldsymbol{D}_u(q)\boldsymbol{F}\mathrm{diag}[\boldsymbol{\mathcal{D}}_u]\sqrt{N}\boldsymbol{F}^H(1:N,1:L)\boldsymbol{a}_u(q) + \boldsymbol{z}\end{aligned}, \quad (4\text{-}30)$$

where $\boldsymbol{\mathcal{P}}_u$ and $\boldsymbol{\mathcal{D}}_u$ represent the pilot and data vectors associated with user u. Specifically, $\boldsymbol{\mathcal{P}}_u \bigcup \boldsymbol{\mathcal{D}}_u = \boldsymbol{X}_u$ and $\boldsymbol{\mathcal{P}}_u \bigcap \boldsymbol{\mathcal{D}}_u = \varnothing$. Following (4-30), an OFDMA block due to all the users is given by

$$\begin{aligned}\boldsymbol{r} &= \sum_{u=1}^{U} \boldsymbol{r}_u \\ &= \sum_{u=1}^{U}\sum_{q=-Q}^{Q} \boldsymbol{D}_u(q)\boldsymbol{F}\mathrm{diag}[\boldsymbol{\mathcal{P}}_u]\sqrt{N}\boldsymbol{F}^H(1:N,1:L)\boldsymbol{a}_u(q) \\ &+\sum_{u=1}^{U}\sum_{q=-Q}^{Q} \boldsymbol{D}_u(q)\boldsymbol{F}\mathrm{diag}[\boldsymbol{\mathcal{D}}_u]\sqrt{N}\boldsymbol{F}^H(1:N,1:L)\boldsymbol{a}_u(q) + \boldsymbol{z}\end{aligned}. \quad (4\text{-}31)$$

After FFT demodulation, (4-31) becomes

$$
\begin{aligned}
&\boldsymbol{y} \\
&= \boldsymbol{F}^H \boldsymbol{r} \\
&= \sum_{u=1}^{U} \sum_{q=-Q}^{Q} \boldsymbol{F}^H \boldsymbol{D}_u(q) \boldsymbol{F} \mathrm{diag}[\boldsymbol{\mathcal{P}}_u] \sqrt{N} \boldsymbol{F}^H (1:N, 1:L) \boldsymbol{a}_u(q) \\
&\quad + \sum_{u=1}^{U} \sum_{q=-Q}^{Q} \boldsymbol{F}^H \boldsymbol{D}_u(q) \boldsymbol{F} \mathrm{diag}[\boldsymbol{\mathcal{D}}_u] \sqrt{N} \boldsymbol{F}^H (1:N, 1:L) \boldsymbol{a}_u(q) + \boldsymbol{Z} \\
&= \sum_{u=1}^{U} \sum_{q=-Q}^{Q} [\boldsymbol{E}_P]_{u,q} \boldsymbol{a}_u(q) + \sum_{u=1}^{U} \sum_{q=-Q}^{Q} [\boldsymbol{E}_D]_{u,q} \boldsymbol{a}_u(q) + \boldsymbol{Z}
\end{aligned}
\quad , \qquad (4\text{-}32)
$$

where

$$
[\boldsymbol{E}_P]_{u,q} = \boldsymbol{F}^H \boldsymbol{D}_u(q) \boldsymbol{F} \mathrm{diag}[\boldsymbol{\mathcal{P}}_u] \sqrt{N} \boldsymbol{F}^H (1:N, 1:L),
$$

$$
[\boldsymbol{E}_D]_{u,q} = \boldsymbol{F}^H \boldsymbol{D}_u(q) \boldsymbol{F} \mathrm{diag}[\boldsymbol{\mathcal{D}}_u] \sqrt{N} \boldsymbol{F}^H (1:N, 1:L).
$$

By forming an augmented matrix

$$
\boldsymbol{E}_P = \begin{bmatrix} [\boldsymbol{E}_P]_{1,-Q} & \cdots & [\boldsymbol{E}_P]_{1,Q} & \cdots & [\boldsymbol{E}_P]_{U,-Q} & \cdots & [\boldsymbol{E}_P]_{U,Q} \end{bmatrix}
$$

and

$$
\boldsymbol{\mathcal{A}} = \begin{bmatrix} \boldsymbol{a}_1(-Q)^T & \cdots & \boldsymbol{a}_1(Q)^T & \cdots & \boldsymbol{a}_U(-Q)^T & \cdots & \boldsymbol{a}_U(Q)^T \end{bmatrix}^T,
$$

the OFDMA block given by (4-32) can be rewritten as

$$
\boldsymbol{y} = \boldsymbol{E}_P \boldsymbol{\mathcal{A}} + \boldsymbol{E}_D \boldsymbol{\mathcal{A}} + \boldsymbol{Z}. \qquad (4\text{-}33)
$$

In (4-33), it is obvious that the second item, which contains all the data symbols, appears as intractable interference, unless the channel is static or semi-static. Therefore, the estimation accuracy using frequency-domain pilot is generally lower than using time-domain pilot, as will be shown by simulation results.

Similar to the scenario of time-domain pilot, LS, LMMSE techniques can be used to estimate CIR on the basis of (4-33). The feasibility of Maximum-Likelihood

depends on the statistic characteristic of the interference item $\boldsymbol{E}_D\boldsymbol{\mathcal{A}}$.

As an example and to avoid the need of channel statistics, the LS technique is considered. From the signal model given by (4-33), a LS channel estimator is the solution of the least square problem $\min_{\boldsymbol{G}_{LS-F}} \left\| \mathbf{G}_{LS-F}\boldsymbol{E}_P - \boldsymbol{\mathcal{A}} \right\|^2$, and is given by

$$\boldsymbol{G}_{LS-F} = \left(\boldsymbol{E}_P^H \boldsymbol{E}_P \right)^{-1} \boldsymbol{E}_P^H . \tag{4-34}$$

According to the study in [101], to give reasonably good LS estimations in the presence of ICI from data, not all the *N* symbols in $\boldsymbol{y}$ are necessary, since using more symbols also collects more interference power from data. However, it is necessary that all the pilot symbols are collected for channel estimation, since these samples have the largest power from pilot symbols and lack of any of them may result in accuracy degradation. From this point of view, channel estimation can be performed based on $\boldsymbol{y}_c$, which is a portion of one whole OFDMA block $\boldsymbol{y}$, with at least all the pilot positions included. This is shown in Fig.4.6.

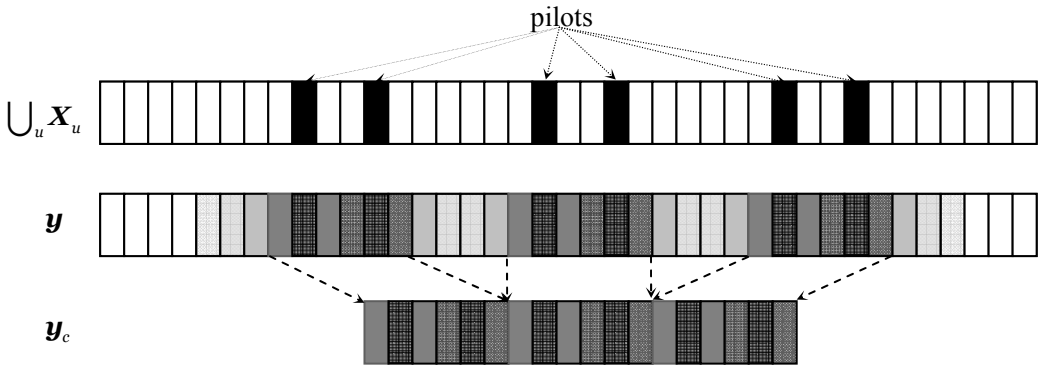

Fig.4.6: Samples selection for channel estimation from the FFT-demodulated OFDMA block

From (4-33), the collected samples $\boldsymbol{y}_c$ is mathematically expressed as

$$\boldsymbol{y}_c = \bar{\boldsymbol{E}}_P\boldsymbol{\mathcal{A}} + \bar{\boldsymbol{E}}_D\boldsymbol{\mathcal{A}} + \bar{\boldsymbol{Z}} , \tag{4-35}$$

where $\bar{\boldsymbol{E}}_P$, $\bar{\boldsymbol{E}}_D$ and $\bar{\boldsymbol{Z}}$ are carved from $\boldsymbol{E}_P$, $\boldsymbol{E}_D$ and $\boldsymbol{Z}$, by selecting the rows leading to the entries in $\boldsymbol{y}_c$. The resultant LS estimation algorithm has the same form as (4-34) except that $\bar{\boldsymbol{E}}_P$ replaces $\boldsymbol{E}_P$.

So far BEM-based channel estimation has been considered for OFDMA Uplink for both time-domain and frequency domain estimation. Before moving on to simulation results, it is worthwhile to analytically study performance of the above estimation algorithms.

4.4 CRLB Analysis for LS Estimators

Cramer-Rao Lower Bound (CRLB) is the lowest MSE that an unbiased estimator can attain. In this section, CRLB will be derived for the LS estimators.

For the convenience of statement, the LS used in time-domain estimation will be referred to as LS-T. Similarly, the LS used in frequency-domain estimation will be mentioned as LS-F. CRLB of BEM coefficients estimation will be first derived, CRLB of CIR estimation can be then calculated as to be shown soon.

Generally for a complex signal

$$\boldsymbol{\alpha} = \boldsymbol{\Phi}\boldsymbol{\lambda} + \boldsymbol{\eta} \tag{4-36}$$

where $\boldsymbol{\Phi}$ is known, white complex noise $\boldsymbol{\eta}$ admits Gaussian distribution $\mathcal{CN}\left(0, \boldsymbol{R}_{\boldsymbol{\eta}}\right)$ and $\boldsymbol{\lambda}$ contains the parameters to be estimated from $\boldsymbol{\alpha}$. The CRLB of unbiased estimation is given by

$$\boldsymbol{C}_{\boldsymbol{\lambda}_e} - \boldsymbol{J}^{-1}\left(\boldsymbol{\lambda}_e\right) \geq \boldsymbol{0}, \tag{4-37}$$

with

$$\boldsymbol{J}(\boldsymbol{\lambda}_e)=2\begin{bmatrix}\mathrm{Re}(\boldsymbol{P}) & -\mathrm{Im}(\boldsymbol{P})\\ \mathrm{Im}(\boldsymbol{P}) & \mathrm{Re}(\boldsymbol{P})\end{bmatrix}+2\begin{bmatrix}\mathrm{Re}(\bar{\boldsymbol{P}}) & -\mathrm{Im}(\bar{\boldsymbol{P}})\\ \mathrm{Im}(\bar{\boldsymbol{P}}) & \mathrm{Re}(\bar{\boldsymbol{P}})\end{bmatrix}, \tag{4-38}$$

where

$$\boldsymbol{\lambda}_e=\left[\mathrm{Re}[\boldsymbol{\lambda}^T] \quad \mathrm{Im}[\boldsymbol{\lambda}^T]\right]^T, \tag{4-39}$$

and matrices $\boldsymbol{P}$ and $\bar{\boldsymbol{P}}$ are given by

$$\boldsymbol{P}(m,n)=\left(\boldsymbol{\Phi}^H\boldsymbol{R}_{\boldsymbol{\eta}}^{-1}\boldsymbol{\Phi}\right)_{m,n}+\mathrm{trace}\left(\boldsymbol{R}_{\boldsymbol{\eta}}^{-1}\left(\frac{\partial\boldsymbol{R}_{\boldsymbol{\eta}}}{\partial\boldsymbol{\lambda}_e^*(m)}\right)\boldsymbol{R}_{\boldsymbol{\eta}}^{-1}\left(\frac{\partial\boldsymbol{R}_{\boldsymbol{\eta}}}{\partial\boldsymbol{\lambda}_e^*(n)}\right)^H\right), \tag{4-40}$$

$$\bar{\boldsymbol{P}}(m,n)=\mathrm{trace}\left(\boldsymbol{R}_{\boldsymbol{\eta}}^{-1}\left(\frac{\partial\boldsymbol{R}_{\boldsymbol{\eta}}}{\partial\boldsymbol{\lambda}_e^*(m)}\right)\boldsymbol{R}_{\boldsymbol{\eta}}^{-1}\left(\frac{\partial\boldsymbol{R}_{\boldsymbol{\eta}}}{\partial\boldsymbol{\lambda}_e^*(n)}\right)^H\right). \tag{4-41}$$

Note that the operator $'\geq'$ stands for positive semi-definite.

A. CRLB for LS-T

In time-domain estimation, the received signal $\boldsymbol{r}\sim\mathcal{CN}\left(\boldsymbol{D}\boldsymbol{\mathcal{A}},\sigma_n^2\boldsymbol{I}\right)$. Correspondingly,

$$\boldsymbol{P}=\sigma_n^{-2}\boldsymbol{D}^H\boldsymbol{D}, \tag{4-42}$$

$$\bar{\boldsymbol{P}}=\boldsymbol{0}. \tag{4-43}$$

The CRLB for LS-T is thus given by

$$\boldsymbol{C}_{\boldsymbol{\mathcal{A}}_e}-\boldsymbol{J}^{-1}\left(\boldsymbol{\mathcal{A}}_e\right)\geq\boldsymbol{0} \tag{4-44}$$

with

$$\boldsymbol{J}_{\mathrm{T}}^{-1}\left(\boldsymbol{\mathcal{A}}_e\right)=\sigma_n^2\left(\boldsymbol{D}^H\boldsymbol{D}\right)^{-1}. \tag{4-45}$$

where

$$\boldsymbol{\mathcal{A}}_e=\left[\mathrm{Re}[\boldsymbol{\mathcal{A}}^T] \quad \mathrm{Im}[\boldsymbol{\mathcal{A}}^T]\right]^T. \tag{4-46}$$

B. CRLB for LS-F

For the frequency-domain estimation, in (4-36), we have

$$\boldsymbol{\Phi\lambda} = \mathcal{P}_F \boldsymbol{\mathcal{A}} , \tag{4-47}$$

$$\boldsymbol{R}_{\boldsymbol{\eta}} = \mathbb{E}\big|_{\boldsymbol{X}} \left(\boldsymbol{\mathcal{D}}_F \boldsymbol{\mathcal{A}} \boldsymbol{\mathcal{A}}^H \boldsymbol{\mathcal{D}}_F^H \right) + \sigma_n^2 \boldsymbol{I} . \tag{4-48}$$

To determine the CRLB, it is necessary to solve $\mathbb{E}\big|_{\boldsymbol{X}} \left(\boldsymbol{\mathcal{D}}_F \boldsymbol{\mathcal{A}} \boldsymbol{\mathcal{A}}^H \boldsymbol{\mathcal{D}}_F^H \right)$ and its partial derivative with respect to $\boldsymbol{\mathcal{A}}^* (i)$ for $i = 1,2...(2Q+1)LU$.

First, starting from (4-28), it is easy to show that $\boldsymbol{\mathcal{D}}_F \boldsymbol{\mathcal{A}}$ can be also expressed as

$$\begin{aligned} \boldsymbol{\mathcal{D}}_F \boldsymbol{\mathcal{A}} &= \sqrt{N} \sum_{u=1}^{U} \sum_{q=-Q}^{Q} \boldsymbol{F}^H \boldsymbol{D}_q \boldsymbol{F} \mathrm{diag}\left[\boldsymbol{F}^H (:,1:L) \boldsymbol{a}_{u,q} \right] \boldsymbol{M}_u^{\mathrm{d}} \boldsymbol{X} \\ &= \boldsymbol{\mathcal{E}} \mathrm{diag}\left[\left(\boldsymbol{I}_{(2Q+1)U} \otimes \boldsymbol{F}^H (:,1:L) \right) \boldsymbol{\mathcal{A}} \right] \boldsymbol{M}_{\mathrm{Aug}}^{\mathrm{d}} \left(\boldsymbol{1}_{(2Q+1)U} \otimes \boldsymbol{X} \right) \end{aligned} , \tag{4-49}$$

where

$$\boldsymbol{\mathcal{E}} = \boldsymbol{1}_U^T \otimes \left(\boldsymbol{F}^H \left[\boldsymbol{D}_{-Q} \boldsymbol{F} ... \boldsymbol{D}_Q \boldsymbol{F} \right] \right) , \tag{4-50}$$

$$\boldsymbol{M}_{\mathrm{Aug}}^{\mathrm{d}} = \begin{bmatrix} \boldsymbol{I}_{(2Q+1)} \otimes \boldsymbol{M}_1^{\mathrm{d}} & & \boldsymbol{O} \\ & \ddots & \\ \boldsymbol{O} & & \boldsymbol{I}_{(2Q+1)} \otimes \boldsymbol{M}_U^{\mathrm{d}} \end{bmatrix} , \tag{4-51}$$

and $\boldsymbol{M}_u^{\mathrm{d}}$ is the masking matrix that identifies data symbols of user *u*. Following this result, the variance matrix is given by

$$\begin{aligned} &\boldsymbol{R}_{\boldsymbol{\eta}} \\ &= \sigma_s^2 \boldsymbol{\mathcal{E}} \mathrm{diag}\left[\left(\boldsymbol{I}_{(2Q+1)U} \otimes \boldsymbol{F}^H (:,1:L) \right) \boldsymbol{\mathcal{A}} \right] \boldsymbol{M}_{\mathrm{Aug}}^{\mathrm{d}} \left(\boldsymbol{1}_{(2Q+1)U} \otimes \boldsymbol{I}_N \right) \boldsymbol{M}_{\mathrm{Aug}}^{\mathrm{d}} \mathrm{diag}\left[\boldsymbol{\mathcal{A}}^H \left(\boldsymbol{I}_{(2Q+1)U} \otimes \boldsymbol{F}^H (:,1:L) \right)^H \right] \boldsymbol{\mathcal{E}}^H \\ &\quad + \sigma_n^2 \boldsymbol{I}_N \end{aligned} \tag{4-52}$$

Following (4-52), the partial derivative $\dfrac{\partial \boldsymbol{R}_{\boldsymbol{\eta}}}{\partial \boldsymbol{\mathcal{A}}^* (i)}$ can be easily shown to be given by

$$\frac{\partial \boldsymbol{R}_{\boldsymbol{\eta}}}{\partial \boldsymbol{\mathcal{A}}^{*}(i)}$$
$$= \sigma_s^2 \boldsymbol{\mathcal{E}} \mathrm{diag}\left[\left(\boldsymbol{I}_{(2Q+1)U} \otimes \boldsymbol{F}^{H}(:,1:L)\right)\boldsymbol{\mathcal{A}}\right] \boldsymbol{M}_{\mathrm{Aug}}^{\mathrm{d}} \left(\boldsymbol{1}_{(2Q+1)U} \otimes \boldsymbol{I}_N\right) \boldsymbol{M}_{\mathrm{Aug}}^{\mathrm{d}} \mathrm{diag}\left[\left(\boldsymbol{I}_{(2Q+1)U} \otimes \boldsymbol{F}^{H}(:,1:L)\right)^{*} \boldsymbol{e}_i\right] \boldsymbol{\mathcal{E}}^{H} \tag{4-53}$$

where $\boldsymbol{e}_i$ is the *i*-th column of an identity matrix $\boldsymbol{I}_{(2Q+1)LU}$. Substituting (4-52) and (4-53) into (4-37) and (4-38), the CRLB for LS-F can be obtained.

After the CRLB of BEM coefficients estimation is obtained as shown above, the CRLB of CIR estimation can be determined. Specifically, the channel responses is calculated from $\boldsymbol{\mathcal{A}}_e$ by

$$\boldsymbol{h} = \left[\boldsymbol{B} \vdots j\boldsymbol{B}\right] \boldsymbol{\mathcal{A}}_e = \bar{\boldsymbol{B}} \boldsymbol{\mathcal{A}}_e , \tag{4-54}$$

where

$$\boldsymbol{B} = \boldsymbol{I}_U \otimes \begin{bmatrix} \boldsymbol{b}_{-Q} & \boldsymbol{0}_{N\times(L-1)} & \boldsymbol{b}_{-Q+1} & \boldsymbol{0}_{N\times(L-1)} & \cdots & \boldsymbol{b}_{Q} & \boldsymbol{0}_{N\times(L-1)} \\ \boldsymbol{0}_{N\times 1} & \boldsymbol{b}_{-Q} & \boldsymbol{0}_{N\times(L-1)} & \boldsymbol{b}_{-Q+1} & \boldsymbol{0}_{N\times(L-1)} & \cdots & \cdots \\ \boldsymbol{0}_{N\times 2} & \boldsymbol{b}_{-Q} & \boldsymbol{0}_{N\times(L-1)} & \boldsymbol{b}_{-Q+1} & \boldsymbol{0}_{N\times(L-1)} & \cdots & \cdots \\ \cdots & & & \cdots & & & \cdots \\ \boldsymbol{0}_{N\times(L-1)} & \boldsymbol{b}_{-Q} & \boldsymbol{0}_{N\times(L-1)} & \boldsymbol{b}_{-Q+1} & \boldsymbol{0}_{N\times(L-1)} & \cdots & \cdots \end{bmatrix}, \tag{4-55}$$

with column vector

$$\boldsymbol{b}_q = \exp\left(\frac{j2\pi qn}{gN}\right)\Bigg|_{n=0}^{N-1} .$$

The matrix $\boldsymbol{B}$ transforms BEM coefficients back to CIR.

With (4-54) and (4-55), the CRLB of CIR estimation is given by [98]:

$$\boldsymbol{C}_{\hat{\boldsymbol{h}}} - \bar{\boldsymbol{B}} \boldsymbol{C}_{\hat{\boldsymbol{\mathcal{A}}}_e} \bar{\boldsymbol{B}}^{T} \geq \boldsymbol{0} . \tag{4-56}$$

4.5 Numerical Results and Discussion

In this section, numerical results will be presented to evaluate and compare the aforementioned channel estimators.

System setup and parameters used in this part of simulation is as below:

1. 64-subcarrier interleaved OFDMA Uplink with 4 users.
2. QPSK modulated random symbols are used as pilots.
3. 3-ray multipath time-selective Rayleigh fading channel.
4. Unless otherwise specified, the normalized Doppler spread $f_dT = 0.05$.
5. Unless otherwise specified, CFO of the four users are 0.15, -0.1, 0.2 and 0.1.

4.5.1 Performance of Estimation

Example 1. Comparison between LS-T and LMMSE-T

In this example, LS-T and LMMSE-T are compared. The oversampling index g is taken to be 10 when $f_dT \le 0.1$ and 1 when $f_dT > 0.1$. In Fig. 4.7, average estimation MSE (MSE averaged over the 4 users, 3 paths and 64 symbols) is plotted versus normalized Doppler spread f_dT. From this result, it can be seen that: First, the LS-T estimator performs considerably close to the CRLB-T. Second, although having estimation bias, the LMMSE-T estimator always performs better than unbiased estimators in the range of Doppler spread examined. Finally, the LMMSE-T has its performance more and more close to the LS estimator when f_dT increases.

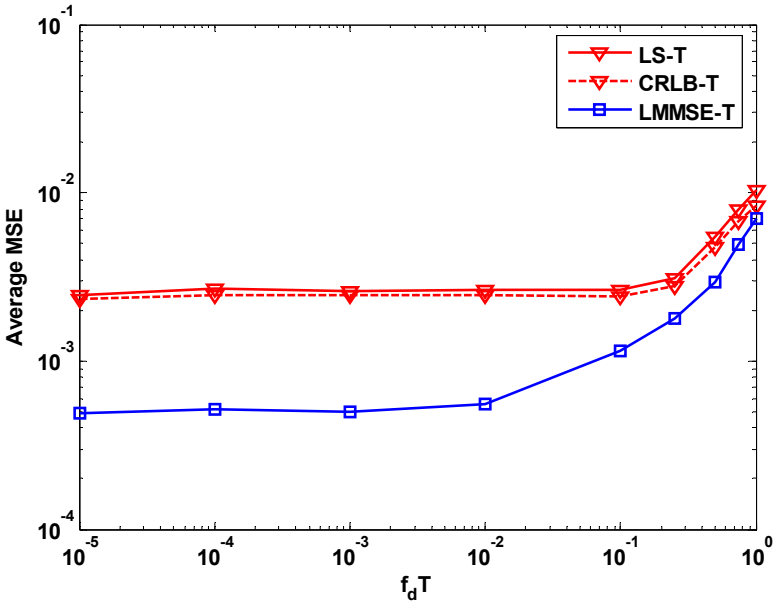

Fig. 4.7: MSE performance of LS-T and LMMSE, SNR=15dB.

Example 2. Comparison between LS-T and LS-F

In Fig. 4.8, average MSE is plotted versus f_dT for the LS-T and LS-F estimators. As a benchmark, their CRLB are also plotted. The oversampling index g is taken to be 10 when $f_dT \le 0.1$ and 1 when $f_dT > 0.1$. Only pilot symbols are collected for channel estimation when using LS-F. Clearly, using time-domain pilot pattern gains significant performance improvement. As channel changes faster, performance of the LS-F strays away from the CRLB-F.

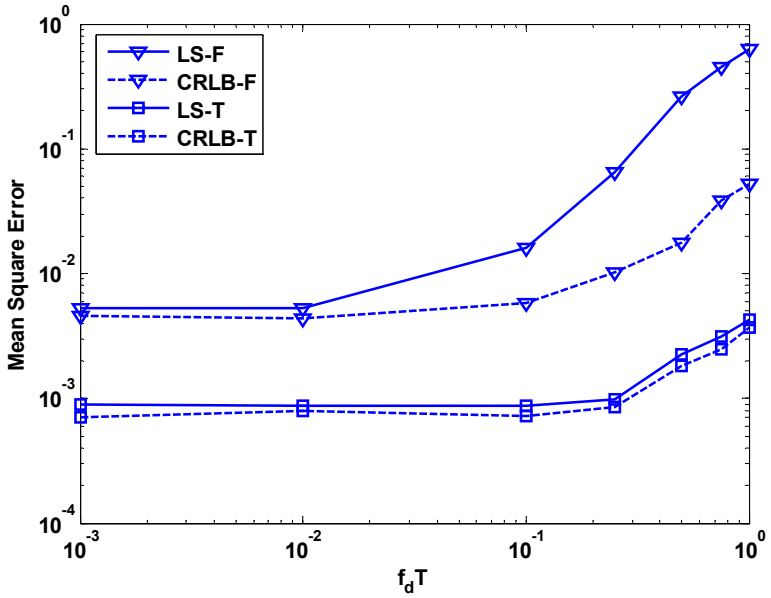

Fig. 4.8: Comparison between LS-T and LS-F, SNR=20dB

From the results shown in Fig. 4.7 and Fig. 4.8, the LMMSE channel estimator using the time-domain pilot will be proposed for possible use in OFDMA uplink, and the following simulations will be mainly aimed at examining this estimation scheme.

Example 3. Investigation on the length of pilot block

In practice, it is preferable to use a pilot block as short as possible. In this example, average MSE is plotted against the length of pilot block L_P to see how long the pilot block should be to acquire favorable estimation. The results are shown in Fig.4.9.

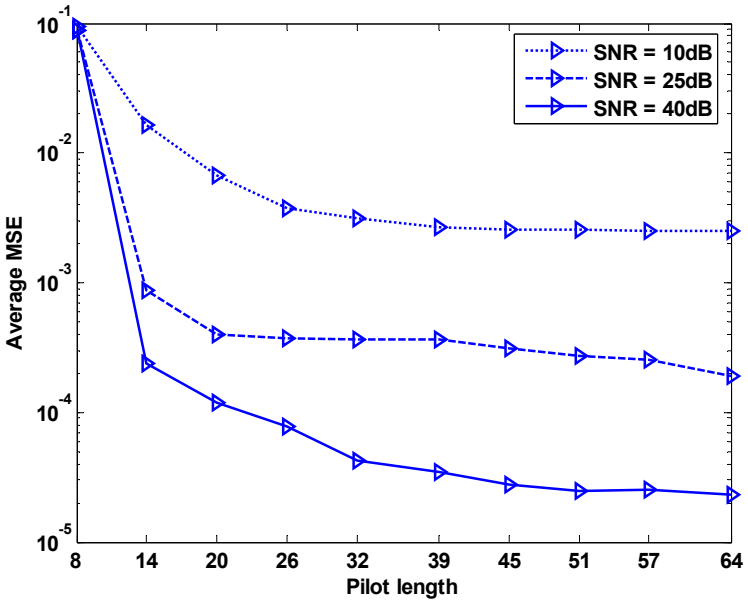

Fig.4.9: Average MMSE versus pilot block length. $f_d T = 0.05$, $g = 20$, using linear interpolation with interpolation length $M = 1$.

From the result in Fig.4.9, it can be seen that, when the pilot block length exceeds a certain value, using longer pilot blocks will not give significant performance improvement. This phenomenon can be interpreted by analyzing the rank of matrix $\boldsymbol{D}$. Specifically, from (4-22b), it can be seen that estimation accuracy is closely related to the rank of the matrix $\boldsymbol{D}^H \boldsymbol{D}$. Specifically, if $L_P \geq (2Q+1)LU$, the matrix $\boldsymbol{D}^H \boldsymbol{D}$ has full rank and thus the performance will not be much improved by increasing the pilot block length. On the other hand, if $L_P < (2Q+1)LU$, the matrix $\boldsymbol{D}^H \boldsymbol{D}$ is rank deficient and thus performance improvement will be significant when the pilot length increases. In this example, $(2Q+1)LU$ is 36. Thus, performance improvement from using longer pilots will be insignificant when $L_P > 36$. Clearly, this is in line with the results shown in Fig.4.9.

According to this result, instead of an entire OFDMA block, a pilot block with length equal to the number of BEM coefficients $(2Q+1)LU$ can be used. Since

$(2Q+1)LU$ is normally smaller than the OFDMA block length N, transmission efficiency can be increased by using shortened pilot blocks.

4.5.2 Performance of ICI Suppression with Channel Estimation

In this part of simulations, the ICI suppression schemes proposed in Chapter 3 is implemented in conjunction with the proposed LMMSE channel estimation. System setup and parameter are the same as those used in Section 4.5.1. Channel coding has not been used.

Example 1. Average Symbol Error Rate

In Fig.4.10, average SER is plotted against SNR with LMMSE channel estimation. The results are also compared with that acquired from perfect CIR. Specifically, the normalized Doppler spread f_dT is 5% and the pilot block length L_P is 36. It can be seen that the proposed channel estimation scheme gives a performance close to the ideal case when the interpolation length is M=1.

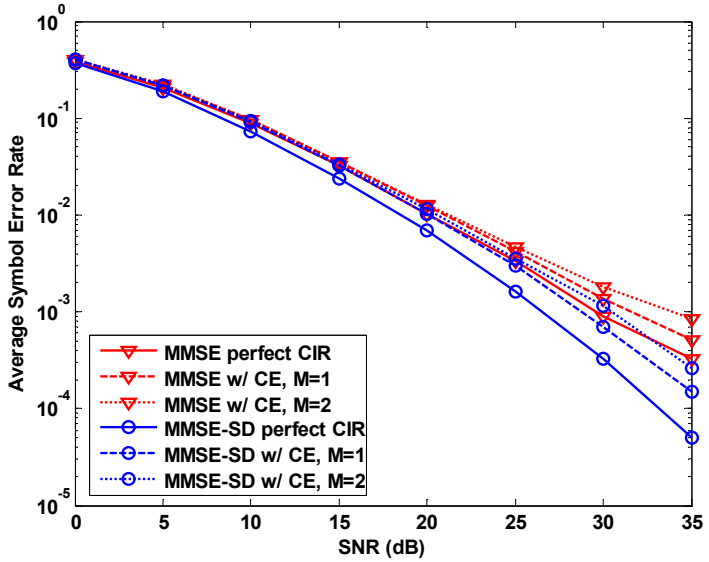

Fig.4.10: Average symbol error rates of MMSE and MMSE-SD with channel estimation at $f_dT = 0.05$, $L_P = 36$. 'CE' in the figure and hereafter stands for 'Channel Estimation'.

Example 2. Random CFO Test

In this simulation, detection performance is examined in a more realistic scenario. Users' CFOs are modeled as independent random variables uniformly distributed in the range $(-\varepsilon,\varepsilon)$, and average SER is simulated for $\varepsilon = 0$, 0.35 and 0.5. From the results presented in Fig.4.11, it can be seen that, when CFO reaches 35% of the subcarrier spacing, performance loss compared with no CFO scenario is only 1dB and 0.5dB for MMSE and MMSE-SD, respectively. Hence, by using the proposed estimation and detection schemes, the strict requirement on the accuracy of coarse synchronization, such as the 2% limit stated in IEEE802.16 standard, can be dramatically relaxed.

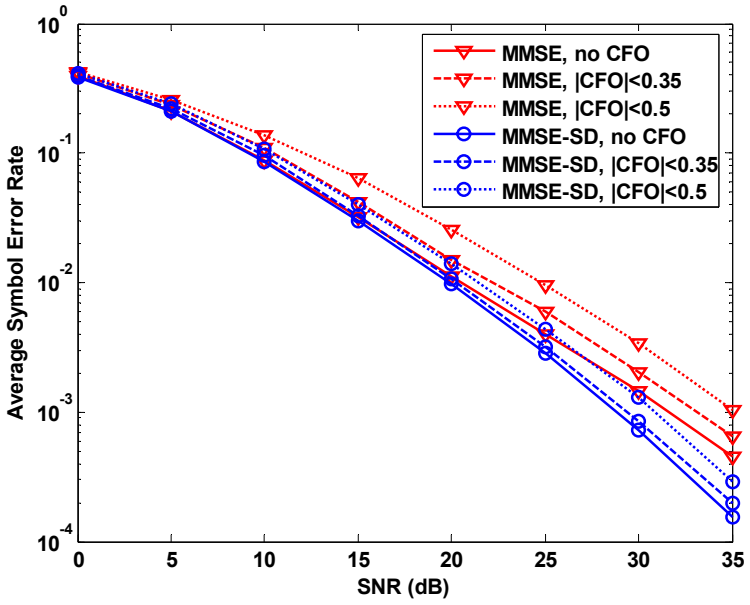

Fig.4.11: Average symbol error rates of MMSE and MMSE-SD under different CFO ranges with channel estimation, $f_d T = 0.05$, $L_p = 36$, $M = 1$.

Example 3. Immunity to CFO Estimation Errors

CFO estimation error is inevitable in real applications and it affects estimation and detection performance. In this simulation, users' CFO estimation error is modeled

as independent white Gaussian random variables $\mathcal{N}\left(0,\sigma^2\right)$, where σ^2 is equal to the mean square error (MSE) in CFO estimation. Average SER is plotted against CFO standard deviation σ (root MSE) in Fig.4.12.

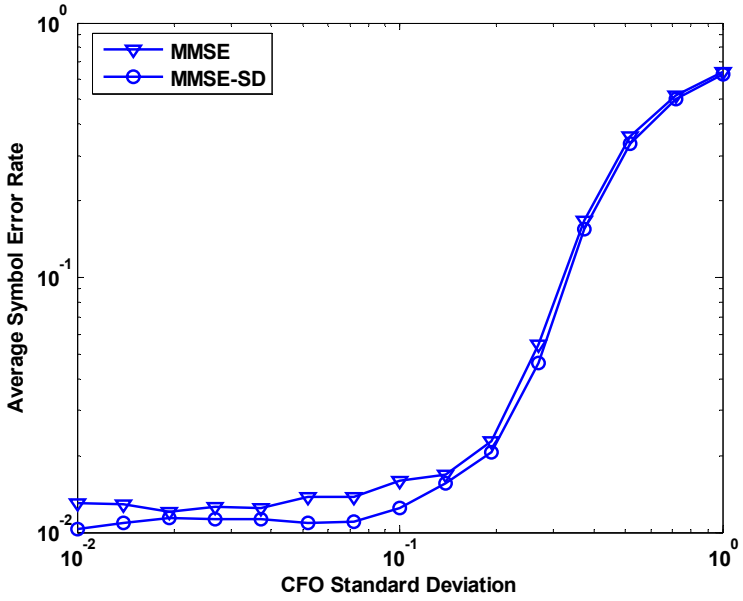

Fig.4.12: Immunity to CFO estimation errors with channel estimation, SNR = 20 dB, $f_dT = 0.05$, $M = 1$, $L_P = 36$.

Clearly, both MMSE and MMSE-SD have insignificant performance loss until the CFO estimation errors exceed 0.1, which is quite a large value in CFO estimation. This result shows that the proposed MMSE and MMSE-SD schemes are sufficiently robust to the CFO errors arising from commonly used CFO estimation algorithms.

Example 4. Immunity to Near-Far Effects

To demonstrate the immunity to near–far effects when channel information is not perfect, the same simulation shown in Fig.3.9 is rerun. Apparently, if channel estimation is used, the near–far resistance is degraded due to channel estimation errors. One approach to maintain the performance is using power control. If this is difficult to be

implemented, a more advanced interpolation scheme can be used to reduce channel estimation errors and improve the near-far resistance.

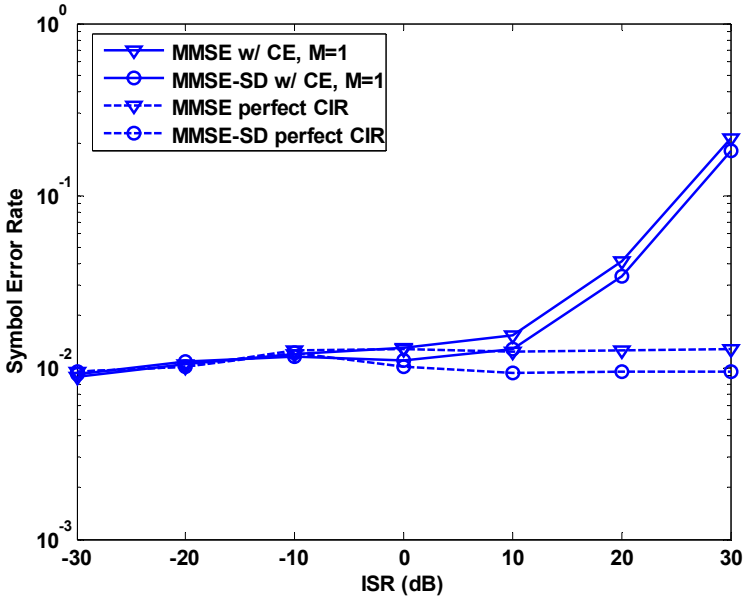

Fig.4.13: Symbol error rate against Interference Signal power Ratio, SNR = 20 dB, $f_d T = 0.05$, $L_P = 36$. Every interfering user induces the same ISR over user 1.

Chapter 5

Low Complexity ICI Suppression in Interleaved OFDMA System Uplink

Interleaved OFDMA is the system that deploys interleaved subcarrier allocation[†]. It owns the largest frequency diversity. As discussed in [7], sufficient frequency diversity is crucial to system capacity in delay sensitive applications. Therefore, interleaved OFDMA is a popular choice for real-time systems, such as multimedia broadcasting system. Moreover, interleaved OFDMA system has a particular signal structure, which can be made use of to develop low-complexity ICI suppression algorithms.

In this chapter, a novel detection structure with lower complexity in ICI suppression is studied for interleaved OFDMA system uplink. Specifically, the interleaved signaling in frequency domain shows a periodic feature in time domain [20][28][29]. By making use of this periodic structure, dimension of FFT demodulation and detection can be considerably reduced.

In Section 5.1, the temporal periodicity of an interleaved OFDMA block is introduced and signature vectors are formulated. Based on the signal model, a signature vector-based multiuser detector is proposed and investigated in Section 5.2. Comparative studies on complexity and performance are given in Section 5.3 and 5.4, respectively.

[†] The study in this work is based on the regular interleaving used in static OFDMA systems

5.1 Signature Vectors in Interleaved OFDMA Signaling

Supposing there are N subcarriers accommodating U users, with each user using P subcarriers. An interleaved OFDMA system deploys interleaved subcarrier allocation as illustrated in Fig.5.1.

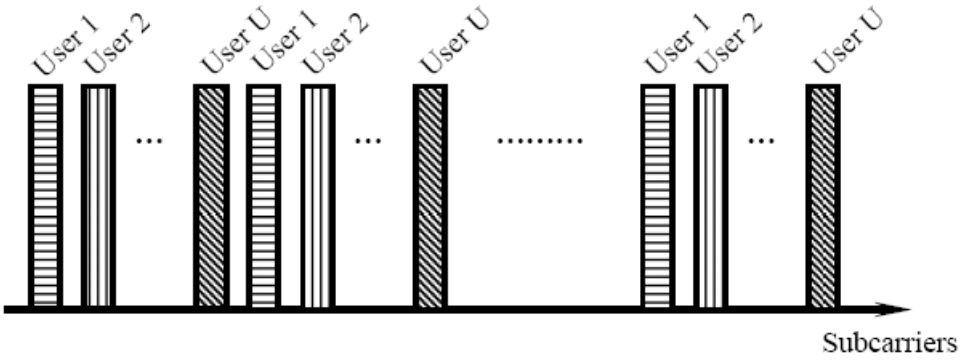

Fig.5.1: Interleaved OFDMA subcarrier allocation, each bar stands for one subcarrier.

Mathematically, an arbitrary user u will be assigned with the subcarriers indexed by $u+pU$, $p=0,1..P-1$. Therefore, an OFDMA block transmitted from user u is given by

$$x_u(n)=\frac{1}{\sqrt{N}}\sum_{p=0}^{P-1}X_u(p)\exp\left[\frac{j2\pi(u+pU)n}{N}\right],\qquad -N_g\le n\le N-1,\quad (5\text{-}1)$$

where N_g stands for the length of cyclic prefix. After transmission in a doubly selective fading channel and front processing, the signal received from user u is given by

$$r_u(n)=\exp\left(\frac{j2\pi\varepsilon_u n}{N}\right)\sum_{l=0}^{L-1}x_u(n-l)h_u(n,l)+z(n),\qquad 0\le n\le N-1,\qquad (5\text{-}2)$$

where ε_u is the CFO of user u, normalized by subcarrier spacing $1/T$. Due to the same reason as stated in Section 3.2, time delay has been omitted in (5-2). Using the BEM channel model developed in Chapter 4, (5-2) can be rewritten as

$$
\begin{aligned}
r_u(n) &= e^{\frac{j2\pi\varepsilon_u n}{N}} \sum_{l=0}^{L-1} x_u(n-l)\left[\sum_{q=-Q}^{Q} a_{u,l}(q) e^{\frac{j2\pi qn}{gN}}\right] + z(n) \\
&= \sum_{q=-Q}^{Q} e^{\frac{j2\pi(\varepsilon_u+q/g)n}{N}} \frac{1}{\sqrt{N}} \sum_{p=0}^{P-1}\left[\sum_{l=0}^{L-1} a_{u,l}(q) e^{\frac{-j2\pi(u+pU)l}{N}}\right] X_u(p) e^{\frac{j2\pi(u+pU)n}{N}} + z(n), \\
&= \frac{1}{\sqrt{N}} \sum_{q=-Q}^{Q} e^{\frac{j2\pi\varepsilon_u(q)n}{N}} \sum_{p=0}^{P-1} H_{u,q}(p) X_u(p) e^{\frac{j2\pi(u+pU)n}{N}} + z(n)
\end{aligned}
$$

$$0 \le n \le N-1, \quad (5\text{-}3)$$

with

$$\varepsilon_u(q) = \varepsilon_u + q/g, \quad (5\text{-}4)$$

$$H_{u,q}(p) = \sum_{l=0}^{L-1} a_{u,l}(q) e^{\frac{-j2\pi(u+pU)l}{N}}, \quad (5\text{-}5)$$

where $a_{u,l}(q)$ stands for the q-th BEM coefficient describing path l of user u, and g is the oversampling index. In (5-3), denoting sample index n by

$$n = n_o + mP,$$

$$0 \le n_o \le P-1 \text{ and } 0 \le m \le U-1, \quad (5\text{-}6)$$

it follows that

$$r_u(n_o + mP) = \sum_{q=-Q}^{Q} b_{u,q}(m) s_{u,q}(n_o), \quad (5\text{-}7)$$

where

$$b_{u,q}(m) = \frac{1}{\sqrt{U}} e^{\frac{j2\pi\left[u+\varepsilon_u(q)\right]m}{U}}, \quad (5\text{-}8)$$

$$s_{u,q}(n_o) = \frac{1}{\sqrt{P}} \sum_{p=0}^{P-1} H_{u,q}(p) X_u(p) e^{\frac{j2\pi n_o\left[u+pU+\varepsilon_u(q)\right]}{N}}. \quad (5\text{-}9)$$

As can be seen, for each BEM basis index q, $b_{u,q}(m)s_{u,q}(n_o)$ with $0 \le n_o \le P-1$ and $0 \le m \le U-1$ shows a periodic feature. Following (5-7), each OFDMA block can be rearranged into a $Q \times P$ matrix, as given by

$$\boldsymbol{r}_u = \sum_{q=-Q}^{Q} \boldsymbol{b}_{u,q} \boldsymbol{s}_{u,q}^T , \tag{5-10}$$

with

$$\boldsymbol{b}_{u,q} = \frac{1}{\sqrt{U}} \left[1 \quad e^{\frac{j2\pi\left[u+\varepsilon_u(q)\right]}{U}} \quad \ldots \quad e^{\frac{j2\pi\left[u+\varepsilon_u(q)\right](U-1)}{U}} \right]^T , \tag{5-11}$$

$$\boldsymbol{s}_{u,q} = \boldsymbol{D}\left(\varepsilon_u(q)\right) \boldsymbol{F}_u \boldsymbol{H}_{u,q} \boldsymbol{X}_u , \tag{5-12}$$

where

$$\boldsymbol{D}\left(\varepsilon_u(q)\right) = \mathrm{diag}\left[1 \quad e^{\frac{j2\pi\varepsilon_u(q)}{N}} \quad \ldots \quad e^{\frac{j2\pi(P-1)\varepsilon_u(q)}{N}} \right],$$

$$\boldsymbol{H}_{u,q} = \mathrm{diag}\left[H_{u,q}(0) \quad H_{u,q}(1) \quad \ldots \quad H_{u,q}(P-1) \right],$$

contain CFO and channel frequency response associated with the q-th basis, and

$$\left[\boldsymbol{F}_u\right]_{n_o,p} = \frac{1}{\sqrt{P}} \exp\left[\frac{j2\pi n_o (u + pU)}{N} \right]$$

is the IFFT modulation matrix corresponding to user u. It is easy to show that $\boldsymbol{F}_u \boldsymbol{F}_u^H = \boldsymbol{F}_u^H \boldsymbol{F}_u = \boldsymbol{I}_P$, which indicates that matrix $\boldsymbol{F}_u^H$ is the corresponding FFT demodulation matrix to user u.

Following (5-10), an OFDMA block received due to multiuser signals is

$$\begin{aligned} \boldsymbol{r} &= \sum_{q=-Q}^{Q} \sum_{u=1}^{U} \boldsymbol{b}_{u,q} \boldsymbol{s}_{u,q}^T + \boldsymbol{z} \\ &= \sum_{q=-Q}^{Q} \boldsymbol{B}_q \boldsymbol{S}_q^T + \boldsymbol{z} \end{aligned} , \tag{5-13}$$

where

$$\boldsymbol{B}_q = \left[\boldsymbol{b}_{1,q} \quad \boldsymbol{b}_{2,q} \quad \ldots \quad \boldsymbol{b}_{U,q} \right],$$

$$\boldsymbol{S}_q = \left[\boldsymbol{s}_{1,q} \quad \boldsymbol{s}_{2,q} \quad \ldots \quad \boldsymbol{s}_{U,q} \right].$$

According to the definition given by (5-11), it can be shown that

$$\left[\boldsymbol{B}_q^H \boldsymbol{B}_q\right]_{i,j} = \frac{1}{U}\frac{\sin\left(\pi\left(j-i+\varepsilon_j(q)-\varepsilon_i(q)\right)\right)}{\sin\left(\pi\left(j-i+\varepsilon_j(q)-\varepsilon_i(q)\right)/U\right)} e^{\frac{j\pi(U-1)\left(j-i+\varepsilon_j(q)-\varepsilon_i(q)\right)}{U}}. \quad (5\text{-}14)$$

Clearly if all the users have no CFO or exactly the same CFO, (5-14) becomes

$$\left[\boldsymbol{B}_q^H \boldsymbol{B}_q\right]_{i,j} = \begin{cases} 1 & i = j \\ 0 & i \neq j \end{cases}. \quad (5\text{-}15)$$

This result implies that, in ideal case, the vectors $\boldsymbol{b}_{u,q}$, u=1,2…U, are orthonormal vectors that can be opted for identifying users. For this reason, the vector $\boldsymbol{b}_{u,q}$ is referred to as signature vector of user u, on basis q. Note that the subscript q indexes a signal replica associated with the q-th BEM basis. All the $2Q+1$ replicas can be combined with a diversity technique, such as Equal Gain Combining (EGC), Maximum Ratio Combing (MRC) and so on. Motivated by these findings, a novel detection structure can be used to suppress ICI and exploit Doppler diversity, as shown in Fig.5.2(a) and (b).

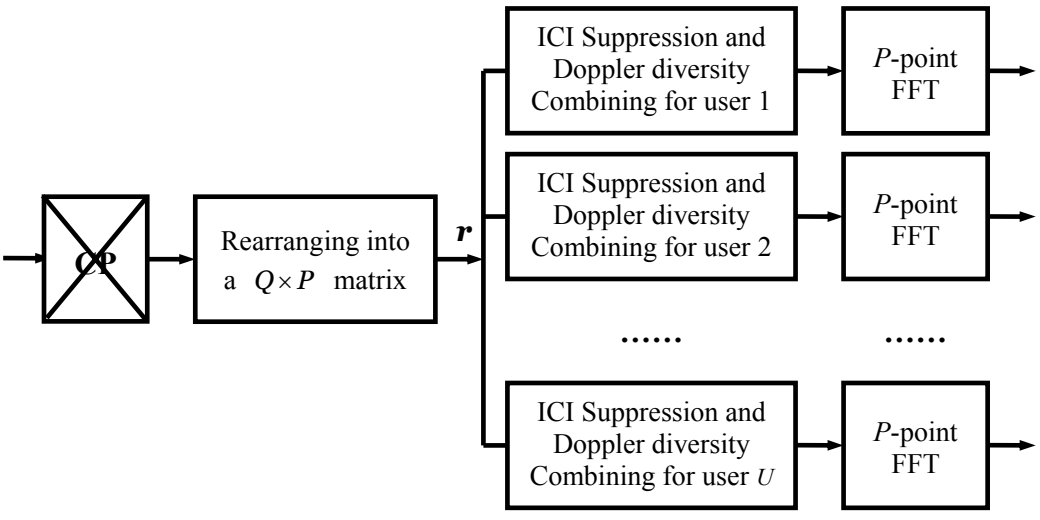

(a)

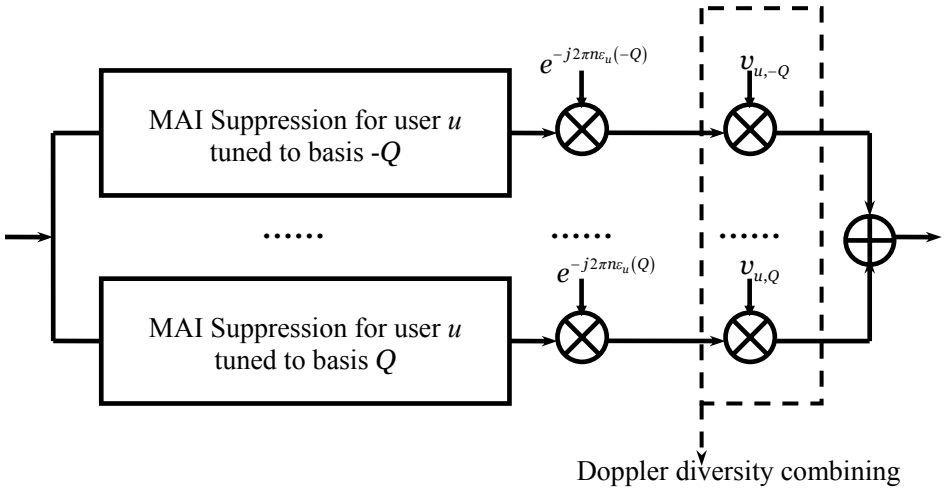

(b)

Fig.5.2: (a) Novel parallel detection structure for the interleaved OFDMA uplink (b) ICI suppression and Doppler diversity combining for each user.

In the detection scheme shown above, there are a total of U branches, each of which detects one user. In the ICI suppression and Doppler diversity combining unit shown in Fig.5-2(b), the signature vector is used to suppress MAI (or cross ICI), then self ICI is suppressed and Doppler diversity is exploited by combining multiple replicas (weights circled in the dashed square are used to exploit diversity gain). After ICI suppression and diversity combining, P-point FFT demodulates the information symbols. For convenience, the detector shown in Fig.5.2 is referred to as the signature-vector based detector in following discussions.

Apparently, the crucial issue to be considered at the moment is how to suppress MAI by taking advantage of signature vectors. It is easy to see that the MAI suppression modules in parallel diversity branches would have no difference but tuning to different BEM bases. To this end, for clarity and convenience, the signature-vector detector will be particularly studied in static and quasi-static frequency selective fading

channels in the remainder of this chapter. In such a scenario, only one branch is needed in diversity combining. Mathematically, over static and quasi-static fading channels, BEM basis index Q is equal to zero. (5-13) thus degenerates to

$$\boldsymbol{r} = \sum_{u=1}^{U} \boldsymbol{b}_u \boldsymbol{s}_u^T + \boldsymbol{z} . \tag{5-16}$$

Note that the subscript index $q = 0$ is omitted in (5-16). The integrated detection procedure under such a case of scenario is redrawn in Fig.5.3 for the convenience to the sequent discussion.

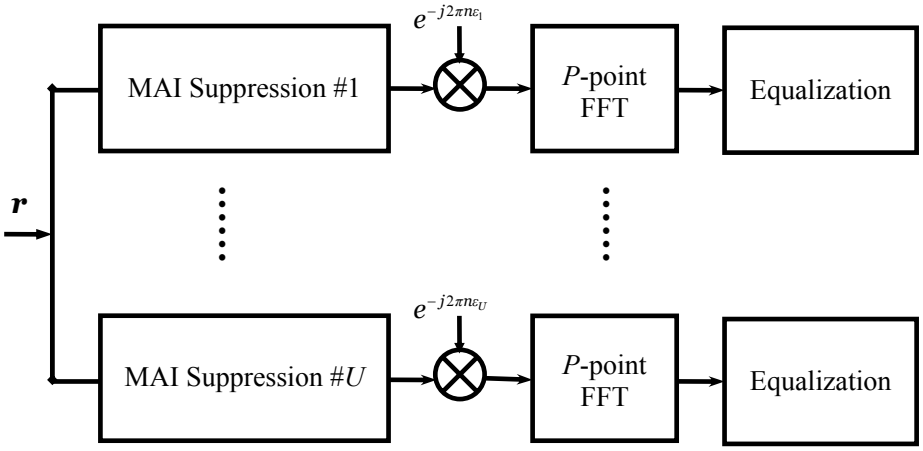

Fig.5.3: Signature-vector based detector in static and quasi-static fading channels.

5.2 Signature Vector-based Multiuser Detection

As shown in Fig.5.3, ICI suppression in the signature-vector based detector is formed of two steps, which cancel cross ICI and self ICI in a row. Unlike current MAI suppression schemes, which normally attempt to suppress MAI in the frequency domain after self ICI suppression and FFT demodulation, the signature-vector detector suppresses MAI in time domain prior to self ICI suppression and FFT demodulation. With the help of signature vectors, MAI can be suppressed by both linear and nonlinear

schemes, similar to those discussed in Chapter 3. In what follows, the linear suppression schemes: Matched Filtering, Zero Forcing and MMSE will be investigated and compared with the schemes proposed in previous work.

5.2.1 Matched Filtering

In Matched Filtering (MF), signature vectors are directly used as weight vectors in MAI suppression. Output of detection branch *u* is given by

$$\begin{aligned}\boldsymbol{y}_u &= \boldsymbol{F}_u^H \boldsymbol{D}(-\varepsilon_u)\left(\boldsymbol{b}_u^H \boldsymbol{r}\right)^T \\ &= \boldsymbol{H}_u \boldsymbol{X}_u + \sum_{v\neq u} \rho_{uv} \boldsymbol{F}_u^H \boldsymbol{D}(\varepsilon_v - \varepsilon_u) \boldsymbol{F}_v \boldsymbol{H}_v \boldsymbol{X}_v , \\ &\quad + \boldsymbol{F}_u^H \boldsymbol{D}(-\varepsilon_u) \boldsymbol{Z}^{\mathrm{T}} \boldsymbol{b}_u^*\end{aligned} \tag{5-17}$$

where

$$\boldsymbol{D}(\alpha) = diag\left[\exp\left(\frac{j2\pi n_o \alpha}{N} \right) \right]_{n_o=0,1\ldots P-1} .$$

$$\rho_{uv} = \boldsymbol{b}_u^H \boldsymbol{b}_v = \frac{1}{U} \frac{\sin\left(\pi\left(v-u+\varepsilon_v-\varepsilon_u\right)\right)}{\sin\left(\pi\left(v-u+\varepsilon_v-\varepsilon_u\right)/U\right)} e^{\frac{j\pi(U-1)(j-i+\varepsilon_v-\varepsilon_u)}{U}} .$$

As was discussed in Chapter 3, using matched filtering leads to a detection output equal to that generated by a conventional OFDMA detector, named as single-user detector in [24]. Using this equivalence, (5-17) will be used to analytically evaluate the residual MAI of a conventional detector in the presence of near-far effects. This is particularly interesting in an interleaved OFDMA system since the system is most vulnerable to MAI. As in Chapter 3, a simple statistical large-scale fading model is used to induce near-far effects. Specifically, a propagation loss $1/\sqrt{d_u^\beta}$ is used to scale the signal received from user *u*, with d_u standing for the distance between the

user and the base station, β being the attenuation index (ranges from 2 to 4 in radio channels). Following this, (5-17) can be rewritten into

$$\begin{aligned}\boldsymbol{y}_u = &\frac{1}{\sqrt{d_u^{\beta}}}\boldsymbol{H}_u\boldsymbol{X}_u + \sum_{v\neq u}\rho_{uv}\frac{1}{\sqrt{d_v^{\beta}}}\boldsymbol{F}_u^H\boldsymbol{D}\left(\varepsilon_v-\varepsilon_u\right)\boldsymbol{F}_v\boldsymbol{H}_v\boldsymbol{X}_v \\ &+\boldsymbol{F}_u^H\boldsymbol{D}\left(-\varepsilon_u\right)\boldsymbol{Z}^{\mathrm{T}}\boldsymbol{b}_u^*\end{aligned}. \tag{5-18}$$

From (5-18), output SIR of a conventional OFDMA detector for user *u* is given by

$$\mathrm{SIR}_u = \frac{\mathrm{trace}\left(\boldsymbol{H}_u\boldsymbol{H}_u^H\right)}{\sum_{v\neq u}\left(\frac{d_u}{d_v}\right)^{\beta}\left|\rho_{uv}\right|^2\mathrm{trace}\left(\boldsymbol{H}_v\boldsymbol{H}_v^H\right)}. \tag{5-19}$$

Using (5-19), Probability Density Function (PDF) of post-MF SIR in a 3-ray Rayleigh multipath slow fading channel is simulated and plotted in Fig.5.4.

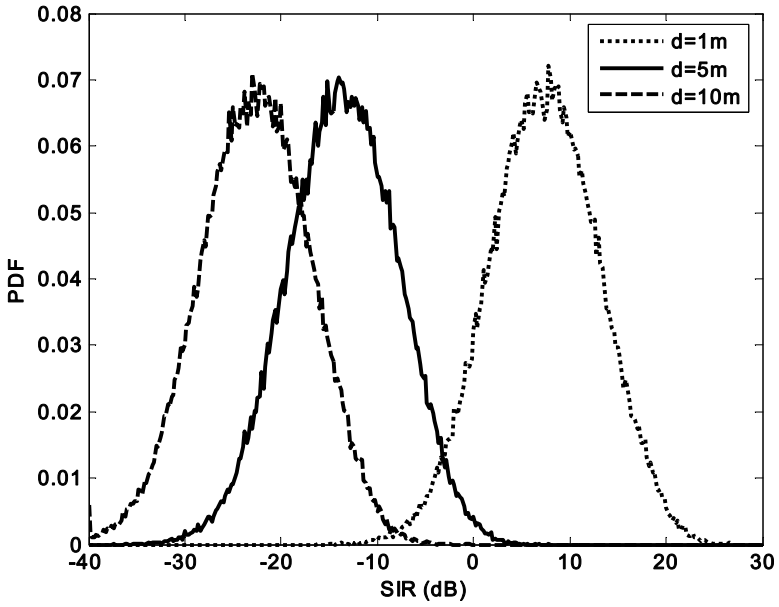

Fig.5.4: output SIR Probability Density Function (PDF) of the conventional OFDMA detector. A total of 16 users are uniformly distributed within a circle centered at the base station. The radius of the circle is 10m and the desired user is placed d meters away from the BS.

Apparently, the conventional OFDMA detector has poor immunity to the near-far problem. As a matter of fact, the detection schemes that attempt to further clean the residual MAI on the top of matched filtering are also affected by the near-far problem.

For example, the Parallel Interference Cancellation (PIC) [27] and Successive Interference Cancellation (SIC) [27], may suffer from the near-far problem for the following reasons:

1. PIC itself also has poor immunity to the near-far problem. The use of PIC to reinforce a conventional detector usually does not help improving near-far immunity.
2. Although SIC has immunity to the near-far problem, the immunity highly depends on the accuracy of hard decision in each round of cancellation. Due to the poor performance of a conventional detector, SIC may suffer from serious error propagation problem, which cancels its near-far immunity.

A straight way to avoid performance degradation caused by the near-far problem, as in CDMA systems, is power control. Generally speaking, the use of power control may introduce a new concern on extra processing delay and computational load. For example, the use of power control in high mobility environments usually suffers from the processing delay, with the result that control information may become outdated when received by mobile stations. For this reason, it is worthwhile to develop detection schemes with sufficient immunity to the near-far problem. Fortunately, the signal structure given in (5-16) enables us to implement Zero Forcing and MMSE schemes, which are near-far resistant as shown in Chapter 3.

5.2.2 Zero Forcing

In this chapter, zero forcing is not obtained by solving a least square problem. Instead, for the multiuser signal given by (5-16), as proved in [36], a zero-forcing MAI

suppression weight vector associated with user u can be solved from

$$\min_{\boldsymbol{w}_{ZF,u}=\boldsymbol{U}_S\boldsymbol{d}_u} \mathbb{E}\left\|\boldsymbol{w}_{\mathrm{ZF},u}^H \boldsymbol{B}\boldsymbol{S}\right\|^2 \quad \text{subject to} \quad \boldsymbol{w}_{\mathrm{ZF},u}^H \boldsymbol{b}_u = 1 \tag{5-20}$$

where $\boldsymbol{B}=\begin{bmatrix}\boldsymbol{b}_1 & \boldsymbol{b}_2 & \cdots & \boldsymbol{b}_U\end{bmatrix}$ contains the signature vectors of all the users, and $\boldsymbol{U}_{\mathrm{S}}$ contains signal subspace eigenvectors of autocorrelation matrix $\boldsymbol{R}=\mathbb{E}\left\{\boldsymbol{r}\boldsymbol{r}^H\right\}$. Specifically, the signal subspace eigenvectors are those associated with eigenvalues which are larger than noise power (see Appendix E). The relation $\boldsymbol{w}_{ZF,u}=\boldsymbol{U}_{\mathrm{S}}\boldsymbol{d}_u$ conveys that the weight vector lies in the signal subspace spanned by $\mathrm{Range}\left(\boldsymbol{U}_{\mathrm{S}}\right)$, with $\boldsymbol{d}_u$ containing all the coordinates. Solving (5-20), a subspace ZF MAI suppression weight vector for user u is given by

$$\boldsymbol{w}_{\text{SB-ZF},u}=\frac{\boldsymbol{U}_{\mathrm{S}}\left(\boldsymbol{\Lambda}_{\mathrm{S}}-\sigma_n^2\boldsymbol{I}\right)^{-1}\boldsymbol{U}_{\mathrm{S}}^H\boldsymbol{b}_u}{\boldsymbol{b}_u^H\boldsymbol{U}_{\mathrm{S}}\left(\boldsymbol{\Lambda}_{\mathrm{S}}-\sigma_n^2\boldsymbol{I}\right)^{-1}\boldsymbol{U}_{\mathrm{S}}^H\boldsymbol{b}_u}, \tag{5-21}$$

where $\boldsymbol{\Lambda}_{\mathrm{S}}$ contains all the signal subspace eigenvalues associated with $\boldsymbol{U}_{\mathrm{S}}$, and σ_n^2 stands for the power of background noise. Derivation of (5-21) is given in Appendix E. It is worthwhile to point out that the solution of (5-20) is not necessarily expressed in terms of subspace parameters. But the subspace expression given by (5-21) helps revealing the relation between zero forcing and MMSE MAI suppression schemes, and also helps analyze the detector's resistance against CFO estimation errors, as will be shown soon.

To implement the ZF MAI suppression (5-21), autocorrelation matrix $\boldsymbol{R}$ is first approximated by calculating

$$\hat{\boldsymbol{R}} = \sum_{i=1}^{l} \boldsymbol{r}_i \boldsymbol{r}_i^H \,, \tag{5-22}$$

where $\boldsymbol{r}_i$, $i = 1,2...l$, are successively collected reception matrix. As discussed in [36], (5-22) is an asymptotically exact estimation of the autocorrelation matrix, with bounded estimation error. The estimate $\hat{\boldsymbol{R}}$ is then decomposed into subspace parameters, which are shared by all the detection branches for MAI suppression.

5.2.3 MMSE

As have been discussed in Section 3.3, the MMSE cancellation scheme normally obtains better performance than ZF by decreasing the enhancement on background noise. MMSE MAI suppression is designed as solution of the optimization problem:

$$\min_{\boldsymbol{w}_{\mathrm{M},u}} \mathbb{E}\left\| \boldsymbol{H}_u \boldsymbol{X}_u - \boldsymbol{F}_u^H \boldsymbol{D}\left(-\varepsilon_u\right)\left(\boldsymbol{w}_{\mathrm{M},u}^H \boldsymbol{Y}\right)^T \right\|^2 \quad \text{subject to} \quad \boldsymbol{w}_{\mathrm{M},u}^H \boldsymbol{b}_u = 1 \,. \tag{5-23}$$

By resorting to the Lagrange multiplier method, the solution can be shown to be

$$\boldsymbol{w}_{\mathrm{M},u} = \frac{\boldsymbol{R}^{-1}\boldsymbol{b}_u}{\boldsymbol{b}_u^H \boldsymbol{R}^{-1} \boldsymbol{b}_u} \,, \tag{5-24}$$

where $\boldsymbol{R}$ is the autocorrelation matrix $\mathbb{E}\left\{\boldsymbol{r}\boldsymbol{r}^H\right\}$, as given in last section. At the moment, it is noteworthy that an unconstrained MMSE MAI suppression has been studied in [28], where the linear constraint $\boldsymbol{w}_{\mathrm{M},u}^H \boldsymbol{b}_u = 1$ is not added, and the corresponding solution is given by

$$\tilde{\boldsymbol{w}}_{\mathrm{M},u} = \boldsymbol{R}^{-1}\boldsymbol{b}_u \,. \tag{5-25}$$

In fact, the MAI suppression schemes given by (5-24) and (5-25) would give the same

detection performance since they are almost the same except for a scalar scaling coefficient, which does not affect the SINR after MAI suppression. However, the use of linear constraint makes some difference when the above two MAI suppression schemes are implemented by adaptive algorithms, as will be shown soon.

For the constrained MMSE scheme, substituting

$$\boldsymbol{R}^{-1} = \boldsymbol{U}_{\mathrm{S}}\boldsymbol{\Lambda}_{\mathrm{S}}^{-1}\boldsymbol{U}_{\mathrm{S}}^{H} + \boldsymbol{U}_{\mathrm{N}}\boldsymbol{\Lambda}_{\mathrm{N}}^{-1}\boldsymbol{U}_{\mathrm{N}}^{H}$$

into (5-24) yields

$$\boldsymbol{w}_{\mathrm{M},u} = \frac{\boldsymbol{U}_{\mathrm{S}}\boldsymbol{\Lambda}_{\mathrm{S}}^{-1}\boldsymbol{U}_{\mathrm{S}}^{H}\boldsymbol{b}_u}{\boldsymbol{b}_u^{H}\boldsymbol{U}_{\mathrm{S}}\boldsymbol{\Lambda}_{\mathrm{S}}^{-1}\boldsymbol{U}_{\mathrm{S}}^{H}\boldsymbol{b}_u}, \tag{5-26}$$

where the orthogonality between the signal and noise subspaces, i.e., $\boldsymbol{U}_{\mathrm{N}}^{H}\boldsymbol{b}_u = 0$, has been used. By comparing this subspace expression with (5-21), it is clear that zero forcing and MMSE MAI suppression schemes are asymptotically the same at high SNR region.

5.2.4 Performance Analysis and Discussion

Before moving along to numerical results, there are still some important discussion and analysis worthy of deeper investigation. In this section, the ZF and MMSE MAI suppression schemes will be studied on their: 1. resistance against CFO estimation error and, 2. computational complexity. At the end of this section, an adaptive algorithm will also be developed and discussed.

A. Performance in the Presence of Erroneous CFO Estimation

As can be seen from (5-11), a signature vector is a function of CFO. Therefore,

CFO estimation errors will give rise to signature vector mismatch. To examine robustness to erroneous CFO estimation, output SINR of the ZF and MMSE MAI suppression schemes can be derived as a function of CFO estimation error. Without loss of generality, user 1 is assumed to be the desired user in the derivation below.

From a subspace point of view, a mismatched signature vector $\hat{\boldsymbol{b}}_1$ (i.e., the signature vector calculated from estimated CFO) can be decomposed into two components, with one in signal subspace and the other in noise subspace [36]. Mathematically,

$$\hat{\boldsymbol{b}}_1 = \boldsymbol{b}_1^s + \boldsymbol{b}_1^n = \boldsymbol{B}\boldsymbol{c} + \boldsymbol{b}_1^n, \tag{5-27}$$

where $\boldsymbol{b}_1^s$ and $\boldsymbol{b}_1^n$ correspond to the signal and noise subspace components, $\boldsymbol{B} = [\boldsymbol{b}_1, \boldsymbol{b}_2 ... \boldsymbol{b}_U]$, and $\boldsymbol{c}$ is the coordinates vector of $\boldsymbol{b}_1^s$ in the signal subspace spanned by $\boldsymbol{B}$. If the mismatched signature vector given by (5-27) is used to suppress MAI, weight vectors of the zero forcing and MMSE schemes can be uniformly expressed in terms of subspace parameters as given by

$$\boldsymbol{w} = \frac{\boldsymbol{U}_{\mathrm{S}} \boldsymbol{\Lambda} \boldsymbol{U}_{\mathrm{S}}^H \hat{\boldsymbol{b}}_1}{\hat{\boldsymbol{b}}_1^H \boldsymbol{U}_{\mathrm{S}} \boldsymbol{\Lambda} \boldsymbol{U}_{\mathrm{S}}^H \hat{\boldsymbol{b}}_1} = \frac{\boldsymbol{U}_{\mathrm{S}} \boldsymbol{\Lambda} \boldsymbol{U}_{\mathrm{S}}^H \boldsymbol{B}\boldsymbol{c}}{\boldsymbol{c}^H \boldsymbol{B}^H \boldsymbol{U}_{\mathrm{S}} \boldsymbol{\Lambda} \boldsymbol{U}_{\mathrm{S}}^H \boldsymbol{B}\boldsymbol{c}}, \tag{5-28}$$

where $\boldsymbol{\Lambda} = \boldsymbol{\Lambda}_{\mathrm{S}} - \sigma_n^2 \boldsymbol{I}$ for ZF and $\boldsymbol{\Lambda} = \boldsymbol{\Lambda}_{\mathrm{S}}$ for MMSE. From (5-28), the SINR of detection output can be easily shown to be

$$\mathrm{SINR} = \frac{|\mu_1|^2 \sigma_1^2 \mathrm{trace}\left(\boldsymbol{H}_1 \boldsymbol{H}_1^H\right)}{\sum_{v=2}^{U} \left[|\mu_v|^2 \sigma_v^2 \mathrm{trace}\left(\boldsymbol{H}_v \boldsymbol{H}_v^H\right) \right] + \|\boldsymbol{w}\|^2 \sigma_n^2}, \tag{5-29}$$

where $\mu_u = \boldsymbol{w}^H \boldsymbol{b}_u$, $u = 1, 2, ... U$. Using the method presented in [36], μ_u and $\|\boldsymbol{w}\|^2$

can be obtained for the zero-forcing scheme, as given by

$$\mu_u = \frac{c_u^* \sigma_u^{-2}}{\boldsymbol{c}^H \boldsymbol{B}^H \boldsymbol{U}_S \boldsymbol{\Lambda} \boldsymbol{U}_S^H \boldsymbol{B} \boldsymbol{c}} \quad , \tag{5-30}$$

$$\|\boldsymbol{w}\|^2 = \frac{\boldsymbol{c}^H \boldsymbol{P}^{-1} \left(\boldsymbol{B}^H \boldsymbol{B}\right)^{-1} \boldsymbol{P}^{-1} \boldsymbol{c}}{\left|\boldsymbol{c}^H \boldsymbol{B}^H \boldsymbol{U}_S \boldsymbol{\Lambda} \boldsymbol{U}_S^H \boldsymbol{B} \boldsymbol{c}\right|^2}, \tag{5-31}$$

where c_u is the u-th entry of coordinates vector $\boldsymbol{c}$, and $\boldsymbol{P} = \mathrm{diag}\left[\sigma_1^2 \quad \sigma_2^2 \quad \ldots \quad \sigma_U^2\right]$. Correspondingly,

$$\begin{aligned} &\mathrm{SINR}_{\mathrm{ZF}} \\ &= \frac{\sigma_1^{-2} \left|c_1^*\right|^2 \mathrm{trace}\left(\boldsymbol{H}_1 \boldsymbol{H}_1^H\right)}{\sum_{v=2}^{U} \left[\sigma_v^{-2} \left|c_v^*\right|^2 \mathrm{trace}\left(\boldsymbol{H}_v \boldsymbol{H}_v^H\right)\right] + \sigma_n^2 \boldsymbol{c}^H \boldsymbol{P}^{-1} \left(\boldsymbol{B}^H \boldsymbol{B}\right)^{-1} \boldsymbol{P}^{-1} \boldsymbol{c}}. \end{aligned} \tag{5-32}$$

Obviously, only the coordinate vector $\boldsymbol{c}$ is needed to finally obtain output SINR. Fortunately, $\boldsymbol{c}$ can be easily derived as a function of the CFO estimation error. Let $\varepsilon_1 + \Delta\varepsilon$ denote estimated CFO and $\Delta\varepsilon$ denote CFO estimation error, according to (5-11), the mismatched signature vector $\hat{\boldsymbol{b}}_1$ is given by

$$\begin{aligned} \hat{\boldsymbol{b}}_1 &= \frac{\left[1 \quad e^{\frac{j2\pi(\varepsilon_1+\Delta\varepsilon)}{U}} \quad \ldots \quad e^{\frac{j2\pi(U-1)(\varepsilon_1+\Delta\varepsilon)}{U}}\right]^T}{\sqrt{U}}, \\ &= \boldsymbol{E}\boldsymbol{b}_1 \end{aligned} \tag{5-33}$$

where

$$\boldsymbol{E} = \begin{bmatrix} 1 & & \boldsymbol{o} \\ & e^{j2\pi\Delta\varepsilon/U} & \\ & & \ldots \\ \boldsymbol{o} & & e^{j2\pi(U-1)\Delta\varepsilon/U} \end{bmatrix}$$

contains the CFO estimation error. From (5-27) and (5-33), we have

$$\hat{\boldsymbol{b}}_1 = \boldsymbol{B}\boldsymbol{c} + \boldsymbol{b}_1^n = \boldsymbol{E}\boldsymbol{B}\boldsymbol{e}_1, \tag{5-34}$$

where $\boldsymbol{e}_k$ is the k-th column of a $U \times U$ identity matrix. Premultiplying (5-34) by $\boldsymbol{B}^H$ yields

$$\boldsymbol{B}^H\boldsymbol{B}\boldsymbol{c}+\boldsymbol{B}^H\boldsymbol{b}_1^n=\boldsymbol{B}^H\boldsymbol{B}\boldsymbol{c}=\boldsymbol{B}^H\boldsymbol{E}\boldsymbol{B}\boldsymbol{e}_1, \tag{5-35}$$

and thus

$$\boldsymbol{c}=\left(\boldsymbol{B}^H\boldsymbol{B}\right)^{-1}\boldsymbol{B}^H\boldsymbol{E}\boldsymbol{B}\boldsymbol{e}_1, \tag{5-36}$$

where the first equation in (5-35) results from the orthogonality between signal and noise subspaces. Substituting (5-36) into (5-32) gives the output SINR of the zero-forcing detector as a function of CFO estimation error. Note that (5-32) also applies to the MMSE detector at high SNR region since the MMSE and ZF schemes are asymptotically the same.

As a special case, if there is no CFO estimation error, $\Delta\varepsilon=0$, the CFO estimation error matrix $\boldsymbol{E}$ will become an identity matrix. In such a scenario, according to (5-36), $\boldsymbol{c}=[1,0...0]^T$, and thus the system becomes MAI-free with an output SINR given by

$$\text{SINR}=\frac{\sigma_1^2}{\sigma_n^2\left[\left(\boldsymbol{B}^H\boldsymbol{B}\right)^{-1}\right]_{1,1}}. \tag{5-37}$$

Consequently, the zero-forcing detector is MAI-free provided that the CFO estimation is accurate enough. According to the relation between MMSE and zero-forcing schemes, MMSE can be also regarded as MAI-free in high SNR region.

B. Complexity Analysis

System complexity is an important concern in practical implementations. As an expected advantage, the proposed zero forcing and MMSE detectors, including MAI suppression, CFO compensation and FFT demodulation, have low complexity due to the reduced processing dimension. To demonstrate this, complexity will be analyzed

and compared with the PIC detector proposed in [27]. The number of complex multiplications involved in FFT demodulation, CFO compensation and MAI suppression is adopted as the metric for complexity comparison.

With u active users in system, the amount of complex multiplications required by the zero-forcing and MMSE detectors are shown in Table 5-1.

TABLE 5-1. COMPLEXITY IN TERMS OF MULTIPLICATIONS

Zero Forcing	$U^3 + U^2P + u^3 + Uu^2 + \left(3U^2 + U + P^2 + P\log_2 P\right)u$
MMSE	$U^3 + U^2P + \left(2U^2 + U + P^2 + P\log_2 P\right)u$

U is the number of subchannels, P is the number of subcarriers used by each user.

With the same system setup, the PIC detector [27] normally has higher complexity because it deploys circular convolution, instead of FFT, for CFO compensation. The study tried to reduce complexity by truncating the convolution vector, and obtained a complexity of

$$\frac{N}{2}\log_2 N + 2x_{\mathrm{I}}PuJ\,, \tag{5-38}$$

where J is the length of the truncated convolution vector, and x_{I} is the number of PIC iterations. As described therein, (5-38) is valid provided that J is much smaller than N. However, the value of J depends on users' CFO. If the users' CFOs exceed 20% of the subcarrier spacing, the value of J becomes large and the complexity will be much larger than that given by (5-38).

To illustrate the complexity advantage of the proposed detectors, a 512-subcarrier 16-subchannel interleaved OFDMA system is considered. Fig.5.5 plots the number of complex multiplications against the number of users for the PIC, ZF and MMSE

detectors. Obviously, ZF and MMSE detectors have much lower complexity than PIC detector. Moreover, it can be seen that the proposed schemes is particularly suitable for the system with a relatively large number of users.

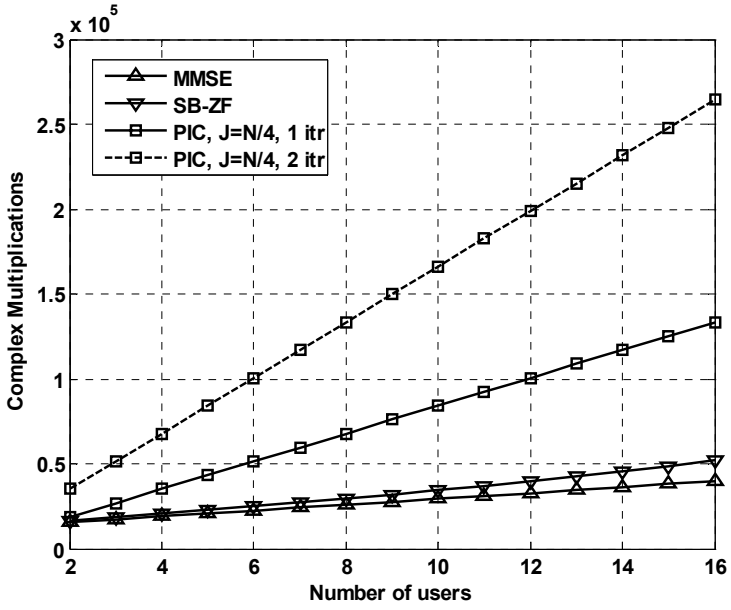

Fig.5.5: Complexity comparison for the PIC, SB-ZF and MMSE detectors in an interleaved OFDMA system with $N = 512$, $Q = 16$ and $P = 32$.

C. Adaptive Implementation of MMSE MAI Suppression

Adaptive MMSE algorithms attract considerable interest due to its lower complexity and its capability to track slow channel variations. Adaptive algorithms have been extensively studied since early 1940s, and widely used in the signal processing and communication fields. In this dissertation, an adaptive Least Mean Square (LMS) algorithm is developed for the unconstrained MMSE and constrained MMSE schemes to find out the difference made by the a linear constraint. Table 5-2 presents the LMS algorithm for these two MMSE schemes.

TABLE 5-2. LMS ALGORITHMS FOR MAI SUPPRESSION

UNCONSTRAINED LMS
Set $\boldsymbol{w}_u(0) = \boldsymbol{b}_u$, for all $u = 1,2,\ldots U$
$\boldsymbol{w}_u(k+1) = \boldsymbol{w}_u(k) + \mu\left[\boldsymbol{YD}(-\varepsilon_u)\boldsymbol{F}_u^H(\sigma_u\boldsymbol{H}_u\boldsymbol{X}_u)^* - \boldsymbol{YY}^H\boldsymbol{w}_u(k)\right]$
CONSTRAINED LMS
Set $\boldsymbol{w}_u(0) = \boldsymbol{b}_u$, for all $u = 1, 2\ldots U$
$\boldsymbol{w}_u(k+1)$ $= \boldsymbol{w}_u(k) + \mu\left(\boldsymbol{I} - \boldsymbol{b}_u\boldsymbol{b}_u^H\right)\boldsymbol{Y}\left[\boldsymbol{D}(-\varepsilon_u)\boldsymbol{F}_u^H(\sigma_u\boldsymbol{H}_u\boldsymbol{X}_u)^* - \boldsymbol{Y}^H\boldsymbol{w}_u(k)\right] + \boldsymbol{b}_u\left[1 - \boldsymbol{b}_u^H\boldsymbol{w}_u(k)\right]$

To compare, the constrained and unconstrained LMS algorithms are simulated in a decision-directed† mode in a 3-ray multipath slow Rayleigh fading channel. Fig.5.6(a) shows their output SINR convergence curves. Due to the error propagation problem, unconstrained LMS takes much longer time to converge. In Fig.5.6(b), an abrupt channel change is added in the simulation. Again, as a result of error propagation, the unconstrained LMS converges to a solution quite far away from the optimum, whereas the constrained algorithm is able to efficiently recover and converge to a favorable solution close to the optimum. The robustness of the constrained algorithm stems from the linear constraint, which protects the energy of the desired signal from deteriorating severely when decision errors occur.

† Decision directed adaptation: an adaptive method that uses the hard decisions into the training sequence.

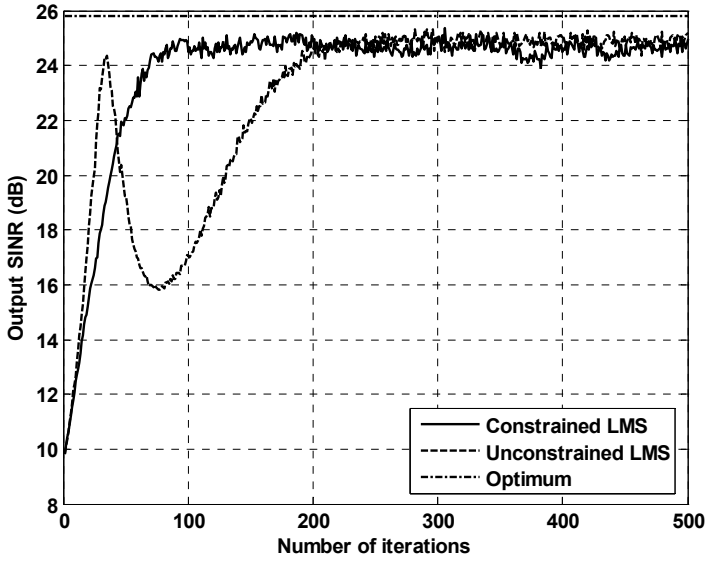

(a)

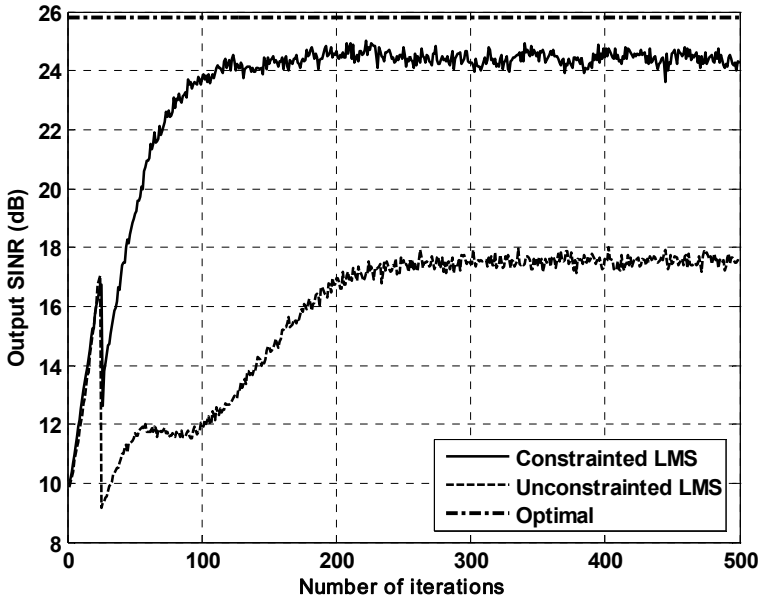

(b)

Fig.5.6. Performance comparison between the constrained and unconstrained LMS algorithms in a decision-directed mode. (a) Convergence curve in a static channel. (b) Recovery curve in the presence of channel change.

5.3 Numerical Results

This section presents some simulation results to demonstrate performance of the proposed detectors. A 128-subcarrier 4-subchannel interleaved OFDMA system is used in the simulation. In Example 1, Example 2, Example 3, the proposed MMSE detector

is simulated with CFO values fixed as 0.12, -0.15, 0.2 and 0.25 for the four users. The PIC scheme proposed in [27] is also simulated and compared with the MMSE scheme. When simulating the PIC scheme, two PIC iterations are used to suppress MAI. In Example 4, to demonstrate performance in a more realistic scenario, the MMSE scheme is simulated by modeling users' CFOs as independent random variables. Finally in Example 5, the proposed ZF and MMSE schemes are compared. Channel coding has not been used in all the results to be presented.

Example 1. Multipath Rayleigh Fading Channel with QPSK Modulation

In this simulation, the wireless channel is modeled as multipath Rayleigh fading with 3-ray delay spread. QPSK is used for modulation. All the users locate within a circular area of 10m radius surrounding the BS. Specifically, the desired user locates at a distance of 5m from the BS, and the other three users are uniformly distributed. To examine the immunity to near-far effects, BER is simulated under both perfect and imperfect power control. From the results shown in Fig.5.7, it can be seen that the PIC scheme has an error floor, which becomes much higher in the absence of power control. In contrast, the MMSE scheme has no error floor, and is able to maintain its performance when there is no power control. This result reveals that the MMSE scheme is able to effectively combat near-far effects, and using such a scheme, the stringent requirement on power control can be relaxed.

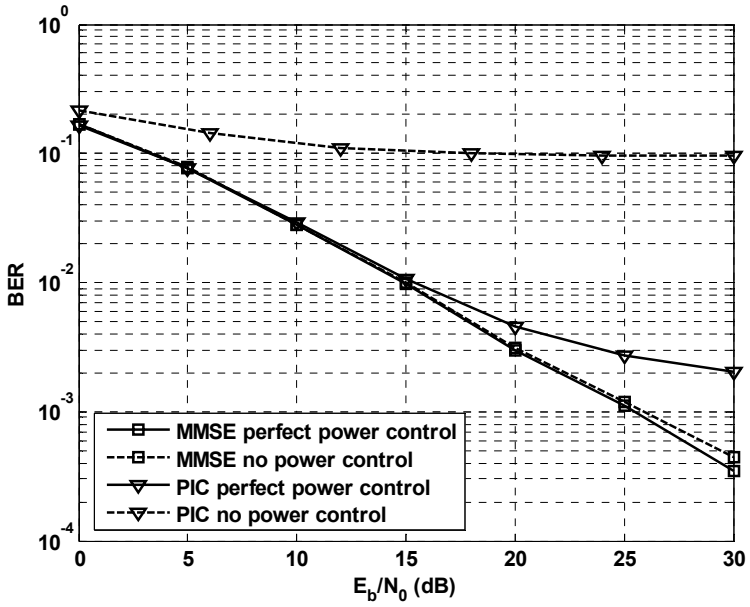

Fig.5.7: BER performance comparison of the MMSE and PIC detectors with and without power control.

In order to see how system load affects performance, BER is simulated for different number of users under perfect power control and shown in Fig.5.8. Clearly, compared with the PIC scheme, the MMSE scheme has smaller performance degradation when system load increases. Thus, by using the proposed MMSE detector, an existing user in the system will be less affected by the admission of new users.

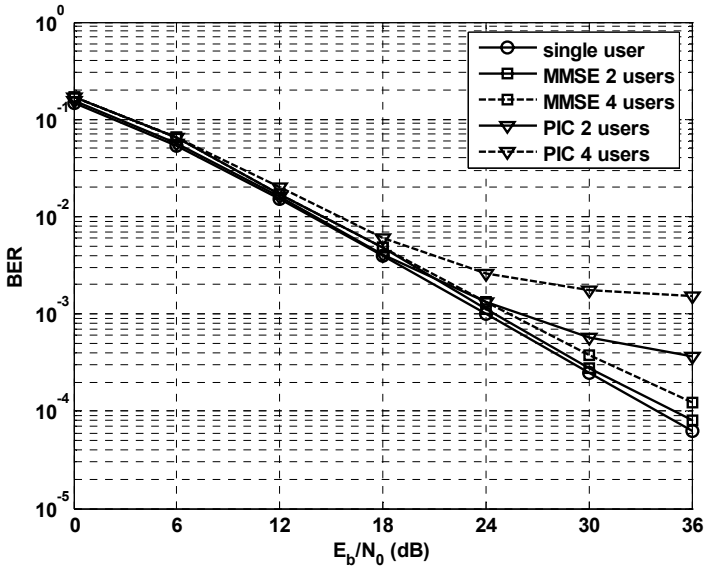

Fig.5.8: BER performance for different number of users under perfect power control

Example 2. Multipath Rayleigh Fading Channel with $\pi/4$ - DQPSK modulation

In this example, time-varying multipath fading channel is considered. The channel is modeled as 2-ray Rayleigh fading with 1-sample delay spread and 20Hz Doppler frequency offset. $\pi/4$-DQPSK modulation with differential demodulation is used to avoid channel estimation. BER performance is simulated at 0dB input SIR (perfect power control) and -20dB input SIR (imperfect power control). As can be seen from results shown in Fig.5.9, under perfect power control, the MMSE scheme outperforms the PIC scheme by 3dB at 5×10^{-3} BER. Furthermore, under imperfect power control, the MMSE scheme is able to give roughly the same performance, while the PIC scheme has a severely degraded performance.

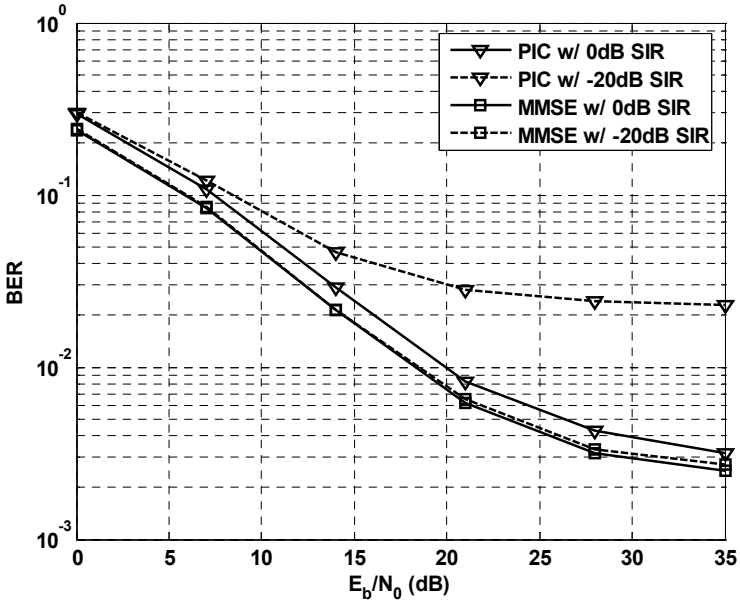

Fig.5.9: BER performance in a time-selective multipath Rayleigh fading channel with differential modulation

Example 3. Performance in the presence of CFO estimation error

To illustrate robustness of the proposed scheme to erroneous CFO estimation, users' CFO estimation error is modeled as independent zero mean Gaussian random variables

with a variance equal to the mean square error in CFO estimation. With the same setup as in Example 1, output SINR is plotted versus the CFO estimation standard deviation in Fig. 5.10.

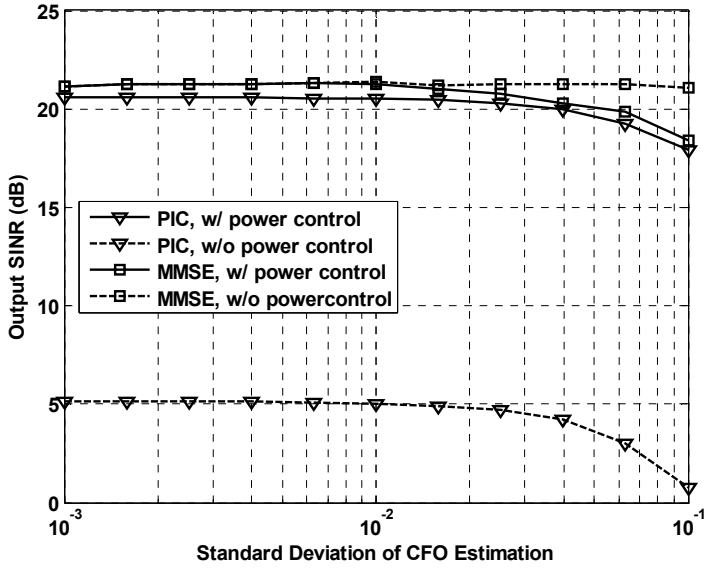

Fig. 5.10: Output SINR versus CFO estimation errors, $E_b/N_0 = 20\text{dB}$, Under imperfect power control, each of the interference users has a power 20dB higher than the desired user.

As can be seen, under perfect power control, the MMSE and PIC schemes have approximately the same resistance to CFO estimation errors. However, when power control is imperfect, the MMSE scheme becomes more robust to CFO estimation errors than the PIC scheme. Furthermore, by comparing the resistance of MMSE in the two scenarios, it can be seen that the MMSE scheme becomes less resistant to CFO estimation errors when the interference becomes weaker. This is because the MMSE scheme attempts to minimize the output power and retain the desired user's signal. When there is a CFO estimation error, the desired user may therefore also appear as interference and get cancelled out in an effect similar to that of incidental cancellation in antenna arrays [102][103]. To further improve the resistance, quadratic constraints can be introduced to give a more reasonable response to the desired user even if its signature

vector is not perfect [104].

To see how the interference power affects the resistance of the proposed scheme, it is assumed that the desired user has the same input SIR over each of the interference users at the receiver. Output SINR is plotted against input SIR with CFO estimation in Fig. 5.11. Specifically, the deterministic CFO estimation scheme proposed in [20] is used. As can been seen, the MMSE detector has a reasonably good performance over a broad range of input SIR. In the weak interference region, degradation caused by CFO estimation errors is insignificant. Note that, when the interference is weak, the PIC scheme outperforms the MMSE scheme by 2dB. This reveals a small noise enhancement price paid by using the MMSE scheme.

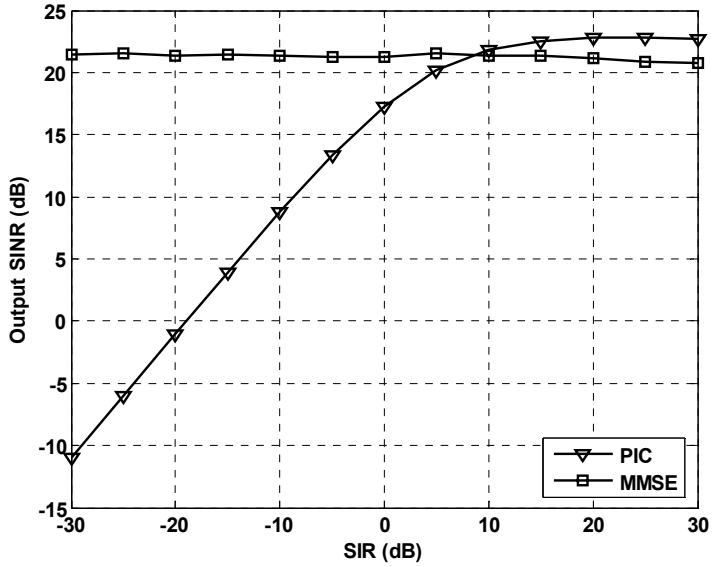

Fig. 5.11: Output SINR versus input SIR with CFO estimation, $E_b/N_0 = 20\text{dB}$.

Example 4. Random CFO Test

To demonstrate the feasibility of the proposed scheme in a realistic scenario, users' CFOs are modeled as independent random variables uniformly distributed in the range $(-\varepsilon, \varepsilon)$. BER is plotted against E_b/N_o for different values of ε. System setup is

the same as that in Example 1. As can be seen from Fig.5.12, with CFO up to 25% of the subcarriers spacing, BER performance exhibits only 0.5dB degradation. In IEEE802.16 standard, the requirement on the CFO after coarse synchronization is limited to 2%. Clearly, by using the proposed scheme, stringent requirement on coarse frequency synchronization can also be relaxed.

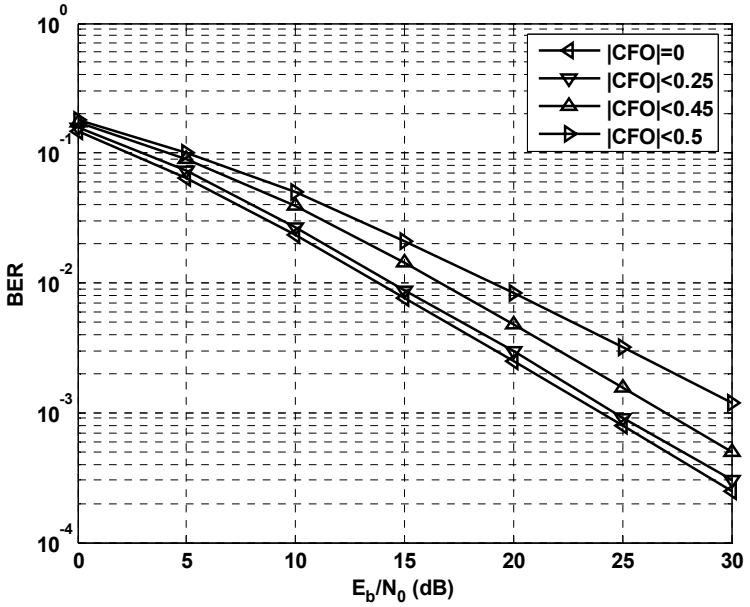

Fig.5.12: BER performance under random CFO test. When $|\varepsilon| \to 0.5$, different users may become so close that they can hardly be separated, and severe performance degradation can be seen.

Example 5. Comparison between ZF and MMSE

Finally, performance of the proposed ZF and MMSE detectors are compared. It is assumed that the desired user has the same input SIR over each of the interference users. BER is plotted against the input ISR at different E_b/N_o in Fig.5.13. It can be seen that the ZF scheme has a constant BER over the whole ISR range, whereas BER of the MMSE scheme has an upper bound lay by ZF in strong interference region. Moreover, performance gap between the two schemes decreases as E_b/N_o increases. This is in

agreement with our discussion in Section 5.2.3 that the ZF and MMSE schemes have the same asymptotic performance.

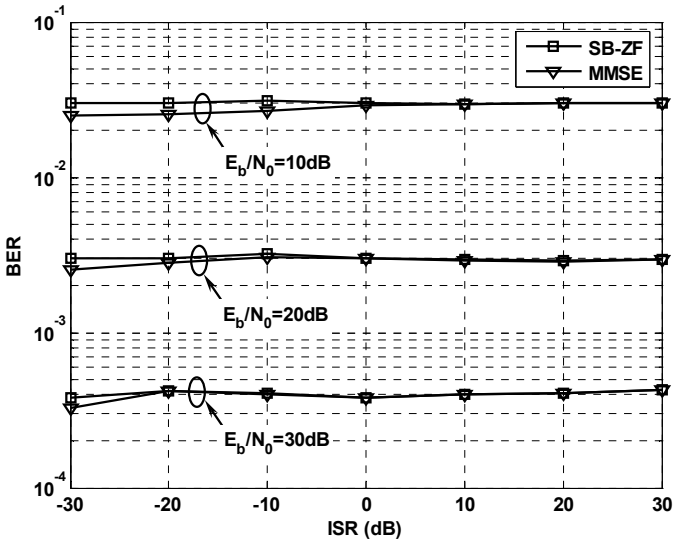

Fig.5.13: BER performance of the SB-ZF and the MMSE scheme under different E_b/N_0 .

Chapter 6

Conclusions and Future Work

6.1 Conclusions

This dissertation mainly considered the physical layer design of OFDMA systems uplink, with the emphasis on two crucial issues: channel estimation and signal detection.

The study started from the issue of ICI suppression. The first contribution of this work is that the scope of study has been extended from static or semi static multipath fading channels to time-variant multipath fading channels. This extension has its practical significance since OFDMA has been appointed to support mobile communications in 4G systems and the channel cannot be assumed to be static or semi-static if velocity of motion is moderate or high. A signal model has been formulated in the presence of channel variations. Particularly, an OFDMA symbol block received at the base station has a linear relation with the transmitted multiuser OFDMA symbol block. Based on this signal model, typical linear detection schemes and nonlinear schemes have been investigated. MMSE and MMSE-SD techniques are proposed to suppress ICI, as they are capable of effectively suppressing ICI and background noise from the multiuser signal. Moreover, the MMSE-SD scheme is able to exploit the time diversity owned by time-variant channels. By using MMSE-SD, faster channel variation will lead to better system performance. It has also been found

that most of the current CFO compensation-based ICI suppression schemes are in fact performing matched filtering and thus become a special case of the framework built in this dissertation. In Chapter 5, the interleaved OFDMA system is particularly considered, as this system has been shown to be preferred for most of the mobile applications [7][10]. In such a system, each received OFDMA block can be rearranged into a matrix form and the ICI suppression schemes formulated on the basis of this novel signal model has much smaller detection dimension and thus lower complexity. A parallel detection structure, in which the MAI suppression is performed prior to FFT demodulation, is proposed. Since CFO and CIR are requisite knowledge to ICI suppression, post-suppression SINR has also been analytically studied in the presence of erroneous CFO and channel estimation. The results demonstrate that the proposed ICI suppression scheme is robust to the estimation error raised from commonly used CFO and channel estimators.

In Chapter 4, another crucial issue in physical layer design, channel estimation, is considered. BEM-based signal model has been developed to transform rapid time-varying CIR into slow varying BEM coefficients. A time-domain pilot pattern has been proposed for possible use in OFDMA uplink to avoid accuracy drop caused by interference in frequency domain. Least Square, Maximum Likelihood and LMMSE channel estimation schemes have been studied and compared. As one example of the frequency-domain pilot patterns, a BEM-based Least Square estimator is also developed upon the pilot pattern used in WiMAX systems. Cramer-Rao Lower Bounds have been derived for the Least Square estimators. Both analytical and simulation

results demonstrate the performance improvement can be obtained from the proposed time-domain estimation.

6.2 Future Work

Although this dissertation tried to completely study the issue of physical layer design for OFDMA systems uplink transmission. There are still some open topics or possible problems worthy of further research.

First, as mentioned in Chapter 3, the proposed MMSE and MMSE-SD ICI suppression schemes obtain significant performance improvement at the cost of complexity. To make them practically feasible, low-complexity algorithms should be further developed. Notable studies that may help on solving this issue can be found in [105]-[108].

Second, in the discussion of BEM-based estimation schemes, it has been shown that the oversampling index g is related to the estimation accuracy. Specifically, if the value of g is too large, the number of BEM coefficients will exceed the number of pilots and thus the performance will be decreased. On the other hand, for a channel that shows obvious but not severe Doppler spread, if g is too small, the number of bases may not be enough to well approximate the CIR, and again the performance will be affected. Therefore, the value of g should be carefully selected for different channel conditions. How to choose this value based on Doppler spread f_dT , and whether there is an optimal value for g are worthy of further investigation.

Third, the time-domain pilot pattern proposed in this dissertation only makes use

of the timer-domain correlation. Making use of frequency-domain correlation has not been considered yet. In OFDMA system, this is important because:

1. Exploiting frequency-domain correlation saves time that used transmitting pilots and thus helps increasing data efficiency.
2. In OFDMA systems, subcarrier allocation is a popular strategy used to exploit the multiuser diversity and increase system capacity. If adaptive subcarrier allocation is enabled, a subcarrier may be used by different users at different moments.

Therefore, how to design a flexible frequency-domain pilot pattern so that it can be used with adaptive subcarrier allocation schemes is an important and interesting issue to be further studied. Some notable recent studies on the issue of pilot design for OFDMA systems can be found in [109]-[111].

Finally, all the study in this dissertation is based on a single antenna system. The use of multiple antennas (or antennas array) has not been covered yet. A wireless transmitter or receiver equipped with multiple antennas is able to exploit the spatial diversity via space-time coding or suppress the interference via beamforming. The use of multiple antennas extends the two-dimension radio resource (time, frequency) to three-dimension (space, time and frequency). A benefit introduced by spatial processing is that the data rate and spectrum efficiency can be significantly increased [112]. Therefore, combining antennas array is a clear trend in developing future wireless systems, especially OFDM-based systems. For example, in latest IEEE802.16e standard Multiple Input Multiple Output (MIMO) is introduced as a

physical layer technique to be used with OFDMA. To this end, it is of considerable interest to study the use of antennas array in OFDMA systems, particularly in the following directions:

1. ICI suppression through Beamforming

The study presented in this work has covered suppressing ICI in the time and frequency domain. When antennas array is available, array processing techniques, which have been widely studied in the last several decades [113]-[115], can be borrowed to suppression ICI in the spatial domain. More specifically, for one desired user, the ICI from other users can be blocked by placing the array's zero-lobe towards interference users. Clearly, this will disable the simultaneous multiuser detection. How to make use of TDMA together with beamforming in OFDMA system, or, how to arrange the user detection in space, time and frequency domains is still to be investigated.

2. Low-complexity Channel Estimation in a MIMO-OFDMA system

Although MIMO is capable of bringing an amount of benefits, it also brings more channel parameters to estimate. How to design a proper pilot pattern for a MIMO-OFDMA system and estimate the channel with reasonable computational load deserves further investigation. A recent notable contribution on this issue can be found in [117] and [118].

All the issues discussed in this section are still open or developing. Undoubtedly, deeper investigations on these issues will help accelerate the commercialization of OFDMA-based technologies in wireless industry.

Appendix A

Noise Power after Linear Detection

For $N \times N$ matrix $\boldsymbol{A}$ given in (3-19), its rank $r \le N$. It can be decomposed via Singular Value Decomposition (SVD) into

$$\boldsymbol{A} = \boldsymbol{U}\boldsymbol{\Lambda}\boldsymbol{V}^H, \tag{A-1}$$

where $\boldsymbol{\Lambda}$ is a diagonal matrix containing all the singular values, $\boldsymbol{U}$ and $\boldsymbol{V}$ are unitary matrices contains left- and right-singular vectors. From (A-1), the power of noise after linear detection can be derived as below:

1. Matched Filtering

After MF detection, noise vector is given by $\boldsymbol{z}_{p,\mathrm{MF}} = \boldsymbol{A}^H \boldsymbol{Z}$, and its autocorrelation matrix is given by

$$\begin{aligned} \boldsymbol{R}_{\mathrm{MF}} &= \mathbb{E}(\boldsymbol{A}^H \boldsymbol{Z}\boldsymbol{Z}^H \boldsymbol{A}) \\ &= \sigma_n^2 \boldsymbol{A}^H \boldsymbol{A} \\ &= \boldsymbol{V}\sigma_n^2 \boldsymbol{\Lambda}^H \boldsymbol{\Lambda} \boldsymbol{V}^H \end{aligned} . \tag{A-2}$$

2. Zero Forcing

The noise vector after ZF detection is given by

$$\boldsymbol{z}_{p,\mathrm{ZF}} = (\boldsymbol{A}^H \boldsymbol{A})^{-1} \boldsymbol{A}^H \boldsymbol{Z} . \tag{A-3}$$

Autocorrelation matrix of this noise is given by

$$\begin{aligned} \boldsymbol{R}_{\mathrm{ZF}} &= \sigma_n^2 (\boldsymbol{A}^H \boldsymbol{A})^{-1} \\ &= \sigma_n^2 \boldsymbol{V} (\boldsymbol{\Lambda}^H \boldsymbol{\Lambda})^{-1} \boldsymbol{V} \end{aligned} . \tag{A-4}$$

3. MMSE

For MMSE, the weight matrix can be re-written as

$$\boldsymbol{W}_{\text{MMSE}} = \boldsymbol{V}\left(\frac{\sigma_n^2}{\sigma_s^2}\boldsymbol{I} + \boldsymbol{\Lambda}^H\boldsymbol{\Lambda}\right)^{-1}\boldsymbol{\Lambda}^H\boldsymbol{U}^H . \tag{A-5}$$

The noise autocorrelation matrix is given by

$$\begin{aligned}\boldsymbol{R}_{\text{MMSE}} &= \sigma_n^2\left(\boldsymbol{W}_{\text{mmse}}^H\boldsymbol{W}_{\text{mmse}}\right)^{-1} \\ &= \boldsymbol{U}\boldsymbol{\Lambda}\left(\frac{\sigma_n}{\sigma_s^2}\boldsymbol{I} + \sigma_n^{-1}\boldsymbol{\Lambda}^H\boldsymbol{\Lambda}\right)^{-2}\boldsymbol{\Lambda}^H\boldsymbol{U}^H .\end{aligned} \tag{A-6}$$

Eigenvalues of (A-2), (A-4) and (A-6) are the noise power on different subcarriers.

□

Appendix B

Proof of the Lemma

Since matrix $\boldsymbol{G}$ is invertible, premultiplying $\boldsymbol{G}^{-1}$ on both sides of the lemma leads to

$$\boldsymbol{E}^H\left(\boldsymbol{E}\boldsymbol{G}\boldsymbol{E}^H+\sigma^2\boldsymbol{I}\right)^{-1}=\left(\boldsymbol{E}^H\boldsymbol{E}\boldsymbol{G}+\sigma^2\boldsymbol{I}\right)^{-1}\boldsymbol{E}^H, \tag{B-1}$$

which will be proved below as an equivalent of the lemma.

1. If $\boldsymbol{E}$ is nonsingular

   From the Right Hand Side (RHS) of (B-1), we have

$$\begin{aligned}\text{RHS}&=\left(\boldsymbol{E}^H\boldsymbol{E}\boldsymbol{G}\boldsymbol{E}^H\boldsymbol{E}^{-H}+\sigma^2\boldsymbol{I}\right)^{-1}\boldsymbol{E}^H\\&=\boldsymbol{E}^H\left(\boldsymbol{E}\boldsymbol{G}\boldsymbol{E}^H+\sigma^2\boldsymbol{I}\right)^{-1}\boldsymbol{E}^{-H}\boldsymbol{E}^H=\text{LHS}\end{aligned}$$

   Therefore, (B-1) is true if $\boldsymbol{E}$ is nonsingular.

2. If $\boldsymbol{E}$ is singular

   It follows from Woodbury matrix inverse formula that

$$\left(\boldsymbol{E}\boldsymbol{G}\boldsymbol{E}^H+\sigma^2\boldsymbol{I}\right)^{-1}=\frac{1}{\sigma^2}\boldsymbol{I}-\frac{1}{\sigma^2}\boldsymbol{E}\boldsymbol{G}\left(\boldsymbol{E}^H\boldsymbol{E}\boldsymbol{G}+\sigma^2\boldsymbol{I}\right)^{-1}\boldsymbol{E}^H, \tag{B-2}$$

$$\left(\boldsymbol{E}^H\boldsymbol{E}\boldsymbol{G}+\sigma^2\boldsymbol{I}\right)^{-1}=\frac{1}{\sigma^2}\boldsymbol{I}-\frac{1}{\sigma^2}\boldsymbol{E}^H\left(\boldsymbol{E}\boldsymbol{G}\boldsymbol{E}^H+\sigma^2\boldsymbol{I}\right)^{-1}\boldsymbol{E}\boldsymbol{G}. \tag{B-3}$$

Let $\boldsymbol{B}_1$ and $\boldsymbol{B}_2$ denote the LHS and RHS of (B-1). It then follows from (B-2) and (B-3) that

$$\boldsymbol{B}_1=\frac{1}{\sigma^2}\boldsymbol{E}^H-\frac{1}{\sigma^2}\boldsymbol{E}^H\boldsymbol{E}\boldsymbol{G}\boldsymbol{B}_2, \tag{B-4}$$

$$\boldsymbol{B}_2=\frac{1}{\sigma^2}\boldsymbol{E}^H-\frac{1}{\sigma^2}\boldsymbol{B}_1\boldsymbol{E}\boldsymbol{G}\boldsymbol{E}^H. \tag{B-5}$$

Cancelling $\boldsymbol{B}_2$ in (B-4) and $\boldsymbol{B}_1$ in (B-5), we have

$$\boldsymbol{B}_1 = \frac{1}{\sigma^2}\boldsymbol{E}^H - \frac{1}{\sigma^4}\boldsymbol{E}^H\boldsymbol{E}\boldsymbol{G}\boldsymbol{E}^H + \frac{1}{\sigma^4}\boldsymbol{E}^H\boldsymbol{E}\boldsymbol{G}\boldsymbol{B}_1\boldsymbol{E}\boldsymbol{G}\boldsymbol{E}^H, \tag{B-6}$$

$$\boldsymbol{B}_2 = \frac{1}{\sigma^2}\boldsymbol{E}^H - \frac{1}{\sigma^4}\boldsymbol{E}^H\boldsymbol{E}\boldsymbol{G}\boldsymbol{E}^H + \frac{1}{\sigma^4}\boldsymbol{E}^H\boldsymbol{E}\boldsymbol{G}\boldsymbol{B}_2\boldsymbol{E}\boldsymbol{G}\boldsymbol{E}^H. \tag{B-7}$$

Denoting $\boldsymbol{B}_1 - \boldsymbol{B}_2$ by $\boldsymbol{\Delta}$, subtracting (B-7) from (B-6) leads to

$$\boldsymbol{\Delta} = \frac{1}{\sigma^4}\boldsymbol{E}^H\boldsymbol{E}\boldsymbol{G}\boldsymbol{\Delta}\boldsymbol{E}\boldsymbol{G}\boldsymbol{E}^H. \tag{B-8}$$

Since $\boldsymbol{E}$ has full column rank, $\boldsymbol{E}^H\boldsymbol{E}\boldsymbol{G}$ is invertible. (B-8) implies that

$$\operatorname{rank}(\boldsymbol{\Delta}) = \operatorname{rank}\left(\boldsymbol{\Delta}\boldsymbol{E}\boldsymbol{G}\boldsymbol{E}^H\right). \tag{B-9}$$

Since $\boldsymbol{E}$ is singular, (B-9) is true iff

$$\operatorname{rank}(\boldsymbol{\Delta}) = 0, \tag{B-10}$$

which indicates $\boldsymbol{\Delta} = \boldsymbol{0}$, and thus $\boldsymbol{B}_1 = \boldsymbol{B}_2$. Therefore, (B-1) is also true if $\boldsymbol{E}$ is singular, and thus the lemma follows.

□

Appendix C

Calculation of the BEM Autocorrelation Matrix $\boldsymbol{R}$

The BEM coefficients can be modeled as zero-mean complex Gaussian random variables. Since BEM coefficients of different paths are assumed to be independent, it is obvious that in matrix $\boldsymbol{R}$, only the entries associated with the same path is nonzero. Therefore, calculating the autocorrelation matrix for each path will generate all the non-zero entries in $\boldsymbol{R}$. For the l-th path of user u, one can collect the CIR samples during the time interval $[0, N_t]$ to form a column vector. From (4-5), this vector is mathematically given by

$$\boldsymbol{h}_u(l) = \boldsymbol{T}\boldsymbol{a}_u(l), \tag{C-1}$$

where

$$\boldsymbol{a}_u(l) = \left[a_u(-Q;l), a_u(-Q+1;l), \ldots a_u(Q;l)\right]^T \tag{C-2}$$

is the BEM coefficients of the l-th path of user u, and

$$\boldsymbol{T} = \begin{bmatrix} t(0,-Q) & t(0,-Q+1) & \ldots & t(0,Q) \\ t(1,-Q) & t(1,-Q+1) & \ldots & t(1,Q) \\ \ldots & \ldots & \ldots & \ldots \\ t(N_t,-Q) & t(N_t,-Q+1) & \ldots & t(N_t,Q) \end{bmatrix} \tag{C-3}$$

is the bases matrix corresponding to the time interval $[0, N_t]$, with the q-th basis given by

$$t(n,q) = \exp\left(\frac{j2\pi qn}{\lambda N}\right). \tag{C-4}$$

Following this, the relation between the CIR autocorrelation matrix and the BEM coefficient autocorrelation matrix is given by

$$\mathbb{E}\left\{\boldsymbol{h}_u(l)\boldsymbol{h}_u^H(l)\right\} = \boldsymbol{T}\boldsymbol{R}_u(l)\boldsymbol{T}^H . \quad \text{(C-5)}$$

where $\boldsymbol{R}_u(l) = \mathbb{E}\left\{\boldsymbol{a}_u(l)\boldsymbol{a}_u^H(l)\right\}$ is the BEM autocorrelation matrix of the l-th path of user u. In (C-5), the autocorrelation matrix $\mathbb{E}\left\{\boldsymbol{h}_u(l)\boldsymbol{h}_u^H(l)\right\}$ can be calculated for different models of the time-varying channel. For the most well-known Jake's model, the entries in $\mathbb{E}\left\{\boldsymbol{h}_u(l)\boldsymbol{h}_u^H(l)\right\}$ can be calculated from

$$\phi_t(\Delta t) = J_0(2\pi f_d \Delta t), \quad \text{(C-6)}$$

where J_0 is the zero-order Bessel function of the first kind. Consequently, by taking $N_t > 2Q$, $\boldsymbol{R}_u(l)$ can be calculated by

$$\boldsymbol{R}_u(l) = \boldsymbol{T}^{+}\mathbb{E}\left\{\boldsymbol{h}_u(l)\boldsymbol{h}_u^H(l)\right\}\left(\boldsymbol{T}^H\right)^{+}, \quad \text{(C-7)}$$

where $\boldsymbol{T}^{+}$ is the Moore-Penrose pseudo inverse of matrix $\boldsymbol{T}$. From (C-6) and (C-7), $\boldsymbol{R}_u(l)$ can be calculated for all the paths. Therefore, all the nonzero entries in the matrix $\boldsymbol{R}$ can be finally determined.

□

Appendix D

Calculation of Correlation Matrices (4-26) and (4-27)

The definition of $\hat{\boldsymbol{\mathcal{H}}}$ given by (4-24b) can be rewritten as

$$\hat{\boldsymbol{\mathcal{H}}} = \boldsymbol{\mathcal{H}} + \Delta\boldsymbol{\mathcal{H}}, \tag{D-1}$$

where

$$\boldsymbol{\mathcal{H}} = \left[\boldsymbol{h}_u(j,l)^T, \boldsymbol{h}_u(j+M+1,l)^T \ldots \boldsymbol{h}_u(j+KM+K,l)^T \right]^T \tag{D-2}$$

is the same vector formed by actual channel responses and $\Delta\boldsymbol{\mathcal{H}}$ stands for the estimation error vector. Specifically, the elements in $\Delta\boldsymbol{\mathcal{H}}$ can be modeled as zero-mean complex Gaussian random variables with variance σ^2 being MSE of the CIR estimation in pilot blocks.

Following (D-1), the correlation matrices given by (4-26) and (4-27) can be calculated as

$$\begin{aligned} \boldsymbol{R}_{\hat{\mathcal{H}}\hat{\mathcal{H}}} &= \mathbb{E}\left[\hat{\boldsymbol{\mathcal{H}}} \hat{\boldsymbol{\mathcal{H}}}^H \right] \\ &= \mathbb{E}\left[\boldsymbol{\mathcal{H}} \boldsymbol{\mathcal{H}}^H \right] + \mathbb{E}\left[\Delta\boldsymbol{\mathcal{H}} \Delta\boldsymbol{\mathcal{H}}^H \right], \\ &= \boldsymbol{R}_{\mathcal{H}\mathcal{H}} + \sigma^2 \boldsymbol{I} \end{aligned} \tag{D-3}$$

$$\begin{aligned} \boldsymbol{R}_{d\hat{\mathcal{H}}} &= \mathbb{E}\left[\boldsymbol{h}_u(d,l) \hat{\boldsymbol{\mathcal{H}}}^H \right] \\ &= \mathbb{E}\left[\boldsymbol{h}_u(d,l) \boldsymbol{\mathcal{H}}^H \right] + \mathbb{E}\left[\boldsymbol{h}_u(d,l) \right] \mathbb{E}\left[\Delta\boldsymbol{\mathcal{H}}^H \right], \\ &= \mathbb{E}\left[\boldsymbol{h}_u(d,l) \boldsymbol{\mathcal{H}}^H \right] \end{aligned} \tag{D-4}$$

where the second equalities in (D-3) and (D-4) follow the reasonable assumption that $\boldsymbol{\mathcal{H}}$ and $\Delta\boldsymbol{\mathcal{H}}$, $\boldsymbol{h}_u(d,l)$ and $\Delta\boldsymbol{\mathcal{H}}$ are statistically independent. In (D-3) and (D-4), $\boldsymbol{R}_{\mathcal{H}\mathcal{H}}$ and $\mathbb{E}\left[\boldsymbol{h}_u(d,l) \boldsymbol{\mathcal{H}}^H \right]$ simply consist of channel correlation coefficients, which can be easily calculated based on the knowledge of channel statistics. For example, in

the well-known Jake's model, correlation coefficient can be determined as given by

$$\varphi(\Delta t) = J_0(2\pi f_d \Delta t). \tag{D-5}$$

□

Appendix E

Derivation of Subspace ZF MAI Suppression

First, using Lagrange multiplier, solution of (5-20) can be easily shown to be

$$\boldsymbol{w}_{\text{ZF}}=\frac{\left(\boldsymbol{A}\mathbb{E}\left\{\boldsymbol{S}\boldsymbol{S}^{H}\right\}\boldsymbol{A}^{H}\right)^{-1}\boldsymbol{a}_{u}}{\boldsymbol{a}_{u}^{H}\left(\boldsymbol{A}\mathbb{E}\left\{\boldsymbol{S}\boldsymbol{S}^{H}\right\}\boldsymbol{A}^{H}\right)^{-1}\boldsymbol{a}_{u}}. \tag{E-1}$$

Second, the autocorrelation matrix $\boldsymbol{R}$ can be expressed in a subspace decomposition form as

$$\begin{aligned}\boldsymbol{R}&=\boldsymbol{A}\mathbb{E}\left\{\boldsymbol{S}\boldsymbol{S}^{H}\right\}\boldsymbol{A}^{H}+\sigma_{n}^{2}\boldsymbol{I}\\&=\boldsymbol{U}_{\text{S}}\boldsymbol{\Lambda}_{\text{S}}\boldsymbol{U}_{\text{S}}^{H}+\boldsymbol{U}_{\text{N}}\boldsymbol{\Lambda}_{\text{N}}\boldsymbol{U}_{\text{N}}^{H},\end{aligned} \tag{E-2}$$

and thus

$$\boldsymbol{A}\mathbb{E}\left\{\boldsymbol{S}\boldsymbol{S}^{H}\right\}\boldsymbol{A}^{H}=\boldsymbol{U}_{\text{S}}\left(\boldsymbol{\Lambda}_{\text{S}}-\sigma_{n}^{2}\boldsymbol{I}\right)\boldsymbol{U}_{\text{S}}^{H}, \tag{E-3}$$

where

$$\boldsymbol{\Lambda}_{\text{S}}=\text{diag}[\lambda_{1}+\sigma_{n}^{2},\lambda_{2}+\sigma_{n}^{2},...\lambda_{U}+\sigma_{n}^{2}]$$

contains the eigenvalues of the signal subspace, $\boldsymbol{\Lambda}_{\text{N}}=\sigma_{n}^{2}\boldsymbol{I}$ contains the eigenvalues of the noise subspace; $\boldsymbol{U}_{\text{S}}$ and $\boldsymbol{U}_{\text{N}}$ contain the corresponding eigenvectors. Substituting (E-3) into (E-1), a Subspace Zero-Forcing (SB-ZF) solution can be obtained as given by

$$\boldsymbol{w}_{\text{SB-ZF}}=\frac{\boldsymbol{U}_{\text{S}}\left(\boldsymbol{\Lambda}_{\text{S}}-\sigma_{n}^{2}\boldsymbol{I}\right)^{-1}\boldsymbol{U}_{\text{S}}^{H}\boldsymbol{b}_{u}}{\boldsymbol{b}_{u}^{H}\boldsymbol{U}_{\text{S}}\left(\boldsymbol{\Lambda}_{\text{S}}-\sigma_{n}^{2}\boldsymbol{I}\right)^{-1}\boldsymbol{U}_{\text{S}}^{H}\boldsymbol{b}_{u}}. \tag{E-4}$$

□

Bibliography

[1]. J.A.C. Bingham, "Multicarrier Modulation for Data Transmission: An Idea Whose Time Has Come", *IEEE Communications Magazine*, Vol.28, No.5, pp.5-14, May, 1990.

[2]. Tero Ojanpera and Ramjee Prasad, "An overview of air interface multiple access for IMT-2000/UMTS", *IEEE Communications Magazine*, Vol.36, No.9, pp.82-95, September, 1998.

[3]. J. D. Vriendt, P. Lainé, C. Lerouge and X. F. Xu, "Mobile Network Evolution: A Revolution on the Move", *IEEE Communications Magazine*, Vol.40, No.4, pp.104-111, April, 2002.

[4]. K. J. Lu, Yi Qian and Hsiao-Hwa Chen, "Wireless Broadband Access: WiMAX and Beyond - A Secure and Service-Oriented Network Control Framework for WiMAX Networks", *IEEE Communications Magazine*, Vol.45, No.5, pp.124-130, May, 2007.

[5]. D. Niyato and E. Hossain, "Wireless Broadband Access: WiMAX and Beyond - Integration of WiMAX and WiFi: Optimal Pricing for Bandwidth Sharing", *IEEE Communications Magazine*, Vol.45, No.5, pp.140 – 146, May, 2007.

[6]. K. H. Teo, Z. F. Tao and J. Y. Zhang, "The Mobile Broadband WiMAX Standard [Standards in a Nutshell]", *IEEE Signal Processing Magazine*, Vol.24, No.5, pp.144-148, September, 2007.

[7]. H. Liu and G. Q. Li, *OFDM-Based Broadband Wireless Networks – Design and Optimization*, Wiley Inter-Science, 2005.

[8]. S. Hara and R. Prasad, "Overview of multicarrier CDMA", *IEEE Communications Magazine*, Vol.35, No.12, pp.126-133, Dec., 1997.

[9]. H. Rohling and R. Gruneid, "Performance comparison of different multiple access schemes for the downlink of an OFDM communication system", in *Proc. IEEE VTC 1997*, Vol.3, pp.1365-1369, May, 1997.

[10]. M. Y. Shen, G. Q. Li and H. Liu, "Effect of traffic channel configuration on the orthogonal frequency division multiple access downlink performance", *IEEE Trans. on Wireless Commun.*, Vol.4, No.4, pp.1901-1913, July, 2005.

[11]. P. Svedman, S. K. Wilson, L. J. Cimini, Jr. and Björn Ottersten, "Opportunistic Beamforming and Scheduling for OFDMA Systems", *IEEE Trans. on Commun.*,

Vol.55, No.5, May, 2007, pp.941 – 952.

[12]. Ian C. Wong and Brian L. Evans, “Optimal Downlink OFDMA Resource Allocation with Linear Complexity to Maximize Ergodic Rates”, *IEEE Trans. on Wireless Commun.*, Vol.7, No.3, pp.962-971, March, 2008.

[13]. M. Ergen, S. Coleri and P. Varaiya, “QoS aware adaptive resource allocation techniques for fair scheduling in OFDMA based broadband wireless access systems”, *IEEE Trans. on Broadcast.*, Vol.49, No.4, Dec., 2003, pp.362 – 370.

[14]. R. Laroia, S. Uppala, and J. Y. Li, “Designing a mobile broadband wireless access network”, *IEEE Signal Processing Magazine*, Vol.21, No.5, Sept., 2004, pp.20 – 28.

[15]. T. D. Nguyen and Y. N. Han, “A Proportional Fairness Algorithm with QoS Provision in Downlink OFDMA Systems”, *IEEE Commun. Letters*, Vol.10, No.11, Nov., 2006, pp.760 – 762.

[16]. Y. J. Chang, F. T. Chien anf Kuo, C.-C.J., “Cross-layer QoS Analysis of Opportunistic OFDM-TDMA and OFDMA Networks”, *IEEE Journal on Selected Areas in Communications,* Vol.25, No.4, May, 2007, pp.657 – 666.

[17]. M. Moeneclaey, M. V. Bladel and H. Sari, “Sensitivity of Multiple-Access Techniques to Narrow-band Interference”, *IEEE Trans., on Commun.*, Vol.49, No.3, Mar., 2001, pp.497 – 505.

[18]. J. J. Van de Beek, P. O. Borjesson, et al “A Time and Frequency Synchronization Scheme for Multiuser OFDM”, *IEEE J. Select. Areas Commun.*, Vol. 17, pp. 1900-1913, Nov. 1999.

[19]. M. Morelli, “Timing and Frequency Synchronization for the Uplink of an OFDMA Sytem”, *IEEE Trans. on Commun.,* Vol.52, No.2, Feb, 2004, pp.296-306.

[20]. Z. Cao, U. Tureli and Y. D. Yao, “Deterministic Multiuser Carrier-Frequency Offset Estimation for Interleaved OFDMA Uplink”, *IEEE Trans. on Commun.*, Vol. 52, No.9, Sep., 2004, pp.1585-1594.

[21]. S. Barbarossa, M. Pompili and G. B. Giannakis, “Time and Frequency Synchronization of Orthogonal Frequency Division Multiple Access Systems”, in *Proc., IEEE ICC 2001*, pp.1674-1678.

[22]. L Kuang, J Lu and Junli Zheng, “Non-pilot-aided Carrier Frequency Tracking for Uplink OFDMA Systems”, in *Proc. IEEE GLOBECOM '04*. pp. 3193-3196

[23]. A. M. Tonello, “Asynchronous Multicarrier Multiple Access: Optimal and Sub-optimal Detection and Decoding”, *Bell Labs Tech. J.*, Vol.7, No.3, 2003, pp 191-217.

[24]. A. M. Tonello and S. Pupolin, “Performance of Single User Detectors in Multitone Multiple Access Asynchronous Communications”, in *Proc. IEEE Veh. Tech. Conf.*, pp. 199-203, May 2002.

[25]. J. Choi, C. Lee, H. W. Jung and Y. H. Lee, “Carrier Frequency Offset Compensation for Uplink of OFDM-FDMA Systems”, *IEEE Commun. Letters*, Vol.4, No.12, Dec., 2000, pp.414-416.

[26]. H. Yoo and D. Hong, “Edge Sidelobe Suppressor Scheme for OFDMA Uplink Systems”, *IEEE Commun. Letters*, Vol. 7, No. 11, Nov. 2003, pp. 534 – 536.

[27]. D. Huang and K. B. Letaief, “An Interference-Cancellation Scheme for Carrier Frequency Offsets Correction in OFDMA systems”, *IEEE Trans. on Commun.*, Vol.53, No.7, July, 2005, pp.1155-1165.

[28]. Z. Cao, U. Tureli, and Y.D. Yao, “User separation and Frequency-Time Synchronization for the Uplink of Interleaved OFDMA”, *IEEE 36th Asilomar Conference on Signals, Systems and Computers*.

[29]. Z. Cao, U. Tureli and P. Liu, “Optimum Subcarrier Assignment for OFDMA Uplink”, *Conference Record of the Thirty-Seventh Asilomar Conference on Signals, Systems and Computers 2003*., Nov., 2003, pp.708 – 712.

[30]. D. Marabissi, R. Fantacci and S. Papini, “Robust Multiuser Interference Cancellation for OFDM Systems With Frequency Offset”, *IEEE Trans. on Wireless Commun.*, Vol.5, No.11, Nov, 2006, pp.3068 – 3076.

[31]. D. Sreedhar and A. Chockalingam, “MMSE Receiver for Multiuser Interference Cancellation in Uplink OFDMA”, in *Proc. IEEE 63rd Vehicular Tech. Conf.* pp. 2125-2129, 2006.

[32]. S. Manohar, D. Sreedhar, V. Tikiya and A. Chockalingam, “Cancellation of Multiuser Interference Due to Carrier Frequency Offsets in Uplink OFDMA”, *IEEE Trans. on Wireless Commun.*, Vol.6, No.7, July, 2007, pp.2560 – 2571

[33]. A. M. Tonello, “Asynchronous Multicarrier Multiple Access: Optimal and Sub-optimal Detection and Decoding”, *Bell Labs Tech. J.*, Vol.7, No.3, 2003, pp 191-217.

[34]. R. Lupas and S. Verdu, “Near-Far Resistance of Multiuser Detectors in

Asynchronous Channels", *IEEE Trans. on Commun.*, Vol.38, No.4, April, 1990, pp.496-508.

[35]. U. Madhow, "Blind Adaptive Interference Suppression for the Near-Far Resistant Acquisition and Demodulation of Direct-Sequence CDMA Signals", *IEEE Trans. on Signal Processing*, Vol.45, No.1, Jan, 1997, pp.124-136.

[36]. X. D. Wang and H. V. Poor, "Blind multiuser detection: a subspace approach", *IEEE Trans. on Information Theory*, Vol.44, No.2, March, 1998, pp.677 – 690.

[37]. U. Madhow and M. L. Honig, "On the Average Near–Far Resistance for MMSE Detection of Direct Sequence CDMA Signals with Random Spreading", *IEEE Trans. on Information Theory*, Vol.45, No.6, Sep. 1999, pp.2039-2045.

[38]. X. D. Yue and H. Howard Fan, "Near–Far Resistance of Optimum and Suboptimum CDMA Detectors Under Multipath", *IEEE Trans. on Signal Processing*, Vol.53, No.8, Aug, 2005, pp.2898-2917.

[39]. IEEE 802.16e-2005 Part 16: Air Interface for Fixed and Mobile Broadband Wireless Access Systems Amendment for Physical and Medium Access Control Layers for Combined Fixed and Mobile Operation in Licensed Bands.

[40]. H. Yaghoobi, "Scalable OFDMA Physical Layer in IEEE802.16 WirelessMAN", *Intel Tech. J.*, Vol.8, No.3, 2004, pp.201-212.

[41]. Michel C. Jeruchim, Philip Balaban, and K. Sam Shanmugan, *Simulation of Communication Systems: Modeling, Methodology, and Techniques 2nd Ed.*, New York : Kluwer Academic/Plenum Publishers, 2000.

[42]. Cimini, L., Jr., "Analysis and Simulation of a Digital Mobile Channel Using Orthogonal Frequency Division Multiplexing", *IEEE Transactions on Commun.*, Vol.33, No.7, Jul, 1985, pp.665 – 675.

[43]. M. Russell and G. L. Stuber, "Interchannel interference analysis of OFDM in a mobile environment", in *Proc. of 45th IEEE VTC 1995*, Vol.2, Jul, 1995, pp.820 - 824.

[44]. S. N. Diggavi, "Analysis of multicarrier transmission in time-varying channels", in *Proc. IEEE ICC 97*, Vol.3, June, 1997, pp.1191 – 1195.

[45]. P. Robertson and S. Kaiser, "The effects of Doppler spreads on OFDM(A) mobile radio systems," in *Proc. IEEE VTC 1999 Fall*, Sep., 1999, pp.329-333.

[46]. B. Stantchev and G. Fettweis, "Time-variant distortions in OFDM", in *IEEE*

Commun. Letters, Vol.4, No.10, Oct., 2000, pp.312 – 314.

[47]. P. Jung and G. Wunder, "On time-variant distortions in multicarrier transmission with application to frequency offsets and phase noise", in *IEEE Trans. on Commun.*, Vol.53, No.9, Sep., 2005, pp.1561 – 1570.

[48]. Y. Li, L. J. Cimini, and N. R. Sollenberger, "Robust channel estimation for OFDM systems with rapid dispersive fading channels," in *IEEE Trans. on Commun.*, vol. 46, July, 1998, pp.902 – 915.

[49]. W. G. Jeon, K. H. Chang, and Y. S. Cho, "An equalization technique for OFDM systems in time-variant multipath channels," in *IEEE Trans. on Commun.*, Vol. 47, No.1, Jan., 1999, pp.27 – 32.

[50]. Y. P. Zhao and S.-G. Häggman, "Intercarrier interference self-cancellation scheme for OFDM mobile communication systems," *IEEE Trans. Commun.*, vol. 49, No.7, pp. 1185-1191, July 2001.

[51]. P. Schniter, "Low-complexity equalization of OFDM in doubly selective channels", in *IEEE Trans. on Signal Processing*, Vol.52, No.4, April, 2004, pp.1002- 1011

[52]. I. Barhumi, G. Leus and M. Moonen, "Time-varying FIR equalization for doubly selective channels", in *IEEE Trans. on Wireless Commun.*, Vol.4, No.1, Jan., 2005, pp.202- 214

[53]. W. S. Hou and B. S. Chen, "ICI cancellation for OFDM communication systems in time-varying multipath fading channels", in *IEEE Trans. on Wireless Commun.*, Vol.4, No.5, Sep., 2005, pp.2100 - 2110.

[54]. L. Tadjpour, Shang-Ho Tsai and Kuo, C.-C.J., "An Approximately MAI-Free Multiaccess OFDM System in Fast Time-Varying Channels", in *IEEE Trans. on Signal Processing*, Vol.55, No.7, July, 2007, pp.3787 – 3799.

[55]. John G. Proakis, *Digital Communications* 4th Ed., New York: McGraw-Hill, 2001.

[56]. William C. Jakes, *Microwave Mobile Communications*, New York: Wiley, 1974.

[57]. Sergio Verdú, "Optimum multi-user asymptotic efficiency", in *IEEE Trans. on Commun.*, vol. COM-34, No.9, Sep., 1986, pp.890-897.

[58]. R. Lupas and Sergio Verdu, Linear Multiuser Detectors for Synchronous Code-Division Multiple-Access-Channels, in *IEEE Trans. on Info. Theory*,

Vol.35, No. 1, Jan., 1989, pp.123-136.

[59]. Sergio Verdú, *Multiuser detection*, New York: Cambridge University Press, 1998.

[60]. A. Stamoulis, S. N. Diggavi and N. Al-Dhahir, "Intercarrier Interference in MIMO OFDM", in *IEEE Trans. on Signal Processing*, Vol.50, No.10, Oct., 2002, pp.2451 – 2464.

[61]. Roger A. Horn and Charles R. Johnson, *Matrix analysis*, New York: Cambridge University Press, 1985.

[62]. Stephen Boyd and Lieven Vandenberghe, *Convex optimization*, New York: Cambridge University Press, 2005.

[63]. M. K. Varanasi and T. Guess, "Optimum Decision Feedback Multiuser Equalization with Successive Decoding Achieves the Total Capacity of the Gaussian Multiple-Access Channel", in *Proc. of IEEE 31st Asilomar Conference on Signals, Systems and Computers*, Vol.2, Nov., 1997, pp.1405 – 1409.

[64]. Y. S. Choim P. J. Voltz and F. A. Cassara, "On Channel Estimation and Detection for Multicarrier Signals in Fast and Selective Rayleigh Fading Channels", in *IEEE Trans. on Commun.*, Vol.49, No.8, Aug., 2001, pp.1375 – 1387.

[65]. M. K. Tsatsanis and G. B. Giannakis, "Modeling and equalization of rapidly fading channels," *Int. J. Adaptive Contr. Signal Processing.*, Vol.10, No. 2/3, pp. 159-176, 1996.

[66]. G. B. Giannakis and C. Tepedelenlioglu, "Basis Expansion Models and Diversity Techniques for Blind Indentification and Equalization of Time-Varying Channels", in *Proc. of the IEEE*, Vol.86, No.10, Oct., 1998, pp.1969 – 1985.

[67]. H. Liu and G. B. Giannakis, "Deterministic approaches for blind equalization of time-varyingchannels with antenna arrays", in *IEEE Transactions on Signal Processing*, Vol.46, No.11, Nov., 1998, pp.3003-3013.

[68]. C. Tepedelenlioglu and G. B. Giannakis, "Transmitter redundancy for blind estimation and equalization of time- and frequency-selective channels," in *IEEE Trans. on Signal Processing*, Vol. 48, July, 2000, pp. 2029-2043.

[69]. X. Ma and G. B. Giannakis, "Maximum-diversity transmissions over doubly-selective wireless channels," in *IEEE Trans. on Inf. Theory*, Vol.49, Jul.,

2003, pp. 1823-1840.

[70]. G. Leus, S. Zhou, and G. B. Giannakis, “Orthogonal multiple access over time- and frequency-selective fading,” in *IEEE Trans. on Inf. Theory*, Vol. 49, Aug., 2003, pp. 1942-1950.

[71]. Imad Barhumi, Geert Leus and Marc Moonen, “Time-domain and Frequency-domain Per-tone Equalization for OFDM over Doubly Selective Channels”, *Signal Processing (Special Section Signal Processing in Communications)*, Vol.84/11, 2004, pp.2055 – 2066.

[72]. M.-O. Pun, M. Morelli and C.-C. Jay Kuo, “Maximum-Likelihood Synchronization and Channel Estimation for OFDMA Uplink Transmissions”, in *IEEE Trans. on Commun*. Vol.54, No.4, April, 2006, pp 726-736.

[73]. M.-O. Pun, M. Morelli, C.-C. Jay Kuo, "Iterative detection and frequency synchronization for OFDMA uplink transmissions", in *IEEE Trans. on Wireless Commun.*, Vol.6, No.2, Feb., 2007, pp.629 – 639.

[74]. A. Sezgin et al., “On the Impact of Mobility on the Channel Estimation in WiMAX OFDMA-Uplink”, in *Proc. of 17th IEEE PIMRC*, pp.1-5, Sep, 2006.

[75]. M. R. Raghavendra, E. Lior, S. Bhashyam and K. Giridhar, “Parametric Channel Estimation for Pseudo-Random Tile-Allocation in Uplink OFDMA”, in *IEEE Trans. on Signal Processing*, Vol.55, No.11, pp.5370-5381, Nov., 2007.

[76]. Peter Fertl and G. Matz, “Multiuser Channel Estimation in OFDMA Uplink Systems Based on Irregular Sampling and Reduced Pilot Overhead”, in *IEEE ICASSP Conf. Proc*., Vol.3, pp.297-300, April, 2007.

[77]. Yi Ma and R. Tafazolli, “Channel Estimation for OFDMA Uplink: a Hybrid of Linear and BEM Interpolation Approach”, in *IEEE Trans. on Signal Processing*, Vol.55, No.4, April, 2007, pp. 1568 – 1573.

[78]. I. Barhumi, G. Leus and M. Moonen, "Time-varying FIR equalization for doubly selective channels", in *IEEE Trans. on Wireless Commun.*, Vol.4, No.1, Jan., 2005, pp.202- 214.

[79]. P. A. Bello, “Characterization of Randomly Time-Variant Linear Channels”, in *IEEE Trans. on Commun. Sys*., Vol.11, No.4, Dec, 1963, pp.360 – 393.

[80]. P. Hoeher, “A Statistical Discrete-Time Model for the WSSUS Multipath Channel”, in *IEEE Trans. on Vehicular Tech.*, Vol. 41, No. 4, pp. 461-468, November 1992.

[81]. M. K. Tsatsanis, G. B. Giannakis and G. T. Zhou, “Estimation and equalization of fading channels with random coefficients”, in *IEEE ICASSP 96. Conference Proc.*, Vol 2, pp. 1093-1096, May 1996.

[82]. L. M. Davis, I. B. Collings and R. J. Evans, “Identification of Time-Varying Linear Channels”, in *IEEE ICASSP 97 Conference Proc.*, Vol 5, pp. 3921-3924, April 1997.

[83]. R. A. Iltis and A. W. Fuxjaeger, “A Digital DS Spread-Spectrum Receiver with Joint Channel and Doppler Shift Estimation”, in *IEEE Trans. Commun.*, Vol.39, Aug., 1991, pp.1255 – 1267.

[84]. A. W. Fuxjaeger and R. A. Iltis, “Adaptive Parameter Estimation using Parallel Kalman Filtering for Spread Spectrum Code and Doppler Tracking”, in *IEEE Trans. on Commun.*, Vol.42, June, 1994, pp.2227 – 2230.

[85]. A. W. Fuxjaeger and R. A. Iltis, “Acquisition of Timing and Doppler Shift in a Direct Sequence Spread Spectrum System”, in *IEEE Trans. on Commun.*, Vol.42, Oct, 1994, pp.2870 – 2879.

[86]. M. K. Tsatsanis, G. B. Giannakis, and G. Zhou, “Estimation and Equalization of Fading Channels with Random Coefficients,” *Signal Processing*, vol. 53, pp. 211-229, 1996.

[87]. Simon Haykin, *Adaptive Filter Theory*. Prentice Hall, 3rd Edition., 1996.

[88]. D. K. Borah and B. D. Hart, “Frequency-Selective Fading Channel Estimation with a Polynomial Time-Varying Channel Model”, in *IEEE Trans. on Commun.*, Vol. 47, No. 6, June, 1999, pp. 862-873

[89]. X. W. Wang and K. J. Ray Liu, “Channel estimation for multicarrier modulation systems using a time-frequency polynomial model”, in *IEEE Trans. on Commun.,* Vol.50, No.7, July, 2002, pp.1045 – 1048.

[90]. Akbar. M. Sayeed and Behnaam. Aazhang, “Joint Multipath-Doppler Diversity in Mobile Wireless Communications”, in *IEEE Trans. on Commun.*, Vol. 47, No 1, Jan., 1999, pp.123 – 132.

[91]. S. Bhashyam, A. M. Sayeed and B. Aazhang, “Time-Selective Signaling and Reception for Communication over Multipath Fading Channels”, in *IEEE Trans. on Commun.*, Vol. 48, No.1, January 2000.

[92]. Ronald Raulefs, *et al.*, “The Doppler Spread – Gaining Diversity for Future Mobile Radio Systems”, in *IEEE Globecom 2003 Conference Proc.*, Vol.3, pp.

1301-1305, December 2003.

[93]. Byung-Chul Kim, “Doppler Diversity for OFDM Wireless Mobile Communications Part I: Frequency Domain Approach”, in *IEEE 57th VTC Conference Proc.*, Vol. 4, pp. 2677-2681, April 2003.

[94]. Byung-Chul Kim, “Doppler Diversity for OFDM Wireless Mobile Communications Part II: Time-Frequency Processing”, in *IEEE 57th VTC Conference Proc.*, Vol. 4, pp. 2682-2685, April 2003.

[95]. H. K. Lau and S. W. Cheung, “A Pilot Symbol-Aided Technique Used for Digital Signal in Multipath Environments”, in *Proc of IEEE ICC 94’*, Vol.2, May, 1994, pp.1126 – 1130.

[96]. W. G. Jeon, K. H. Chang and Y. S. Cho, "An Equalization Technique for Orthogonal Frequency-Division Multiplexing Systems in Time-Variant Multipath Channels", in *IEEE Trans. on Commun.*, Vol.47, No.1, Jan., 1999, , pp.27-32.

[97]. M. H. Ng and S. W. Cheung, "Bandwidth-Efficient Pilot-Symbol-Aided Technique for Multipath-Fading Channels", in *IEEE Trans. on Vehicular Technology*, Vol.50, No.4, Jul., 2001, pp.1132-1139.

[98]. S. M. Kay, *Fundamentals of Statistical Signal Processing: Estimation Theory*, Prentice Hall, Englewood Cliffs, New Jersey, 1993.

[99]. J. D. Gorman and A. O. Hero, “Lower Bounds For Parametric Estimation with Constrains”, in *IEEE Trans. on Information Theory*, Vol.26, No.6, pp.1285-1301, Nov., 1990.

[100]. A. O. Hero, J. A. Fessler and M. Usman, “Exploring Estimator Bias-Variance Tradeoffs using the Uniform CR Bound”, in *IEEE Trans. on Signal Processing*, Vol.44, No.8, pp.2026-2041, August 1996.

[101]. Z. Tang, R. C. Cannizzaro, G. Leus and P. Banelli, “Pilot-Assisted Time-Varying Channel Estimation for OFDM Systems”, in *IEEE Trans. on Signal Processing*, Vol.55, No.5, pp.2226-2236, May, 2007.

[102]. Harry L. Van Trees, “Optimum Array Processing”, Wiley-Interscience, 2002

[103]. C.C Ko and Z.Y Wu, “Fast algorithm for avoiding incidental cancellation problems in partially adaptive arrays”, *Electronics Letters*, U.K., Vol. 29, No. 12, 1993, pp. 1061 - 1062.

[104]. Z. Tian, K. L. Bell and H. L. Van Trees, “Robust Constrained Linear Receivers for CDMA Wireless Systems”, in *IEEE Trans. on Signal Processing*, Vol.49, No.7, July 2001, pp.1510-1522.

[105]. D. N. Guo, L. K. Rasmussen, S. M. Sun and T. J. Lim, “A Matrix-Algebraic Approach to Linear Parallel Interference Cancellation in CDMA”, in *IEEE Trans. on Commun.*, Vol.48, No.1, Jan., 2000, pp.1- 9.

[106]. R. R. Müller and S. Verdú, “Design and Analysis of Low-Complexity Interference Mitigation on Vector Channels”, in *IEEE J. on Selected Areas in Commun.*, Vol.19, No.8, August, 2001, pp.1429 – 1441.

[107]. P. Schniter, "Low-Complexity Equalization of OFDM in Doubly Selective Channels", in *IEEE Trans. on Signal Processing*, Vol.52, No.4, pp.1002-1011, April, 2004.

[108]. Z. R. Cao, U. Tureli and Y. Dong Yao, “Low-Complexity Orthogonal Spectral Signal Construction for Generalized OFDMA Uplink with Frequency Synchronization Errors”, in *IEEE Trans. on Vehicular Tech*., Vol.56, No.3, pp.1143-1153, May, 2007.

[109]. R. J. Baxley, J. E. Kleider and G. Tong Zhou, “Pilot Design for IEEE 802.16 OFDM and OFDMA”, in *Proc IEEE ICASSP 2007*, Vol. 2, pp.321-324, April, 2007.

[110]. S. Song and A. C. Singer, “Pilot-Aided OFDM Channel Estimation in the Presence of the Guard Band”, in *IEEE Trans. on Commun.*, Vol.55, No.8, pp.1459-1465, August, 2007.

[111]. S Lee, J. Y. Lee and H. S. Lee, "Group-based Pilot Design Method in Mobile OFDMA Systems", in *Proc. IEEE ICACT 2008*, Vol.1, pp.183-186, Feb, 2008.

[112]. A. Paulraj, R. Nabar and D. Gore, *Introduction to Space–Time Wireless Communications*, Cambridge University Press, 2003.

[113]. H. Krim and M. Viberg, "Two decades of array signal processing research: the parametric approach", in *IEEE Signal Processing Magazine*,Vol.13, No.4, July, 1996, pp.67 – 94.

[114]. L. C. Godara, "Application of antenna arrays to mobile communications. II. Beam-forming and direction-of-arrival considerations", in *Proceedings of the IEEE*, Vol.85, No.8, Aug., 1997, pp.1195-1245.

[115]. A. J. Paulraj and C. B. Papadias, "Space-time processing for wireless

communications", in *IEEE Signal Processing Magazine*, Vol.14, No.6, Nov., 1997, pp.49 – 83.

[116]. H. X. Li and H. Liu, "On the Optimality of OFDMA MIMO Channels", in *Proc. of IEEE Asilomar Conf. on Signals, Systems and Computers 06*', pp. 1757 – 1761.

[117]. L. Cariou and J.-F. Helard, "Efficient MIMO channel estimation for linear precoded OFDMA uplink systems", *Electronics Letters*, Vol.43, No.18, Aug., 2007, pp.986 – 988.

[118]. A. Saemi, J.-P. Cances and V. Meghdadi, "Synchronization algorithms for MIMO OFDMA systems", in *IEEE Trans. on Wireless Commun.*, Vol.6, No.12, Dec., 2007, pp.4441 – 4451.

List of Publications

Journal papers

1. S. W. Hou and C. C. Ko, "Multiple-Access Interference Suppression for Interleaved OFDMA System Uplink", in *IEEE Trans. on Vehicular Technology*, Vol.57, No.1, January, 2008, pp.194 – 205.

2. S. W. Hou and C. C. Ko, "Intercarrier Interference Suppression for OFDMA Uplink in Time and Frequency Selective Fading Channels", to appear as a regular paper in *IEEE Trans. on Vehicular Technology.*

3. M. F. Rabbi, S. W. Hou and C. C. Ko, "High Mobility OFDMA Channel Estimation using Basis Expansion Model", under review of *IEEE Transactions on Vehicular Technology*.

Conference papers

1. S. W. Hou and C. C. Ko, 'Subspace-based Multiple Access Suppression in Synchronous Interleaved OFDMA System', in *Proceedings of 64th IEEE Vehicular Technology Conference 2006*.

2. S. W. Hou and C. C. Ko, 'Intercarrier Interference Suppression for OFDMA Uplink in Time and Frequency Selective Fading Channels', in *Proceedings of 67th IEEE Vehicular Technology Conference 2008*.